CHEMICAL APPLICATIONS
OF
HIGH-RESOLUTION NMR ROTARY SPIN ECHOES

by

SAI-ON CHAN

B.Sc., University of Hong Kong, 1961

A THESIS SUBMITTED IN PARTIAL FULFILMENT OF
THE REQUIREMENTS FOR THE DEGREE OF
DOCTOR OF PHILOSOPHY
in the Department
of
Chemistry

SIMON FRASER UNIVERSITY

April, 1969

EXAMINING COMMITTEE APPROVAL

Dr. E. J. Wells
Senior Supervisor

Dr. R. G. Korteling
Examining Committee

Dr. E. M. Voigt
Examining Committee

Dr. M. Bloom
External Examiner
Physics Department
U. B. C.

ABSTRACT

The high-resolution NMR rotary-echo technique developed by Wells and Abramson regains the frequency selectivity lacking in spin-echo methods employing high-power rf pulses. A general theoretical treatment for the decay of the rotary-echo train is made. Closed formulae to include chemical exchange are still lacking but approximate equations for special limiting cases have been derived. The hindered internal rotation about the carbon-nitrogen bond in N,N-dimethylcarbamyl chloride (DMCC) and N,N-dimethylnitrosamine (DMNA) is studied. Activation energies and frequency factors of 15.1 and 25.0 kcal/mole and 2.70×10^{11} and 2.99×10^{13} sec^{-1} respectively are obtained for DMCC and DMNA respectively, comparable to other spin-echo results. Pulsing at sub-audio frequencies, the rotary-echo decay is found sensitive to unresolved scalar coupling to quadrupolar nuclei. The method has been applied to determine the coupling constants $J_{\underline{H}C\underline{C}N}$ in acetonitrile (CH_3CN) and $J_{\underline{H}C\underline{C}l}$ in chloroform ($CHCl_3$), the results produced being in good agreement to those obtained by other means. The fluorine spin-rotation relaxation in liquid chlorodifluoromethane (CHF_2Cl) and difluoromethane (CH_2F_2) has also been studied by the selective rotary-echo technique using an indirect method by which only the proton resonances, whose natural linewidths are dominated by the rapid relaxation by spin-rotation interaction of the fluorine nuclei coupled scalarly to the protons, need be ob-

served. The symmetric and antisymmetric fluorine transition probabilities k_s and k_a respectively for the two systems are determined at various temperatures ranging from 217° to 315° K. The ratios k_s/k_a are found to be about 13 for CHF_2Cl and about 9 for CH_2F_2 independent of temperature indicating that the correlation time τ_1 for the change in angular momentum is much shorter than the correlation time τ_2 for molecular reorientation.

A separate and unrelated study is made on the system N,N-dimethyl-2,3-dihydroxy -3-phenylpropionamide, $\phi CH(OH)CH(OH)CON(CH_3)_2$. Preparation of the compound leads us to a closer study of the usual organic peracid hydroxylation process and the stereochemistry of the epoxide-ring opening. Preliminary observations of the effects of metal ions on the PMR of the system, the hindered internal rotation about the carbon-nitrogen bond and of the effects of differential exchange among the hydroxyl protons are made.

ACKNOWLEDGEMENTS

For his helpful direction and sincere dedication to this research program, the author wishes to express his utmost appreciation and gratitude to Dr. E. J. Wells of the Chemistry Department, Simon Fraser University.

Acknowledgements are also due to Mr. K. H. Abramson for his work on the rotary-echo spectrometer.

Last but not least, the author is indebted to the National Research Council of Canada for the award of a postgraduate scholarship which makes the present work possible.

TABLE OF CONTENTS

LIST OF TABLES

LIST OF FIGURES

CHAPTER I

INTRODUCTION

Since the first successful detection of nuclear magnetic resonance signals in bulk matter in late 1945 by Purcell, Torrey and Pound (1) and by Bloch, Hansen and Packard (2), the subject of nuclear magnetic resonance has developed in a remarkable manner. The advantage of the resonance method is that it enables one to select out of the total magnetic susceptibility a particular contribution of interest—here, the nuclear contribution, though it is in general very weak compared to that of the orbital electrons.

By doing NMR experiments, we are using a nucleus as a magnetic probe to investigate the local magnetic effects inside a molecular system. High-resolution work has shown that magnetic nuclei can detect very small changes in chemical environment and provide a number of important applications in various branches of chemistry and chemical physics. Through modern developments of instrumentation, the method has become one of the most powerful tools for investigating chemical problems. Nowadays, steady-state NMR methods are widely used by organic chemists to assist in structure determination and by inorganic and physical chemists to investigate such problems as isomerism, tautomerism, chemical equilibria, hydrogen bonding, reaction rates, chemical exchange and relaxation processes.

In spite of its usefulness and wide application, the steady-state NMR method suffers from certain limitations (3) in the studies of kinetic rate and relaxation processes. Pulsed NMR methods employing a single rf pulse (4) or a sequence of two or more rf pulses (5, 6) have been shown to be better in some cases. However, a disadvantage of the usual pulsed methods of high rf power is the lack of selectivity on the various homonuclear spin transitions which may occur in a high-resolution spectrum. The current approach to this problem is to restrict attention to systems which, by simplicity or high symmetry, yield relatively simple spectra, or which can be so transformed by judicious isotopic substitution.

From Solomon's rotary-echo experiment (7), it is seen that the selectivity on frequency can be regained. By working in a rotating frame coinciding with a particular transition frequency, and with a rf amplitude low enough not to significantly perturb other nearby transitions one has, in the rotary-echo phenomenon, a tool of low time resolution allowing direct time-dependent measurement on isolated lines of a complex high-resolution spectrum. Such high-resolution rotary spin echoes have been obtained by Wells and Abramson (8) with slight modificaiton of Solomon's method.

In what follows a general aspect of the high-resolution rotary spin echoes will be given, but essentially the greater part of this work deals with applications to a number of chemical

or chemico-physical problems.

A. The Rotating Frame and Spin Echoes

Some insight into the nature of magnetic resonance can be obtained by consideration of the classical motion of a magnetic dipole with angular momentum $\vec{J}$ in a magnetic field $\vec{H}_o$. The equation of motion is

$$\frac{d\vec{J}}{dt} = \vec{\mu} \times \vec{H}_o \tag{1.1}$$

where $\vec{\mu}$ is the magnetic moment of the magnetic dipole. Since $\vec{\mu} = \gamma\vec{J}$, $\vec{J}$ can be eliminated and

$$\frac{d\vec{\mu}}{dt} = \vec{\mu} \times (\gamma\vec{H}_o) \tag{1.2}$$

where γ is the magnetogyric ratio.

In order to solve equation (1.2) it is desirable to transform to a rotating co-ordinate frame of reference. According to the general law of relative motion the time derivative $\frac{d\vec{\mu}}{dt}$ of $\vec{\mu}$ computed in the laboratory frame and its derivative $\frac{\partial\vec{\mu}}{\partial t}$ computed in the rotating frame are related through

$$\frac{d\vec{\mu}}{dt} = \frac{\partial\vec{\mu}}{\partial t} + \vec{\omega} \times \vec{\mu} \tag{1.3}$$

where $\vec{\omega}$ is the angular velocity of the rotating frame with respect to the laboratory frame. Combining (1.2) and (1.3), the motion of the magnetic moment in the rotating frame is given by

$$\frac{\partial\vec{\mu}}{\partial t} = \vec{\mu} \times (\gamma\vec{H}_o + \vec{\omega}) \tag{1.4}$$

which has the same form as (1.2) provided the magnetic field $\vec{H}_o$

is replaced by an effective field $\vec{H}_e = \vec{H}_o + \vec{\omega}/\gamma$. By choosing a rotating frame with $\vec{\omega}$ such that $\vec{H}_e = 0$, we can readily solve for the motion of $\vec{\mu}$ in a static field. Thus with

$$\vec{\omega} = -\gamma\vec{H}_o \tag{1.5}$$

$\frac{\partial\vec{\mu}}{\partial t} = 0$ and the magnetic moment is a fixed vector in the rotating frame. Therefore, with respect to the laboratory frame $\vec{\mu}$ precesses with an angular velocity $\vec{\omega}_o$, called the Larmor frequency of the spin in the applied field $\vec{H}_o$ given by equation (1.5).

If a second magnetic field, alternating at angular frequency $\vec{\omega}_o$ and with amplitude $2H_1$, or rotating at the Larmor frequency $\vec{\omega}_o$ and with amplitude H_1, is applied to the spin perpendicular to the field H_o, a resonance condition is attained. In the rotating frame the effective field H_e is equal to H_1 and is always fixed and perpendicular to the axis of rotation, the z-axis*. Let us take the x-axis in the rotating frame along H_1, then a magnetic moment that is initially parallel to the static field H_o will precess at angular velocity γH_1 in the y-z plane, but remaining perpendicular to H_1 always. If we were to turn on H_1 for a short time t_w, the moment would precess through an angle $\theta = \gamma H_1 t_w$. If t_w were chosen such that $\theta = \pi$, the pulse (generally referred to as a 180° pulse) would simply invert the moment.

---

*An alternating field $2H_1\cos\omega_o t$ can be readily broken up into two rotating components each of amplitude H_1, one rotating clockwise and the other counterclockwise. The component which rotates in the opposite sense to the precession of the magnetic moment can be shown to give negligible effects at or near resonance for H_o sufficiently large.

If $\theta = \pi/2$ (a 90° pulse), the magnetic moment is turned from the z-direction to the y-direction. These are the bases of the spin-echo method.

In actual experiments a large assembly of magnetic nuclei is observed. The inhomogeneity of the applied field across the sample results in a spread $\gamma\Delta H_o$ in Larmor frequencies. High-resolution linewidths are predominantly broadened by this. By the application of rf pulses the magnet inhomogeneity effects can conveniently be removed. It has been shown that the decay of the precessing transverse magnetization following a 90° pulse and caused by destructive interference between the contributions from moments in different parts of the sample, precessing at different Larmor frequencies is not an irreversible process (4). 90° refocussing pulses were first used by Hahn (5). The restoring of the transverse magnetization gives rise to the so-called spin echoes. The technique of 180° refocussing pulses was introduced by Carr and Purcell (6). It is more elegant and the easiest to interpret. These pulses applied at times τ, 3τ, ..., $(2n-1)\tau$, ... after the first 90° pulse give rise to spin echoes at time 2τ, 4τ, ..., $2n\tau$, ... This latter method is the most widely used at present, with the additional modification of Meiboom and Gill (9) of a 90° rf phase shift between the initial 90° pulse and the refocussing 180° pulses.

B. The High-Resolution Rotary Spin Echoes

The high-resolution rotary spin echoes are obtained (8) by a minor modification of Solomon's method (7) in effecting the 180° relative phase change between H_1 and the y-component of the magnetization vector in the rotating frame. The modified method proves to be particularly simple to apply with commercially available high-resolution NMR spectrometers and, in principle, offers some advantages in echo amplitude stability over the old one. In the following we give a simple pictorial description of the method, then the instrumentation, the procedure to obtain a 180° pulse and some discussions on the effects of radiation damping and self-diffusion through the H_1 field gradient.

(a) General description of the rotary-echo method

An assembly of magnetic nuclei is immersed at thermal equilibrium in a strong dc field H_o along the z-axis. For simplicity the high-resolution steady-state spectrum is assumed to be a single line. At time $t = 0$ an oscillatory field of frequency ω_o and amplitude $2H_1$ is gated on exactly at resonance, i.e. $\omega_o = \gamma H_o$. In the frame rotating at the spin transition frequency the field along the x-axis is given by

$$H_1(t) = H_1 + H_1 \cos 2\omega_o t \,. \qquad (1.6)$$

For H_o (and hence ω_o) sufficiently large the time dependent term can be neglected. If H_1 satisfies the condition $\gamma H_1 >> \Delta\omega_{\frac{1}{2}}$, where $\Delta\omega_{\frac{1}{2}}$ is the half width at half height of the

transition*, then the motion of the spin magnetization in the rotating frame is simply a precession about the newly-established constant H_1. This precession has been called "transient nutation" by Torrey (10) and is damped by the dephasing processes in the rotating frame with a decay constant given by

$$R_{2r} = \tfrac{1}{2}(R_1 + R_2) \qquad (1.7)$$

where R_1 and R_2 are the longitudinal and transverse relaxation rates in the laboratory frame. Further the precession is more severely damped by the instrumental inhomogeneity in H_1 generated by a radio frequency solenoid. In the absence of nuclear frequency modulation effects the undesirable dephasing caused by H_1 inhomogeneity in the doubly rotating frame is reversible by a technique analogous to the Carr-Purcell method (6) of removing the effects of the H_0 inhomogeneity in the usual spin-echo experiment.

At time $t = \tau$ the static field H_0 is pulsed off resonance in either direction by an amount $h >> H_1$ for a time t_w sufficient to cause the magnetization to skip through 180° about the z-axis in the first rotating frame**. Following this pulse, the magnet-

---

*The second moment of a spin transition in a liquid sample is unchanged by spinning the sample in the inhomogeneous field H_0, although the central transition may be dramatically narrowed. By $\Delta\omega_{\frac{1}{2}}$ we mean the residual width of this central line, and ignore the effects of the spinning side bands.

**For the general case of a multi-line homonuclear spectrum covering a frequency range Ω, h must satisfy the more stringent condition $h >> \Omega$ so as not to perturb the other transitions.

ization continues to precess as before about H_1 and refocusses along the z-direction at $t = 2\tau$ giving rise to the "rotary spin echo", the maximum of which is observed as the magnetization again dips through the xy-plane at $t = 2\tau + \frac{\pi}{2\gamma H_1}$. As in the Carr-Purcell experiment a sequence of identical 180° pulses can be applied at times $t = (2n - 1)\tau$, and the magnetization is refocussed along the z-axis at times $t = 2n\tau$ giving a rotary-echo sequence. The decay of the echo train is approximately exponential with a decay constant $R_{2\tau}$ given by equation (1.7), diffusion effects being neglected. The magnetization trajectory in the rotating frame is sketched in Fig. 1-1*.

Some advantages of the present method over Solomon's phase shift method are i) the generation of a dc pulse is experimentally simpler than the phase reversal of a high frequency signal ($\nu > 20$ Mhz); and ii) errors in the echo amplitudes down the echo sequence caused by a systematic error in the off-resonance pulse do not accumulate as rapidly as those caused by a systematic error in the phase-switching angle. The present mod-

---

*This figure is helpful for visualizing the physical situation but is not to be taken too literally. It is an oversimplification in that the signal induced in the receiving coil is not related in a simple manner to the bulk nuclear magnetization but is weighted by the coupling between a particular nucleus and the coil. Moreover, the spin locking experiments of Ostroff and Waugh (Phys. Rev. Letters, 16, 1097, (1966)) and Mansfield and Ware (Physics Letters, 22, 133 (1966)) indicate that such diagrams can lead to qualitatively wrong results, and that in general the response should be obtained from a Fourier analysis of the complete pulse sequence.

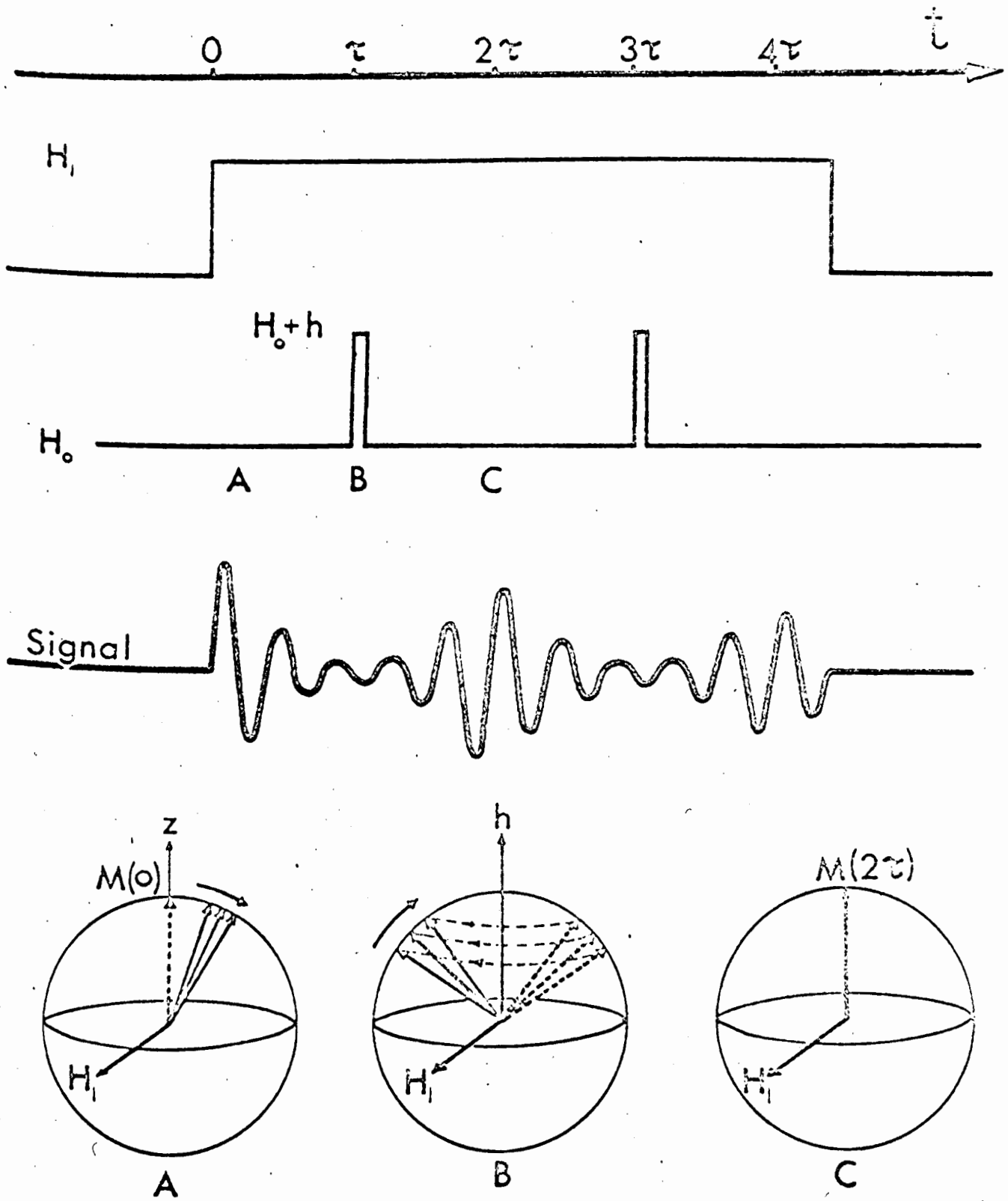

Fig. 1-1. Formation of rotary spin echoes.

ification may be likened in this respect to the Meiboom-Gill modification (9) of the initial Carr-Purcell experiment. A sketch of the relative situations is shown in Fig. 1-2.

(b) Instrumentation

The high-resolution rotary-echo experiment was performed on a Varian A56/60 high-resolution NMR spectrometer which has a single coil probe and external field frequency lock. The timing logic set-up is sketched in Fig. 1-3. A master gating voltage was obtained from the time-base of a Tektronix 547 oscilloscope. This voltage switched the rf field H_1 to the probe coil by means of a Tektronix co-axial switch (5W750 in Type 109 pulse generator) with mercury wetted contacts (a transistor switch in the cathode circuit of the synthesizer rf output stage will also serve the purpose) and simultaneously initiated the negative sawtooth sequence of a Tektronix 162 waveform generator in gated mode. The 25-volt dc pulses were delivered after an empirically adjusted delay to the dc sweep coils from a Tektronix 163 pulse generator driven by the waveform generator. The nuclear signal was fed through the A56/60 receiver and detector circuits in the normal way and on to a readout device from the recorder output jack. Usually the signals were photographed on Polaroid film from the oscilloscope but it was found possible with samples of long relaxation time using low H_1 (< 1mG) to record signals directly on a potentiometric recorder. The modification on the Varian

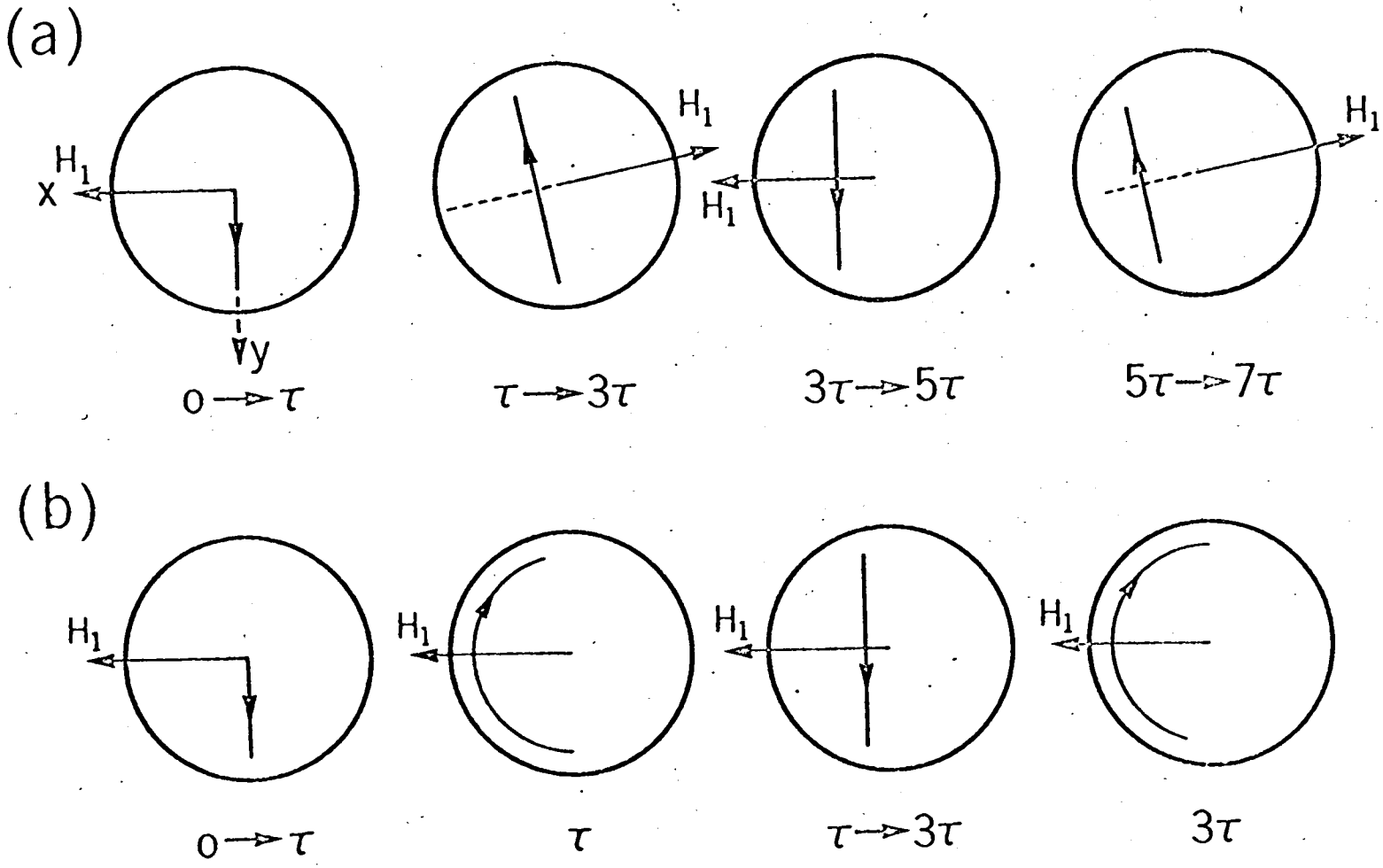

Fig. 1-2. Schematic comparison of the accumulation of systematic errors in (a) Solomon's phase-shift method and (b) the present field-pulse method.

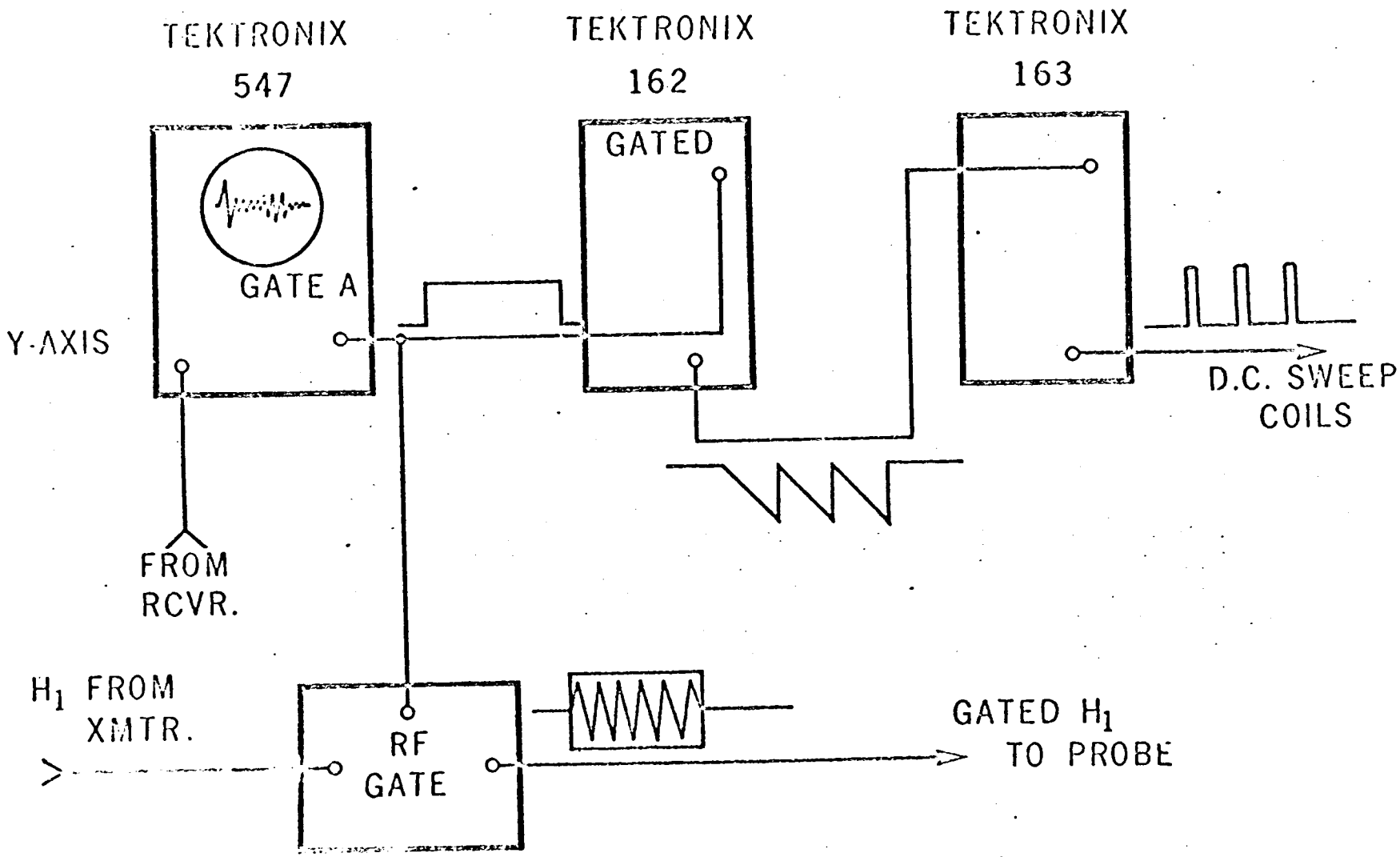

Fig. 1-3. The timing logic for production of rotary spin echoes.

high-resolution NMR spectrometer was straightforward. The bandwidth of the output operational amplifier (Philbrick USA - 3) was extended to about 500 hz by the addition of several extra feed-back capacitors.

The rf leakage through the co-axial switch could not be completely eliminated, but the H_1 present in the nominal OFF position was down some 60 db and was well below saturation level of all transitions. This leakage has the practical advantage of allowing the experimenter to maintain the critical resonance condition on a selected transition between experiments.

For both steady-state and rotary-echo work with the Varian A56/60 high-resolution NMR spectrometer, the sample temperature was maintained in the built-in variable temperature probe by a gas-flow system and the temperature regulated by a Varian V-6040 temperature control. Temperatures were calibrated with the ethylene glycol and methanol samples provided along with the Varian instruments.

(c) Adjustment of the 180° pulse width

The pulse length required to achieve a 180° rotation of the magnetization about the z-axis can be determined in a procedure illustrated in Figs. 1-4 and 1-5.

First a resonance condition on a suitably narrow transition is obtained with a value of H_1 below saturation (the rf leakage serves the purpose well). Under the combined influence of

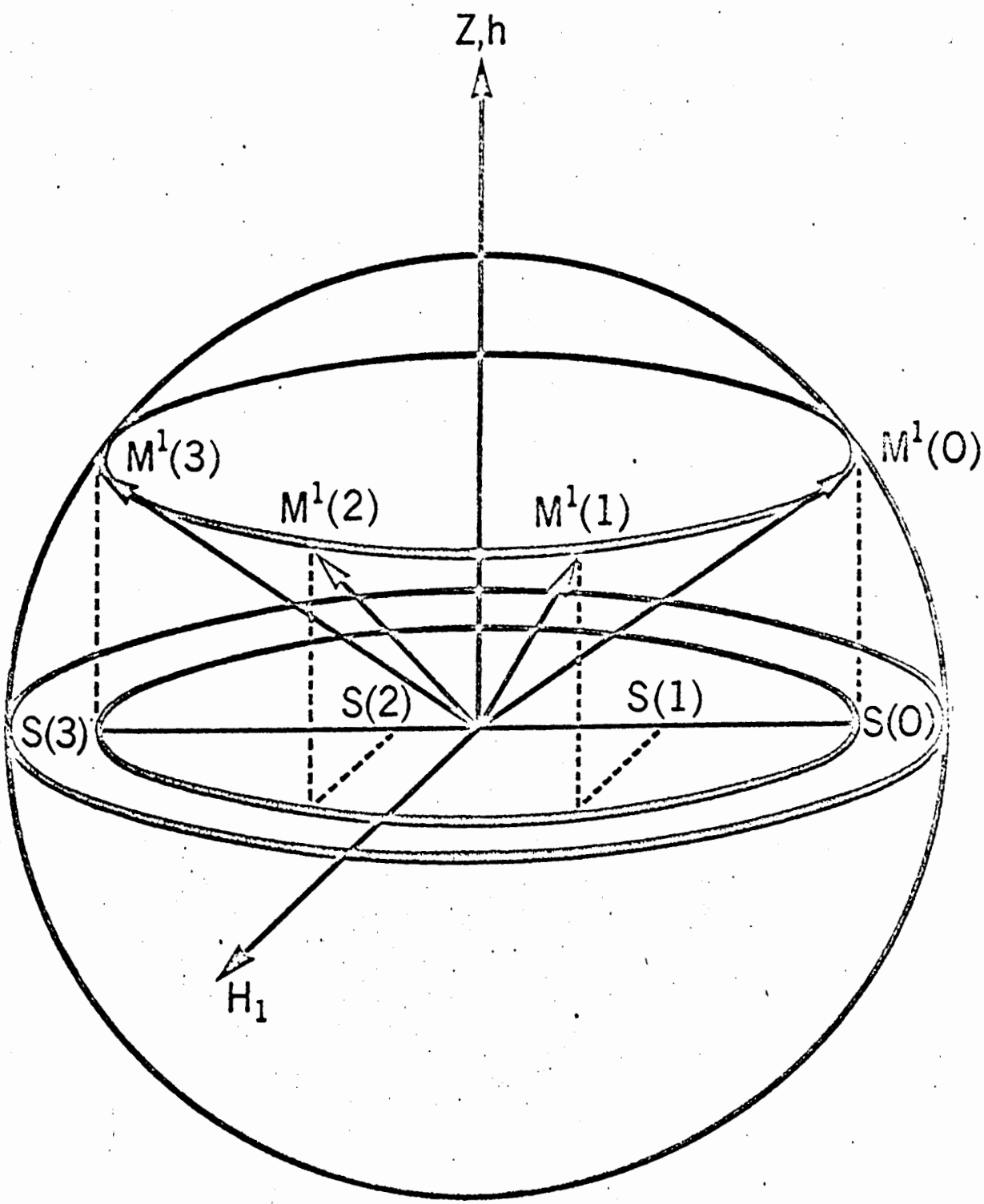

Fig. 1-4. Rotation of the resultant magnetization about the z-axis by dc pulses of different widths.

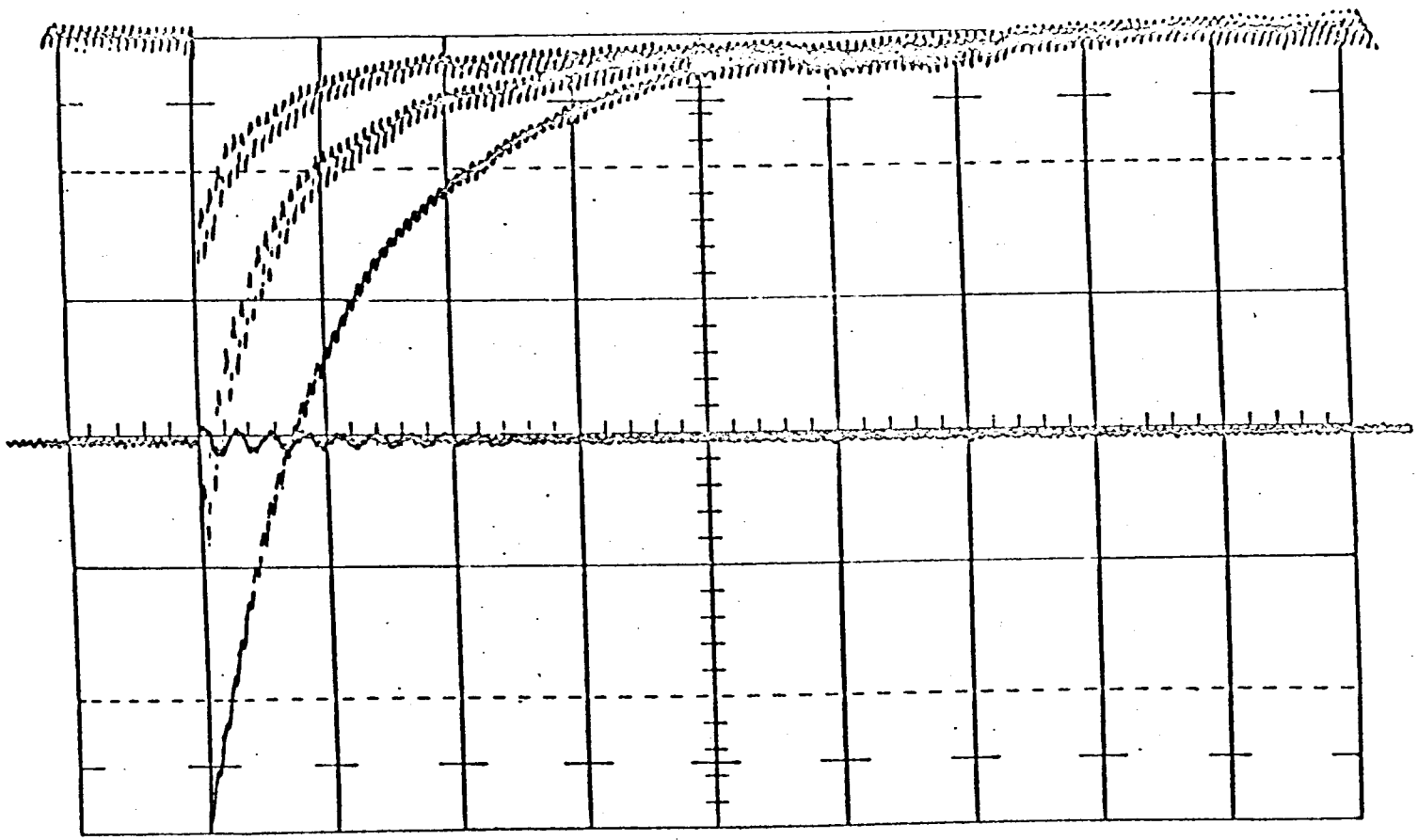

Fig. 1-5. Signal deviations following dc pulses of different widths.

this resonant H_1 and spin-lattice relaxation effects, the spin magnetization comes to a position of equilibrium $M^1(0)$ removed from the thermal equilibrium in the absence of H_1. The detected signal S in absorption mode is proportional to M_y, the component of the magnetization vector along the out-of-phase axis in the rotating frame. Application of a large z-field pulse causes the magnetization to precess about z and the signal following the pulse reflects the new out-of-phase component M'_y. If inhomogeneities in the off-resonance field h are neglected the effect of a correctly-set z-pulse is to take M_y to $-M_y$, i.e. to reverse the sign of the steady-state signal, corresponding to a rotation of the magnetization by 180° about the z-axis in the rotating frame. Thus the 180° pulse width is obtained by adjusting for maximum signal deviation from the steady-state value.

(d) Effects of radiation damping

Radiation damping (11-14) is the phenomenon that energy is dissipated in the form of Joule heat because of the current induced in the transmitter-receiver coil by the precessing magnetization. This energy can only be provided by the nuclear magnetic energy of the misalignment of the magnetization and results in a torque which tends to restore $\vec{M}$ to its equilibrium position parallel to the applied field, without changing the amplitude of $\vec{M}$. The torque can be thought of as one equal to $\vec{M} \times \vec{H}_r$ in the rotating frame, where $\vec{H}_r$ is the radiation field,

parallel to $\vec{H}_1$, produced by the current induced in the coil by the precession of $\vec{M}$. The amplitude of $\vec{H}_r$ is given by (15)

$$H_r = 2\pi\eta Q M \sin\theta \qquad (1.8)$$

where η is the filling factor,

Q is the quality factor of the tuned receiver circuit

and θ is the instantaneous angle between $\vec{M}$ and the z-axis.

The effective field H_1' in the rotating frame at resonance is then given by

$$H_1' = H_1 - H_r \qquad (1.9)$$

and the transitory precession of M is retarded by H_r on the down-swing from its equilibrium position ($0 < \theta < \pi$) and accelerated on the up-swing ($\pi < \theta < 2\pi$). In the absence of dephasing mechanisms which change the amplitude of M, the effect of H_r can only be a small and,in practice, negligible timing error (8) at the signal maxima when M dips through the xy-plane. It is expected that H_r yields only second order effects down the rotary-echo sequence when dephasing effects are taken into account. The situation is analogous to the refocussing of radiation damping effects by 180° pulses in the Carr-Purcell experiment.

(e) Self-diffusion through H_1 field gradient

For simplicity, consider a "single coil" NMR probe where the rf coil acts both as the transmitter as well as the receiver coil. A time-dependent current $I(t) = Ie^{i\omega_0 t}$ flowing through the coil is seen by each nucleus in its frame rotating at the

Larmor frequency ω_o as a constant current I, if displacement current effects due to the time dependence in the laboratory frame can be neglected*. The coil is idealised as a single turn solenoid of radius a in the yz-plane and the sample volume is supposed to be an infinite cylinder of radius r, whose axis coincides with that of the coil along x as in Fig. 1-6.

In cylindrical co-ordinates with the coil centre as origin, the values of the components of the field H_1 in the rotating frame are found to be (16)

$$\left.\begin{aligned} H_x &= H_c \frac{a}{\pi} \frac{1}{[(a+\rho)^2 + x^2]^{\frac{1}{2}}}\left[K + \frac{a^2 - \rho^2 - x^2}{(a-\rho)^2 + x^2}E\right] \\ H_\rho &= H_c \frac{ax}{\pi\rho} \frac{1}{[(a+\rho)^2 + x^2]^{\frac{1}{2}}}\left[-K + \frac{a^2 + \rho^2 + x^2}{(a-\rho)^2 + x^2}E\right] \\ H_\theta &= 0 \end{aligned}\right\} \qquad (1.10)$$

where $H_c = \frac{2\pi I}{ac}$ is the value of the field at the coil centre and K and E are complete elliptic integrals of the first and second kinds respectively in the argument k given by

$$k^2 = \frac{4a\rho}{(a+\rho)^2 + x^2} \quad . \qquad (1.11)$$

The radial component H_ρ is symmetrical about the x-axis, which is also the axis of mechanical spinning. For sufficiently high spinning rate ($\omega_s >> \gamma H_\rho$, which is almost always the case in high-resolution experiments) the radial component at a given nucleus is averaged to zero by the spinning in the absence of

---

*This condition is well satisfied by NMR experiments in currently attainable dc fields.

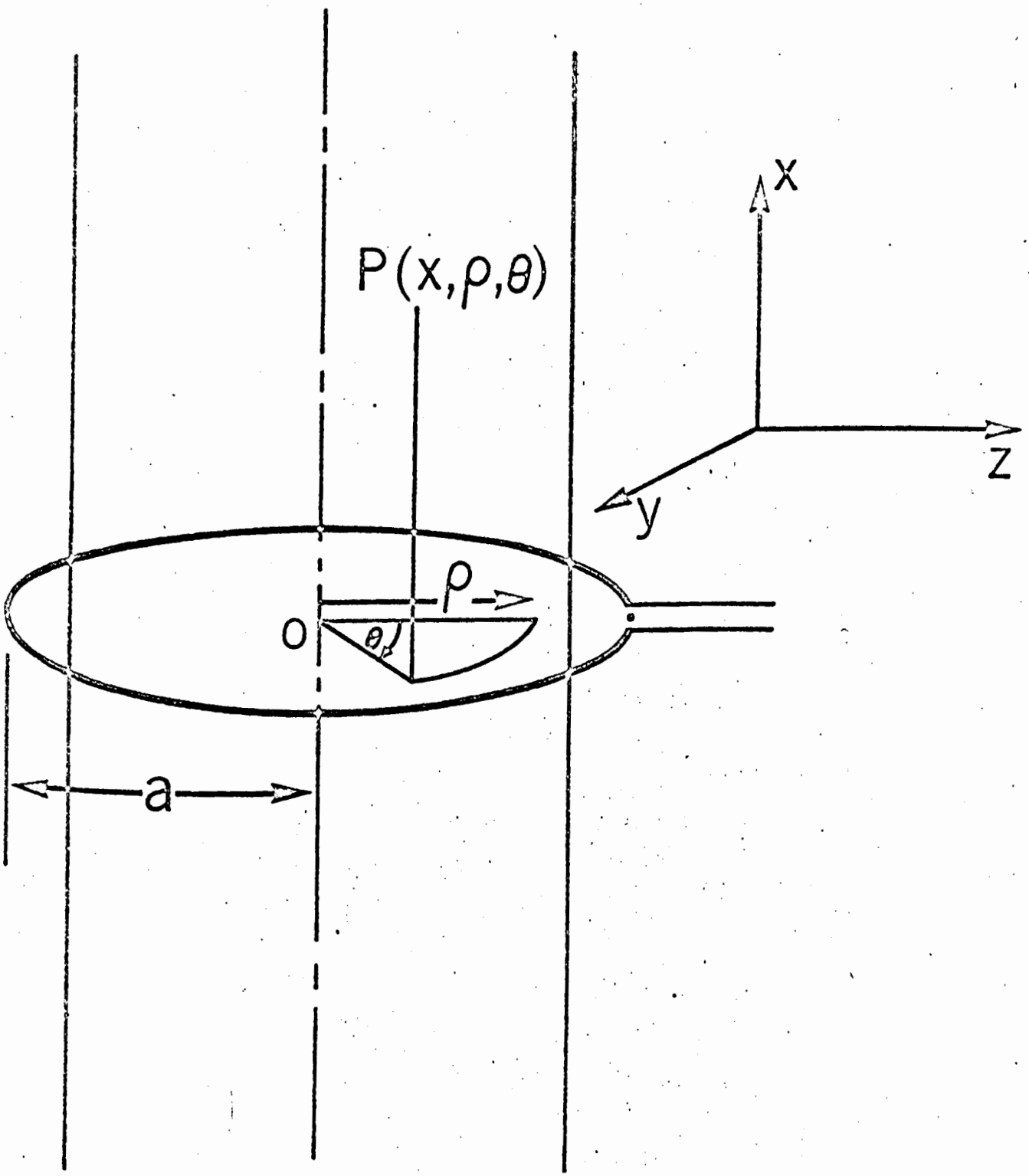

Fig. 1-6. Cylindrical co-ordinates for an idealised sample geometry.

diffusion. Even if diffusion takes place through the radial field gradient, it is expected that the averaged effect of H_ρ is negligible.

The radial and axial dependences of the field H_x are shown in Fig. 1-7 for some given values of the x and ρ co-ordinates from tabulated values of K and E (17). It is seen that the most severe gradient in H_x is at those regions of the sample near the coil wire, i.e. $\rho/a > 0.5$. By selection of sample tube wall thickness one can control ρ_{max} to limit the gradient in H_x. Moreover, the effects of molecular diffusion through the H_1 field gradients can be eliminated completely by rapid pulsing. In the case of moderate pulse rate the effects can be removed by extrapolating the decay rates against some function of the pulse repetition time 2τ to infinite repetition rate, i.e. $2\tau = 0$. The exact form of the extrapolation function will depend on the details of the H_1 field gradients experienced by the active volume of the sample. Empirically it is found that a plot of $R_{2\tau}$ vs $(2\tau)^2$ gives a linear variation within experimental errors and yields correct extrapolated values. Thus the nuclei experience effectively a constant field gradient. A qualitative justification for this is the smallness of the value of the self-diffusion coefficients ($D \approx 10^{-5}$ cm^2sec^{-1}) for most mobile organic liquids. Since the mean square Brownian displacement $\overline{\Delta^2}$ in time t is given by $\overline{\Delta^2} = 2Dt$, the diffusion distance after one second is typically 5×10^{-3} cm or 1% of the sample diameter. Thus

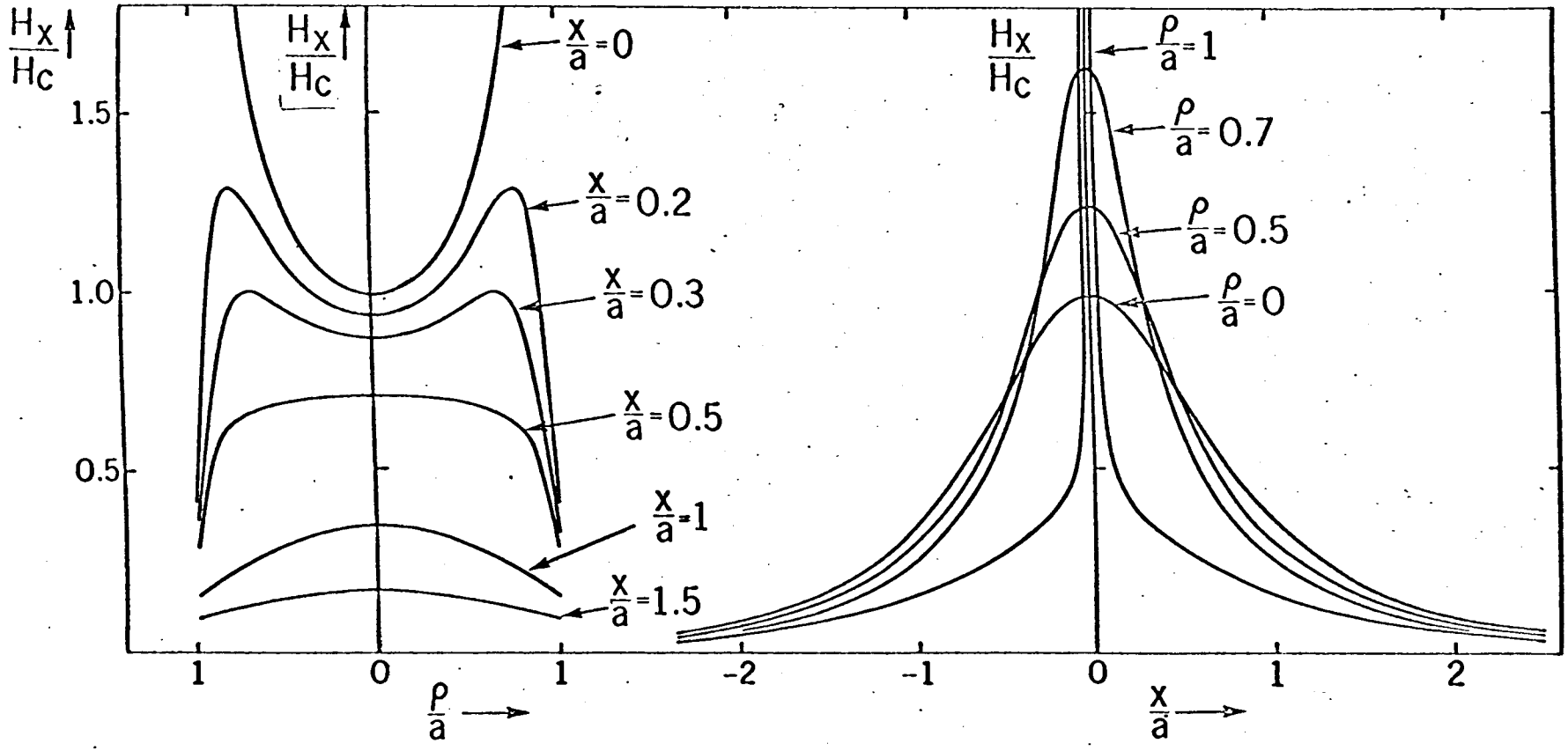

Fig. 1-7. The radial and axial dependences of H_x.

each nucleus diffuses through an essentially constant field gradient for 2τ sufficiently small.

CHAPTER II

THEORY OF THE NMR ROTARY SPIN ECHOES

A general theory is developed from Bloch's equations (18) in matrix form. Using the technique of matrix integral solution of coupled differential equations, an expression for the magnetization at time $2n\tau$ after the nth refocussing pulse is derived in the following section.

A. Theoretical Analysis

In matrix notation, Bloch's equations can be written as

$$\frac{d\vec{M}}{dt} = \underset{\approx}{B}\vec{M} + \vec{C} \tag{2.1}$$

where $\vec{M}$ is a column vector whose entries are the three orthogonal components u, v and M_z of the resultant magnetization with respect to a frame rotating at the Larmor frequency $\omega_o = \gamma H_o$ about the z-axis. Therefore

$$\vec{M} = \begin{bmatrix} u \\ v \\ M_z \end{bmatrix} \tag{2.2}$$

$$\underset{\approx}{B} = \begin{bmatrix} -R_2 & \delta & 0 \\ -\delta & -R_2 & -\omega_1 \\ 0 & \omega_1 & -R_1 \end{bmatrix} \tag{2.3}$$

$$\vec{C} = \begin{bmatrix} 0 \\ 0 \\ R_1 M_o \end{bmatrix} \tag{2.4}$$

and R_1 = longitudinal relaxation rate,

R_2 = transverse relaxation rate,

$\delta = \omega - \omega_o$ = distance from resonance in radians per second,

$\omega_1 = \gamma H_1$,

and M_o = the equilibrium magnetization.

To solve equation (2.1), put

$$\vec{N} = \underset{\approx}{B}\vec{M} + \vec{C}. \tag{2.5}$$

Since $\underset{\approx}{B}$ and $\vec{C}$ are time-independent,

$$\frac{d\vec{N}}{dt} = \underset{\approx}{B}\frac{d\vec{M}}{dt} . \tag{2.6}$$

From equations (2.1), (2.5) and (2.6),

$$\frac{d\vec{N}}{dt} = \underset{\approx}{B}\vec{N},$$

$$\text{therefore } \vec{N}(t) = e^{\underset{\approx}{Bt}}\vec{N}(0). \tag{2.7}$$

Now the effect of the 180° pulse in the rotary-echo method (8) is to change the signs of u and v leaving M_z unchanged.

Therefore $$\underset{\approx}{P}\vec{M} = \begin{bmatrix} -u \\ -v \\ M_z \end{bmatrix}$$

and $$\underset{\approx}{P} = \begin{bmatrix} -1 & 0 & 0 \\ 0 & -1 & 0 \\ 0 & 0 & 1 \end{bmatrix} . \tag{2.8}$$

At $t = \tau$, a pulse P is applied. We introduce the symbols τ_- and τ_+ to refer to times just before and just after the pulse respectively. By (2.7)

$$\vec{N}(\tau_-) = e^{\underset{\approx}{B\tau}}\vec{N}(0),$$

and by (2.5)

$$\vec{M}(\tau_-) = \underset{\approx}{B}^{-1}[e^{\underset{\approx}{B\tau}}\vec{N}(0) - \vec{C}] .$$

Since the effect of the 180° pulse on the magnetization vector is to change $\vec{M}$ into $\underset{\approx}{P}\vec{M}$, therefore

$$\vec{M}(\tau_+) = \underset{\approx}{P}\vec{M}(\tau_-) = \underset{\approx\approx}{PB}^{-1}[e^{\underset{\approx}{B\tau}}\vec{N}(0) - \vec{C}] .$$

By (2.5), $\vec{N}(\tau_+) = \underset{\approx}{BPB}^{-1}[e^{\underset{\approx}{B}\tau}\vec{N}(0) - \vec{C}] + \vec{C}$.

By (2.7), $\vec{N}(2\tau) = e^{\underset{\approx}{B}\tau}\vec{N}(\tau_+)$

$$= e^{\underset{\approx}{B}\tau}\underset{\approx}{BPB}^{-1}e^{\underset{\approx}{B}\tau}\vec{N}(0) + e^{\underset{\approx}{B}\tau}(\underset{\approx}{1} - \underset{\approx}{BPB}^{-1})\vec{C}.$$

Putting $$\underset{\approx}{E} = e^{\underset{\approx}{B}\tau}\underset{\approx}{BPB}^{-1}e^{\underset{\approx}{B}\tau}, \tag{2.9}$$

and $$\vec{D} = (\underset{\approx}{1} - \underset{\approx}{BPB}^{-1})\vec{C}, \tag{2.10}$$

$$\vec{N}(2\tau) = \underset{\approx}{E}\vec{N}(0) + e^{\underset{\approx}{B}\tau}\vec{D}.$$

Repeating the same procedure as before for another pulse, we get $\vec{N}(4\tau) = \underset{\approx}{E}^2\vec{N}(0) + (\underset{\approx}{1} + \underset{\approx}{E})e^{\underset{\approx}{B}\tau}\vec{D}$.

Similarly, $\vec{N}(6\tau) = \underset{\approx}{E}^3\vec{N}(0) + (\underset{\approx}{1} + \underset{\approx}{E} + \underset{\approx}{E}^2)e^{\underset{\approx}{B}\tau}\vec{D}$.

Therefore, in general, we have

$$\vec{N}(2n\tau) = \underset{\approx}{E}^n\vec{N}(0) + \frac{\underset{\approx}{1} - \underset{\approx}{E}^n}{\underset{\approx}{1} - \underset{\approx}{E}}e^{\underset{\approx}{B}\tau}\vec{D}. \tag{2.11}$$

But $\vec{M} = \underset{\approx}{B}^{-1}[\vec{N} - \vec{C}]$

therefore $\vec{M}(2n\tau) = \underset{\approx}{B}^{-1}[\vec{N}(2n\tau) - \vec{C}]$.

Simplifying, we get

$$\vec{M}(2n\tau) = \underset{\approx}{F}^n\vec{M}(0) + (\underset{\approx}{1} - \underset{\approx}{F}^n)[\frac{\underset{\approx}{1}}{\underset{\approx}{1} - \underset{\approx}{F}}e^{\underset{\approx}{B}\tau}(\underset{\approx}{1} - \underset{\approx}{P}) - \underset{\approx}{1}]\vec{G} \tag{2.12}$$

where $$\underset{\approx}{F} = e^{\underset{\approx}{B}\tau}\underset{\approx}{P}e^{\underset{\approx}{B}\tau} \tag{2.13}$$

and $$\vec{G} = \underset{\approx}{B}^{-1}\vec{C}. \tag{2.14}$$

The first term in (2.12) gives an approximately exponential decay of $\vec{M}$ while the second term is a correction arising from the T_1 asymmetry associated with the rotary spin echoes.

This correction oscillates in magnitude, being larger for the odd echoes.

In the usual spin-echo case, the magnetization vectors have axial symmetry along the z-direction about which they precess. In the case of rotary spin echoes, symmetry along the x-axis about which the magnetization vectors precess is destroyed by T_1 relaxation towards the z-direction. The effect of this T_1 asymmetry is shown pictorially in Fig. 2-1. Analytically, the T_1 asymmetry makes the equation (2.1) inhomogeneous and so is there the second non-exponential term in (2.12). However, if T_1 is extremely long or, $\omega_1 >> \frac{1}{T_1}$ the second term drops off or is negligible to good approximation. So in practice the echo amplitudes decay exponentially as the condition $\omega_1 >> \frac{1}{T_1}$ is generally satisfied. Therefore

$$\vec{M}(2n\tau) = \underset{\approx}{F}^n \vec{M}(0) \tag{2.15}$$

holds to good approximation.

B. Nutational Signals Between Pulses

From equations (2.5) and (2.7)

$$\begin{aligned}\vec{M}(t) &= \underset{\approx}{B}^{-1}[e^{\underset{\approx}{B}t}\{\underset{\approx}{B}\vec{M}(0) + \vec{C}\} - \vec{C}] \\ &= e^{\underset{\approx}{B}t}[\vec{M}(0) + \underset{\approx}{B}^{-1}\vec{C}] - \underset{\approx}{B}^{-1}\vec{C}.\end{aligned} \tag{2.16}$$

Including damping due to inhomogeneous fields

$$\vec{M}(t) = e^{-R't}[e^{\underset{\approx}{B}t}\{\vec{M}(0) + \underset{\approx}{B}^{-1}\vec{C}\} - \underset{\approx}{B}^{-1}\vec{C}]. \tag{2.17}$$

Assuming $R_1 = R_2 = R = \frac{1}{2}(R_1 + R_2)$ and diagonalizing $\underset{\approx}{B}$ in (2.3),

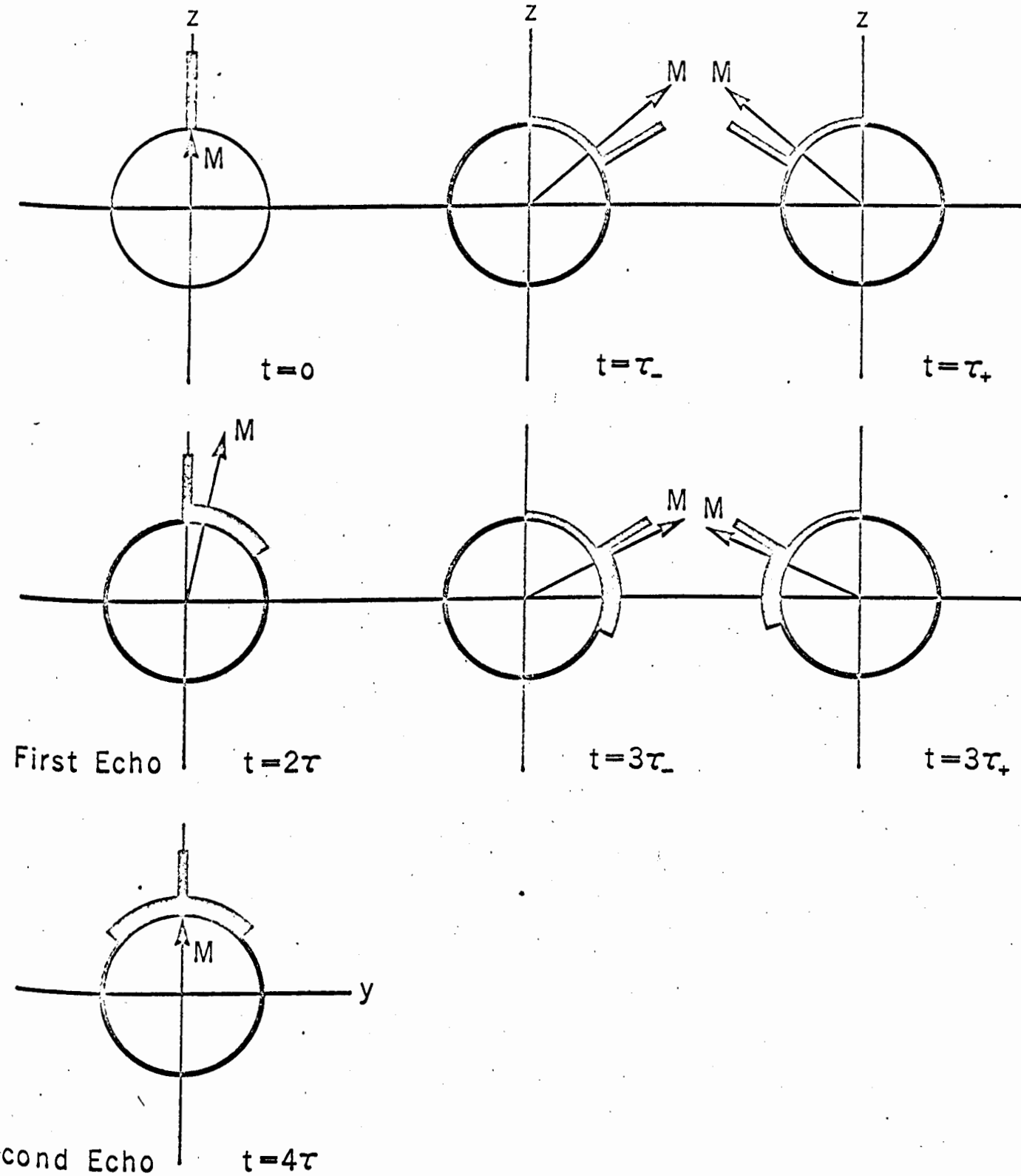

Fig. 2-1. Approximate T_1 effects and its asymmetry in rotary echoes

we get

$$e^{\underset{\approx}{B}t} = \frac{e^{-Rt}}{a^2}\begin{bmatrix} \omega_1^2 + \delta^2\cos at & a\delta\sin at & -\omega_1\delta(1 - \cos at) \\ -a\delta\sin at & a^2\cos at & -a\omega_1\sin at \\ -\omega_1\delta(1 - \cos at) & a\omega_1\sin at & \delta^2 + \omega_1^2\cos at \end{bmatrix} \quad (2.18)$$

where $a^2 = \omega_1^2 + \delta^2$.

Getting the inverse of $\underset{\approx}{B}$ and multiplying to $\vec{C}$ in (2.4), we have

$$\underset{\approx}{B}^{-1}\vec{C} = \frac{M_o}{R^2 + a^2}\begin{bmatrix} \omega_1\delta \\ R\omega_1 \\ -(R^2 + \delta^2) \end{bmatrix} . \quad (2.19)$$

Using equations (2.17)-(2.19) and that $\vec{M}(0) = \begin{bmatrix} 0 \\ 0 \\ M_o \end{bmatrix}$, we get, before any pulse is applied,

$$u(t) = e^{-R't}[\frac{e^{-Rt}}{a}(\delta R\omega_1\sin at + a\delta\omega_1\cos at) - \delta\omega_1]\frac{M_o}{R^2 + a^2} \quad (2.20)$$

$$v(t) = e^{-R't}[e^{-Rt}(R\omega_1\cos at - a\omega_1\sin at) - R\omega_1]\frac{M_o}{R^2 + a^2} \quad (2.21)$$

$$M_z(t) = e^{-R't}[\frac{e^{-Rt}}{a}(R\omega_1^2\sin at + a\omega_1^2\cos at) + R^2 + \delta^2]\frac{M_o}{R^2 + a^2} . \quad (2.22)$$

For $\delta = 0$, equations (2.20)-(2.22) reduce to

$$u(t) = 0, \quad (2.23)$$

$$v(t) = e^{-R't}[e^{-Rt}(R\omega_1\cos\omega_1 t - \omega_1^2\sin\omega_1 t) - R\omega_1]\frac{M_o}{R^2 + \omega_1^2}, \quad (2.24)$$

$$M_z(t) = e^{-R't}[e^{-Rt}(R\omega_1\sin\omega_1 t + \omega_1^2\cos\omega_1 t) + R^2]\frac{M_o}{R^2 + \omega_1^2}. \quad (2.25)$$

If $R \ll \omega_1$, the equations further reduce to

$$u(t) = 0, \quad (2.26)$$

$$v(t) \approx -e^{-R't}\cdot e^{-Rt}M_o\sin\omega_1 t , \quad (2.27)$$

$$M_z(t) \approx e^{-R't}\cdot e^{-Rt}M_o\cos\omega_1 t . \quad (2.28)$$

If $R << \omega_1 << \delta$, equations (2.20)-(2.22) become

$$u(t) \approx e^{-R't}\frac{\omega_1}{a}M_o(e^{-Rt}\cos at - 1), \tag{2.29}$$

$$v(t) \approx e^{-R't}.e^{-Rt}\frac{\omega_1}{a}M_o \sin at\ , \tag{2.30}$$

$$M_z(t) \approx e^{-R't}M_o\ . \tag{2.31}$$

Adding (2.27) and (2.30) together

$$v(t) \approx e^{-(R'+R)t}(M_o^{on}\sin\omega_1 t + \frac{\omega_1}{a}M_o^{off}\sin at) \tag{2.32}$$

gives the nutational signal due to one on-resonance and one far-off-resonance magnetization. This signal consists of the usual damped sine waves of frequency ω_1, modulated by high-frequency oscillations of much smaller amplitudes.

Referring to Fig. 2-2, we notice that, between pulses in a sequence, the nutational signals resemble each other in alternate periods of duration τ in the on-resonance case.

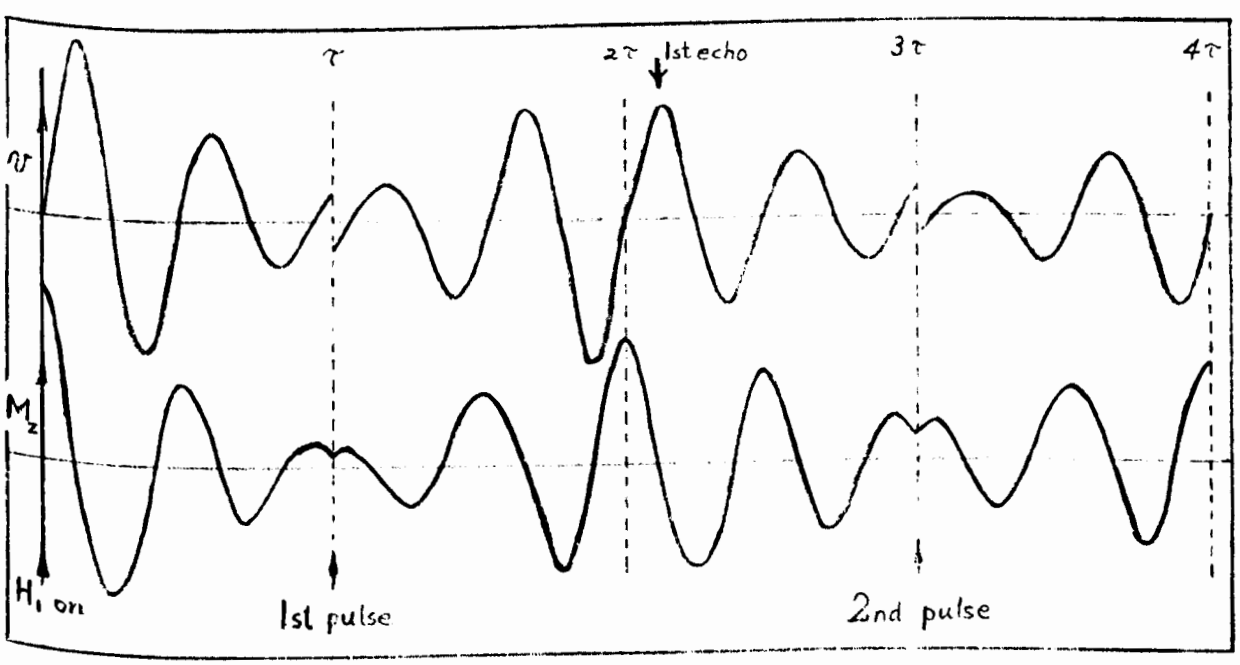

Fig. 2-2. Nutational signals between pulses.

Therefore, from equations (2.27) and (2.28), for periods before each pulse

$$v(t) \approx -e^{-R^*t}M_o \sin\omega_1(t - 2n\tau), \tag{2.33}$$

$$M_z(t) \approx e^{-R^*t}M_o \cos\omega_1(t - 2n\tau) \tag{2.34}$$

where $R^* = R' + R$ and t is between $2n\tau$ and $(2n + 1)\tau$.

For periods after each pulse

$$v(t) \approx e^{-R^*t}M_o \sin\omega_1[2(n + 1)\tau - t], \tag{2.35}$$

$$M_z(t) \approx e^{-R^*t}M_o \cos\omega_1[2(n + 1)\tau - t] \tag{2.36}$$

and t is between $(2n + 1)\tau$ and $2(n + 1)\tau$.

In the off-resonance case, the magnetization vector after a pulse does not precess in the same cone as before; so there is no simple general expression available. But if the dc pulse is applied in such a way that the same cone of precession is followed after each pulse, the same treatment as in the on-resonance case can be applied. In this latter case the pulse changes the sign of y leaving those of x and z unchanged, and the angle of rotation about the z-axis during the pulse duration is smaller than 180°.

C. On- and Off-Resonance Cases

(a) On resonance, $\delta = 0$

$$\text{The matrix } \underset{\approx}{B} = \begin{bmatrix} -R_2 & 0 & 0 \\ 0 & -R_2 & -\omega_1 \\ 0 & \omega_1 & -R_1 \end{bmatrix} . \tag{2.37}$$

If $R_1 = R_2 = R = \frac{1}{2}(R_1 + R_2)$, $\underset{\approx}{B}$ can be diagonalized easily. And

as obtained according to (2.13)

$$\underset{\approx}{F} = e^{-2R\tau}\underset{\approx}{P}\ , \tag{2.38}$$

$$\underset{\approx}{F}^n = e^{-2nR\tau}\underset{\approx}{P} \quad \text{for n odd} \tag{2.39}$$

$$\text{or } e^{-2nR\tau}\underset{\approx}{I} \quad \text{for n even} \tag{2.40}$$

where $\underset{\approx}{I}$ is the identity or unit matrix.

Thus in general, the even echo amplitudes and the odd echo amplitudes each decay exponentially with a rate equal to the mean relaxation rate as was obtained by Torrey (10). The factor $\underset{\approx}{P}$ in the expression on the right hand side of (2.39) for n odd results from the use of a cycle of pulses of order two, and is analogous to the result in the Carr-Purcell experiment (19). In the following, we assume $R_1 = R_2$ unless explicitly taken otherwise owing to nuclear transfer effects, so that the odd echo amplitude progression coincides with the even echo amplitude progression and the decay is exponential for all echoes.

(b) Off resonance, $\delta \neq 0$

For $R_1 = R_2 = R = \frac{1}{2}(R_1 + R_2)$, diagonalization of the matrix

$$\underset{\approx}{B} = \begin{bmatrix} -R & \delta & 0 \\ -\delta & -R & -\omega_1 \\ 0 & \omega_1 & -R \end{bmatrix} \tag{2.41}$$

enables one to get $\underset{\approx}{F}$. And as obtained according to (2.13),

$$\underset{\approx}{F} = \frac{e^{-2R\tau}}{a^4}\begin{bmatrix} \delta^2\{2\omega_1^2(1-\cos a\tau)+\delta^2(1-\cos^2 a\tau)\}-\omega_1^4 & -2a\delta\sin a\tau(\omega_1^2+\delta^2\cos a\tau) & 2\delta\omega_1(1-\cos a\tau)(\omega_1^2+\delta^2\cos a\tau) \\ 2a\delta\sin a\tau(\omega_1^2+\delta^2\cos a\tau) & a^2(2\delta^2\sin^2 a\tau - a^2) & -2a\delta^2\omega_1\sin a\tau(1-\cos a\tau) \\ 2\delta\omega_1(1-\cos a\tau)(\omega_1^2+\delta^2\cos a\tau) & 2a\delta^2\omega_1\sin a\tau(1-\cos a\tau) & \delta^4+\omega_1^4+2\delta^2\omega_1^2\cos a\tau(2-\cos a\tau) \end{bmatrix} \tag{2.42}$$

where $a = (\omega_1^2 + \delta^2)^{\frac{1}{2}}$.

From (2.42) one can hardly see how the echo magnetization $\vec{M}(2n\tau)$ decays because of its complexity but empirically the echo amplitude decays away very rapidly for δ large as the H_o inhomogeneity begins to come into play on top of that of H_1 and the pulses are ineffective in refocussing under such conditions.

D. Effects of the H_o Inhomogeneities

Normally in high-resolution NMR experiments on spin $\frac{1}{2}$ nuclei, the observed linewidth is determined predominantly by the magnet inhomogeneity and the distribution in observed resonance frequencies reflects the distribution of the static field H_o across the active volume of the sample. That a resonance signal has a finite linewidth means that the experimental decay rate R_{exp} is, to an extent, greater than the theoretical decay rate R_{2r} obtained by considering a hypothetical signal represented by a δ-function at the Larmor frequency $\omega_o = \gamma H_o$. The correction necessary to account for this influence on the observed decay rate down the rotary-echo sequence can be obtained in the following treatment.

For $\omega_1 >> R_1$, from equation (2.15)

$$\vec{M}(2n\tau) = \underset{\approx}{F}^n \vec{M}(0) \qquad (2.15)$$

where $\underset{\approx}{F} = \underset{\approx}{F}(\delta, \omega_1)$ is a function of the two independent variables δ and ω_1 and is given by (2.42). For a given value of ω_1, $\underset{\approx}{F}$ is thus a function of δ only. So equation (2.42) reduces to (2.38) when $\delta = 0$. Let us consider the difference in magnetization

between the on-resonance and off-resonance cases at the first and nth echoes for a given value of ω_1.

$$\Delta\vec{M}_1 = \vec{M}_o(2\tau) - \vec{M}_\delta(2\tau) = (\underset{\approx}{F}_o - \underset{\approx}{F}_\delta)\vec{M}(0).$$

$$\begin{aligned}\Delta\vec{M}_n &= \vec{M}_o(2n\tau) - \vec{M}_\delta(2n\tau) = (\underset{\approx}{F}_o{}^n - \underset{\approx}{F}_\delta{}^n)\vec{M}(0) \\ &= (\underset{\approx}{F}_o - \underset{\approx}{F}_\delta)(\underset{\approx}{F}_o{}^{n-1} + \underset{\approx}{F}_o{}^{n-2}\underset{\approx}{F}_\delta + \ldots + \underset{\approx}{F}_\delta{}^{n-1})\vec{M}(0) \\ &\approx n\underset{\approx}{F}_o{}^{n-1}\Delta\vec{M}_1 \qquad (2.43)\end{aligned}$$

assuming $\underset{\approx}{F}_o \approx \underset{\approx}{F}_\delta$ for $\delta/\omega_1 \ll 1$ and thus $\underset{\approx}{F}_o$ commutes with $\underset{\approx}{F}_\delta$. The subscripts o and δ refer to the on- and off-resonance cases respectively. Using (2.38) and (2.42) and that

$$\vec{M}(0) = \begin{bmatrix} 0 \\ 0 \\ M_o \end{bmatrix},$$

$$\begin{aligned}\Delta\vec{M}_n &= n\underset{\approx}{F}_o{}^{n-1}\Delta\vec{M}_1 \\ &= n\underset{\approx}{F}_o{}^{n-1}\,\frac{2\delta\omega_1}{a^4}\begin{bmatrix} -(1 - \cos a\tau)(\omega_1{}^2 + \delta^2\cos a\tau) \\ a\delta\sin a\tau(1 - \cos a\tau) \\ \delta\omega_1\{1 - \cos a\tau(2 - \cos a\tau)\} \end{bmatrix}.\end{aligned} \qquad (2.44)$$

For a rectangular line shape of full width $2\Delta\omega_{\frac{1}{2}}$, the mean error can be calculated as follows:

$$\overline{\Delta\underset{\sim}{M}_n} = n\underset{\approx}{F}_o{}^{n-1}\overline{\Delta\underset{\sim}{M}_1} \qquad (2.45)$$

where

$$\overline{\Delta\underset{\sim}{M}_1} = \frac{1}{2\Delta\omega_{\frac{1}{2}}}\int_{-\Delta\omega_{\frac{1}{2}}}^{\Delta\omega_{\frac{1}{2}}} \Delta\vec{M}_1(\delta)\,d\delta \quad . \qquad (2.46)$$

Integrating for only the M_z component, the component necessary

in the correction calculation, we have

$$\overline{\Delta M_{z\,n}} = nM_o e^{-2nR\tau}\left[\tfrac{2}{3}\beta^2 + \frac{2(\omega_1\tau - 2)}{5}\beta^4 + \frac{\omega_1^2\tau^2 - 8\omega_1\tau}{14}\beta^6 + \ldots\right] \tag{2.47}$$

where $\beta = \Delta\omega_{\frac{1}{2}}/\omega_1$, usually $\ll 1$

and the condition $\cos\omega_1\tau = 0$ has been imposed to get the upper bound of $\overline{\Delta M_{z\,n}}$.

From equation (2.47) and that

$$M_{z\,o}(2n\tau) = M_o e^{-2nR\tau},$$

the relative error

$$\frac{\overline{\Delta M_{z\,n}}}{M_{z\,o}(2n\tau)} = n\left[\tfrac{2}{3}\beta^2 + \frac{2(\omega_1\tau - 2)}{5}\beta^4 + \frac{\omega_1^2\tau^2 - 8\omega_1\tau}{14}\beta^6 + \ldots\right]. \tag{2.48}$$

Neglecting terms with higher order in β than the second,

$$\frac{\overline{\Delta M_{z\,n}}}{M_{z\,o}(2n\tau)} \approx \tfrac{2}{3}\beta^2 n. \tag{2.49}$$

Therefore $$M_{z\,\delta}(2n\tau) \approx (1 - \tfrac{2}{3}\beta^2 n)M_{z\,o}(2n\tau)$$
$$= (1 - \frac{\beta^2}{3\tau}t)M_{z\,o}(2n\tau) \tag{2.50}$$

where $t = 2n\tau$.

Since $$\frac{\beta^2}{3\tau}t \ll 1,$$

$$1 - \frac{\beta^2}{3\tau}t \approx \exp(-\frac{\beta^2}{3\tau}t).$$

Therefore $$M_{z\,\delta}(2n\tau) \approx \exp(-\frac{\beta^2}{3\tau}t)[e^{-R_{2r}t}M_{z\,o}(0)]$$
$$= e^{-R_{exp}t}M_{z\,o}(0), \tag{2.51}$$

and $$R_{exp} = R_{2r} + \frac{\beta^2}{3\tau}. \tag{2.52}$$

This correction $\frac{\beta^2}{3\tau}$ can be made negligible by choosing H_1 sufficiently large, i.e. $H_1 \gg \Delta H_o$.

Some experimental decay rates of the rotary-echo amplitudes in degassed benzene with and without the sample spinning are shown in Table I. The results show that the effect of inhomogeneities in H_o can safely be neglected under ordinary experimental conditions.

Table I. R_{2r} in spinning and non-spinning samples of degassed benzene, $\omega_1 = 10$ hz.

2τ (sec)	$(R_{2r})_n$ Non-Spinning Sample	$(R_{2r})_s$ Spinning Sample	$(R_{2r})_n - (R_{2r})_s$
0.5	0.0862 sec^{-1}	0.0827 sec^{-1}	0.0035 sec^{-1}
0.63	0.0956 sec^{-1}	0.0928 sec^{-1}	0.0028 sec^{-1}

E. Nuclear Overhauser Effect

Overhauser effect in metals (20) arises from the coupling $\vec{I}\cdot\vec{S}$ of the nuclear and electron spins through the longitudinal relaxation mechanism of the S-spins. The pure nuclear analogue of the effect has also been observed in heteronuclear systems by Solomon (21) and by Solomon and Bloembergen (22). If an experimental method is selective enough, such an effect should also be detected among homonuclear systems. The recent works of Kaiser (23), Cocivera (24) and Brooks et al (25) provide enough evidences for this.

For systems containing more than one magnetic nuclear species or more than one group of magnetically equivalent nuclei of the same species, scalar interaction $J\vec{I}_a\cdot\vec{I}_b$ as well as

intermolecular and intramolecular dipole-dipole interactions give rise to cross relaxation in the longitudinal magnetization (21) of the nuclear spins. So for a two-spin system, Bloch's equations for the M_z components are modified to:

$$\frac{dM_{za}}{dt} = -R_{1a}(M_{za} - M_{0a}) - \sigma(M_{zb} - M_{0b}) \qquad (2.53)$$

$$\frac{dM_{zb}}{dt} = -R_{1b}(M_{zb} - M_{0b}) - \sigma(M_{za} - M_{0a}) \qquad (2.54)$$

where R_{1a} and R_{1b} are the conventional longitudinal relaxation rates for the spins A and B respectively and σ is the so-called cross relaxation rate.

To include this nuclear Overhauser effect, let us assume that a rotary-echo experiment be performed on a homonuclear system whose high-resolution spectrum consists of two lines separated by δ. Sitting exactly on resonance at one signal, if δ is sufficiently larger than γH_1, the effect of H_1 on the other is negligible apart from the nuclear Overhauser effect. Then the modified Bloch's equations for the systems are

$$\begin{aligned}
\frac{du}{dt} &= -Ru \\
\frac{dv}{dt} &= -Rv - \omega_1 M_z \\
\frac{dM_z}{dt} &= \omega_1 v - RM_z - \sigma M_z' + RM_0 + \sigma M'_0 \\
\frac{dM_z'}{dt} &= -\sigma M_z - RM_z' + \sigma M_0 + RM'_0
\end{aligned} \qquad (2.55)$$

where the longitudinal and transverse relaxation rates are assumed to be all equal to R, and again the cross relaxation rate is denoted by σ.

In matrix notation, the coefficient $\underset{\approx}{B}$ is given by

$$\underset{\approx}{B} = \begin{bmatrix} -R & 0 & 0 & 0 \\ 0 & -R & -\omega_1 & 0 \\ 0 & \omega_1 & -R & -\sigma \\ 0 & 0 & -\sigma & -R \end{bmatrix}$$

The off-diagonal elements are ω_1 and σ. σ, being usually smaller than R, is of course much smaller than ω_1. Neglecting σ in the array, the matrix can be broken down to a 2 X 2 matrix

$$\begin{bmatrix} -R & -\omega_1 \\ \omega_1 & -R \end{bmatrix}$$

as in the case excluding nuclear Overhauser effect (see page 30). Thus for $\omega_1 >> \sigma$, rotary-echo decays are not affected by the nuclear Overhauser effect to first order.

CHAPTER III

CHEMICAL EXCHANGE STUDIES

The hindered internal rotation about the C-N bond in N,N-dimethylcarbamyl chloride and the N-N bond in N,N-dimethylnitrosamine was studied at various temperatures by the high-resolution rotary-echo method.

A. Hindered Internal Rotation

According to the resonance theory (26), the C-N bond in amides, the N-N bond in nitrosamines and the O-N bond in nitrites can assume double bond character owing to resonance forms of the type

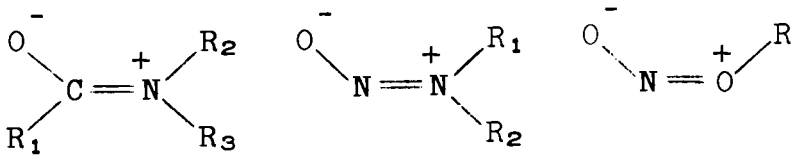

The partial double bond character imparts a planar configuration to such systems and the barrier to internal rotation may be quite high but usually not so high that the cis and trans isomers can be separated by physical methods. Without the necessity of separating the isomers, the NMR technique provides a convenient method to study compounds of such types. In fact, there have been many publications on the application of NMR methods to the study of hindered internal rotation (27).

Because of the variations in the method of experimentation and evaluation of data, discrepancies in various activation par-

ameters reported by independent workers for the same chemical system are great. For N,N-dimethylcarbamyl chloride the steady-state results of Rogers and Woodbrey (28) and of Allerhand and Gutowsky (3) are low in both the activation energy and the frequency factor. Using the spin-echo method aided by a high speed computer, Allerhand and Gutowsky (3) and Krakower (29) produce independently more promising results. Recently, Neuman, Roark and Jonas (30) perform a detailed kinetic study of the system using the computerised total line-shape fitting method. They obtain 16.9 ± 0.5 kcal/mole for the activation energy and a value of -1.6 eu for the entropy of activation. N,N-dimethylnitrosamine has been studied independently by Phillips (31) and Blears (32) using the steady-state NMR method. The reported activation parameters are in reasonably good agreement to the spin-echo values obtained by Abramson et al (33) and Krakower (29). In general, the factors affecting the accuracy of the various NMR methods in the determination of chemical exchange rates are analyzed and discussed in a recent work by Allerhand, Gutowsky, Jonas and Meinzer (34).

B. Exchange Effects in High-Resolution Rotary Echoes

Consider a system in which a nuclear spin is reversibly transferred between two non-equivalent sites A and B uncoupled to each other.

(a) Slow exchange

In the slow exchange region, two distinct signals exist. Sitting on resonance at signal A and off resonance from signal B by $\delta = \omega_a - \omega_b$, the modified Bloch equations as generalized by Hahn and Maxwell (35) and McConnell (36) can be written as

$$\frac{d}{dt}\begin{bmatrix} u_a \\ v_a \\ M_{za} \\ u_b \\ v_b \\ M_{zb} \end{bmatrix} = \begin{bmatrix} -R_{2a}-k_a & 0 & 0 & k_b & 0 & 0 \\ 0 & -R_{2a}-k_a & -\omega_1 & 0 & k_b & 0 \\ 0 & \omega_1 & -R_{1a}-k_a & 0 & 0 & k_b-\sigma \\ k_a & 0 & 0 & -R_{2b}-k_b & \delta & 0 \\ 0 & k_a & 0 & -\delta & -R_{2b}-k_b & -\omega_1 \\ 0 & 0 & k_a-\sigma & 0 & \omega_1 & -R_{1b}-k_b \end{bmatrix} \begin{bmatrix} u_a \\ v_a \\ M_{za} \\ u_b \\ v_b \\ M_{zb} \end{bmatrix} + \begin{bmatrix} 0 \\ 0 \\ R_{1a}M_{oa}+\sigma M_{ob} \\ 0 \\ 0 \\ \sigma M_{oa}+R_{1b}M_{ob} \end{bmatrix} \tag{3.1}$$

where k_a and k_b are the exchange rates out of the sites A and B respectively. The cross relaxation between M_{za} and M_{zb} is included to account for the nuclear Overhauser effect.

Assuming $R_{1a} = R_{1b} = R_{2a} = R_{2b} = R$, $k_a = k_b = k$ and $M_{oa} = M_{ob} = M_o$, (3.2)

the matrix $\underset{\approx}{B} = \begin{bmatrix} -R-k & 0 & 0 & k & 0 & 0 \\ 0 & -R-k & -\omega_1 & 0 & k & 0 \\ 0 & \omega_1 & -R-k & 0 & 0 & k-\sigma \\ k & 0 & 0 & -R-k & \delta & 0 \\ 0 & k & 0 & -\delta & -R-k & -\omega_1 \\ 0 & 0 & k-\sigma & 0 & \omega_1 & -R-k \end{bmatrix}$. (3.3)

Here σ is generally smaller than R and is usually smaller than k except for extremely slow exchange. Its being far off the diagonal makes it justifiable to neglect it along with the off-diagonal k's in the slow exchange limit. With the off-diagonal

k's and σ neglected, the $\underset{\approx}{B}$ matrix can be partitioned into the on-resonance and off-resonance parts.

Now two cases arise. If signal B is very far from resonance, i.e. $\delta >> \omega_1$, the 180° pulses have no refocussing effect on the fanning out magnetization vectors at site B. So the signal B decays rapidly in the rotating frame and has no contribution to the subsequent echoes. Thus only the resonant part of the matrix need be considered. Solution for the on-resonance case leads to a rotary-echo decay rate R_{2r} given by

$$R_{2r} = \frac{1}{2}(R_1 + R_2) + k \qquad (3.4)$$

The term k on the right hand side of equation (3.4) means that the signal A loses magnetization each time a nuclear spin transfers out of site A and does not regain magnetization from site B because the net contribution from the spins transferred back from site B is averaged out to zero. Thus the contribution of k to this decay differs from the contribution to the steady-state linewidth as calculated by Piette and Anderson (37).

If signal B is not very far from resonance, i.e. $\delta \lesssim \omega_1$, both signals A and B contribute to the echo amplitudes, and the situation is complicated as the off-resonance matrix is hard to handle. Considering the situation phenomenologically, the average fractional loss of magnetization as a result of a transfer from one site to another is found (Appendix A) to be $\sin^2\frac{\alpha}{2}$, where $\alpha = \tan^{-1}(\frac{\delta}{\omega_1})$. Thus in the slow exchange region and for

$$\delta \lesssim \omega_1$$

$$R_{2r} = \frac{1}{2}(R_1 + R_2) + (\sin^2\frac{\alpha}{2})k. \qquad (3.5)$$

(b) Fast exchange

In the fast exchange region, only one signal exists and it appears at the first moment of the individual site precession frequencies. On resonance at this signal and with the same notations and assumptions as above, the matrix $\underset{\approx}{B}$ can be written as

$$\begin{bmatrix} -R-k & -\frac{\delta}{2} & 0 & k & 0 & 0 \\ \frac{\delta}{2} & -R-k & -\omega_1 & 0 & k & 0 \\ 0 & \omega_1 & -R-k & 0 & 0 & k-\sigma \\ k & 0 & 0 & -R-k & \frac{\delta}{2} & 0 \\ 0 & k & 0 & -\frac{\delta}{2} & -R-k & -\omega_1 \\ 0 & 0 & k-\sigma & 0 & \omega_1 & -R-k \end{bmatrix}.$$

In fast exchange, σ is negligible compared with k, i.e. $k-\sigma$ is practically equal to k. So cross relaxation has again no effect here. k being large, the matrix cannot be simplified as in the case of slow exchange. And unfortunately, there is no other justifiable approximation that can be taken. Manipulation with the complete 6 X 6 matrix is beyond possible and no closed formula is obtained. Thus for the calculation of exchange rates in the fast exchange region reported in this work

$$R_{2r} = \frac{1}{2}(R_1 + R_2 + \Delta\omega_{ex}) \qquad (3.7)$$

is used, where $\Delta\omega_{ex}$ is the equilibrium line width* due to exchange

*The line observed is the exchange narrowed component while the broad component is not detected because of its great width in high-resolution steady-state measurements and because it decays away very rapidly in rotary-echo measurements.

in a high-resolution steady-state spectrum. And according to Piette and Anderson (37)

$$k = \frac{1}{8} \frac{\delta^2}{\Delta\omega_{ex}} \qquad (3.8)$$

in the fast exchange region.

The fast exchange case is different from the slow exchange case because the site magnitizations are conserved in the former and not in the latter. The validity of equation (3.8) in calculating exchange rates in this region is justified because of this conservative property and that the k is large and the pulse rate $1/2\tau$ (at sub-audio frequencies) is small. So under such experimental conditions the nuclear spins under observation exchange many times between pulses and the equilibrium linewidth can be approximated as in the long τ limit of the BRW theory (38).

C. Experimental

(a) Preparation of samples

Commercially available N,N-dimethylcarbamyl chloride was purified by several vacuum fractionations. N,N-dimethylnitrosamine was prepared by the reaction of dimethylamine hydrochloride (0.25 mole, 20.5 g.) and sodium nitrite (0.3 mole, 21 g. in 50 ml. of 6N hydrochloric acid solution). The mixture was distilled rapidly to dryness and the distillate was treated with an excess of potassium carbonate. The resulting yellow non-acidic aqueous solution was shaken with 4 portions of ether each 50 ml. The ether extract was dried over freshly baked anhydrous potassium

carbonate. Removal of ether under reduced pressure left a yellow oil. The oil was purified by three successive distillations. The boiling point of the final product was 150-151°C.

The samples used in this investigation were prepared in thick-walled cylindrical glass tubes of bore about 3 mm in diameter. The tube containing the sample was mounted on a high vacuum system and the sample was thoroughly degassed by freezing with liquid nitrogen and then allowing it to warm to room temperature under vacuum. This freeze-pump-thaw procedure was repeated several times and the tube was finally sealed off.

(b) Determination of exchange rates

For each temperature, the decay of the rotary-echo amplitudes was photographed for each of eight pulse separations (2τ = .2, .25, .32, .4, .5, .63, .8 and 1 sec.). Then for each photograph corresponding to a certain pulse separation echo amplitudes were plotted against time. The points lying quite closely on a straight line in a semi-log plot showed that the decay was exponential and the slope of the straight line gave the decay rate for that particular pulse separation. The decay rates depend somewhat on the pulse separation indicating self-diffusion effect, etc. Plotting the decay rates against $(2\tau)^2$, the square of the pulse separation (see page 20), and extrapolating to infinite pulse rate (i.e. $2\tau = 0$), the extrapolated decay rate was taken to be the decay rate $R_{2\tau}$ of the rotary-echo train free

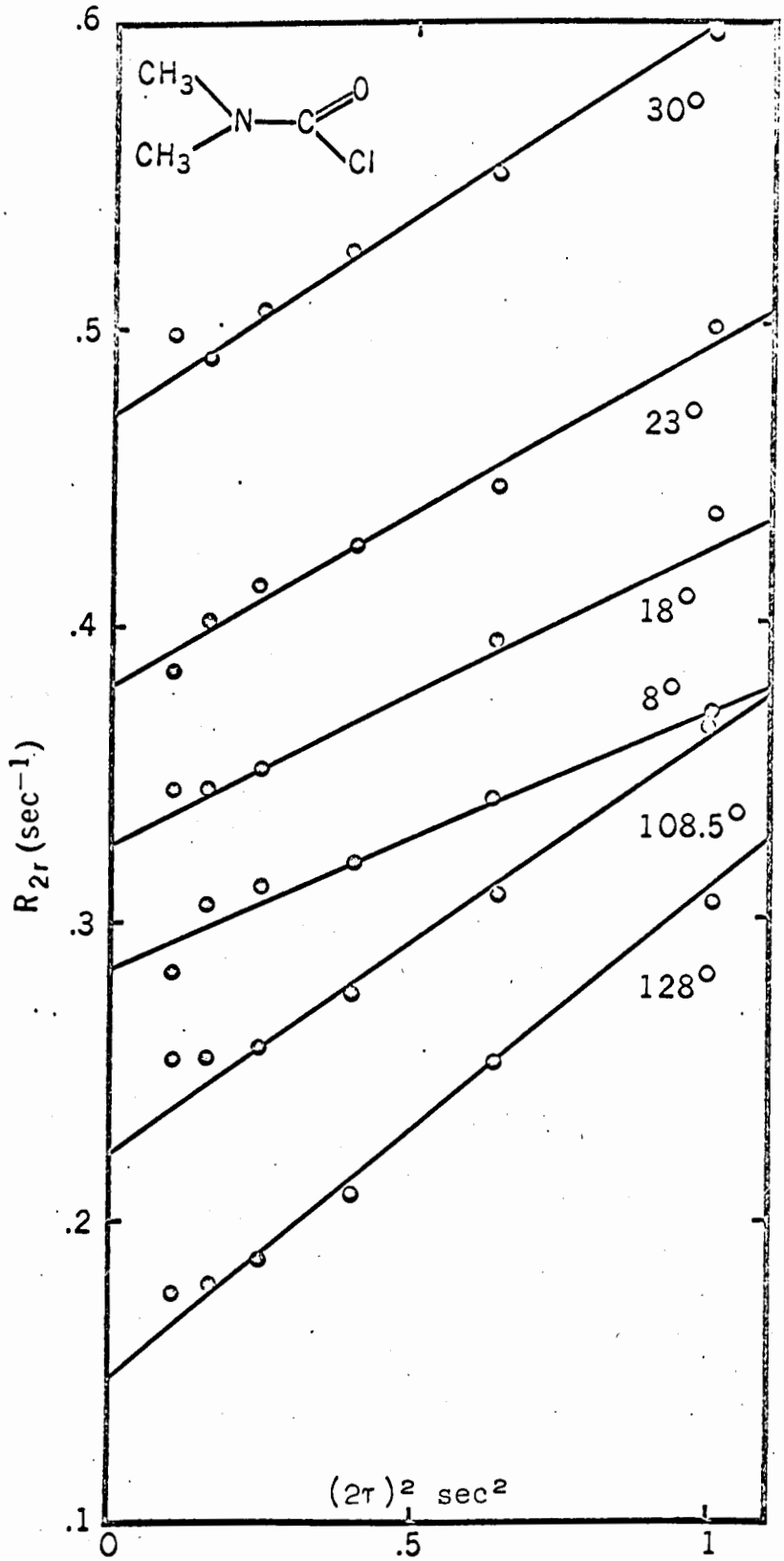

Fig. 3-1. R_{2r} extrapolation plot for N,N-dimethylcarbamyl chloride.

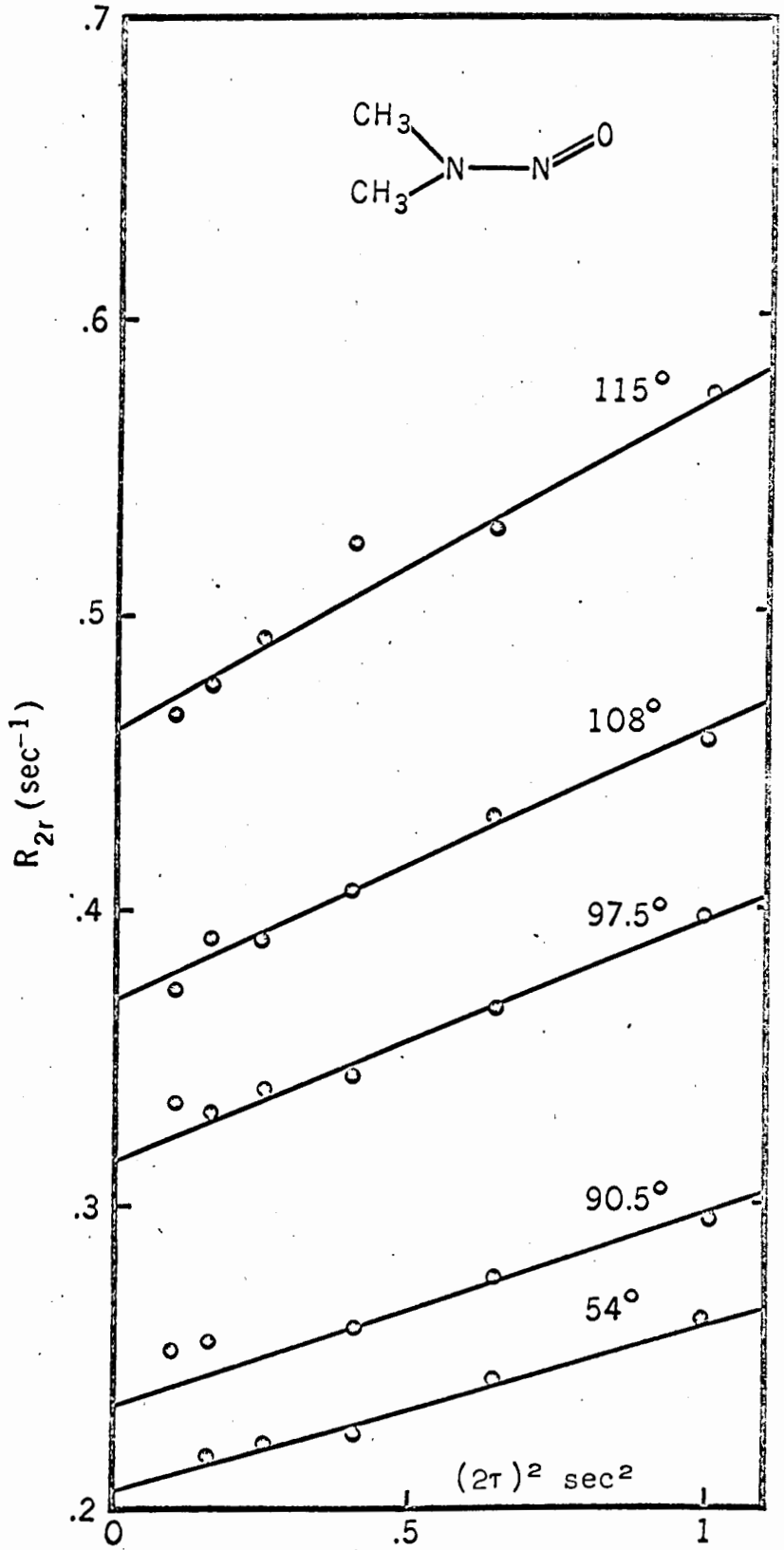

Fig. 3-2. R_{2r} extrapolation plot for N,N-dimethylnitrosamine.

from diffusion effect at a certain temperature. Such extrapolation plots are shown in Figs. 3-1 and 3-2. Slight deviations of points for 2τ small from linear behaviour are presumably due to overlapping of echoes in the train when $\tau < \pi/\omega_1$. Being selective, the rotary-echo method is non-conservative in the magnetization for exchange unlike the spin-echo experiment. Therefore, exchange effects are not pulsed out and, in general, the diffusion extrapolation removes only the effects of diffusion leaving those of the exchange in either the slow or the fast limit unaffected. Then for each temperature, the chemical exchange rate (k) was determined from R_{2r} according to equations (3.4), (3.5) or (3.7) and (3.8) as the case may be. Values of activation energies E_a and frequency factors ν_0 were obtained from the Arrhenius plots,

$$\ln k = \ln \nu_0 - \frac{E_a}{R} \cdot \frac{1}{T} \quad . \tag{3.9}$$

D. Results

(a) N,N-dimethylcarbamyl chloride (DMCC)

T_1 and T_2 values and their temperature dependence for N, N-dimethylcarbamyl chloride were obtained from the published results of Allerhand and Gutowsky (3). The chemical shift between the two methyl resonances was assumed independent of temperature, and the value used in the determination of exchange rate in the fast exchange region for DMCC was our low temperature high-resolution limit of 6.6 hz. The exchange rates at various

Table II. Chemical exchange rates for N,N-dimethylcarbamyl chloride.

Temp. (°C.)	R_{2r}	$\frac{1}{2}(R_1 + R_2)$	k	Remarks
8	.286	.233	.41	
18	.328	.196	1.00	k obtained
23	.380	.182	1.45	according to
27.5	.701	.178	3.49	eqn. (3.5)
30	.472	.170	2.40	
83	.848	.099	130	
92	.525	.094	229	k obtained
108.5	.225	.085	683	according to (3.7) & (3.8)
128	.150	.077	1350	

Table III. Comparison of activation parameters for N,N-dimethylcarbamyl chloride.

Method	E_a ($\frac{kcal}{mole}$)	$\Delta H^{\ddagger}$ ($\frac{kcal}{mole}$) @ 326°K	ν_o	$\Delta S^{\ddagger}$ (eu) @ 326°K	Reference
Rotary-echo	15.1 ± 1.0	14.5	2.70×10^{11}	- 8.1	present
Spin-echo	14.0 ± 0.9	13.4	7.90×10^{10}	-10.5	3
Spin-echo	14.0 ± 0.7	13.4	1.03×10^{11}	-10.3	29
Steady-state (int. ratio)	9.7 ± 0.5	9.1	2.50×10^{7}	-26.8	3
Steady-state (peak sep.)	8.6 ± 1.7	8.0	7.95×10^{6}	-29.0	3
Steady-state (int. ratio)	7.3 ± 0.5	6.7	1.30×10^{6}	-32.6	28
Steady-state (tls fit)	16.9 ± 0.5	16.3	7.95×10^{12}	- 1.6	30

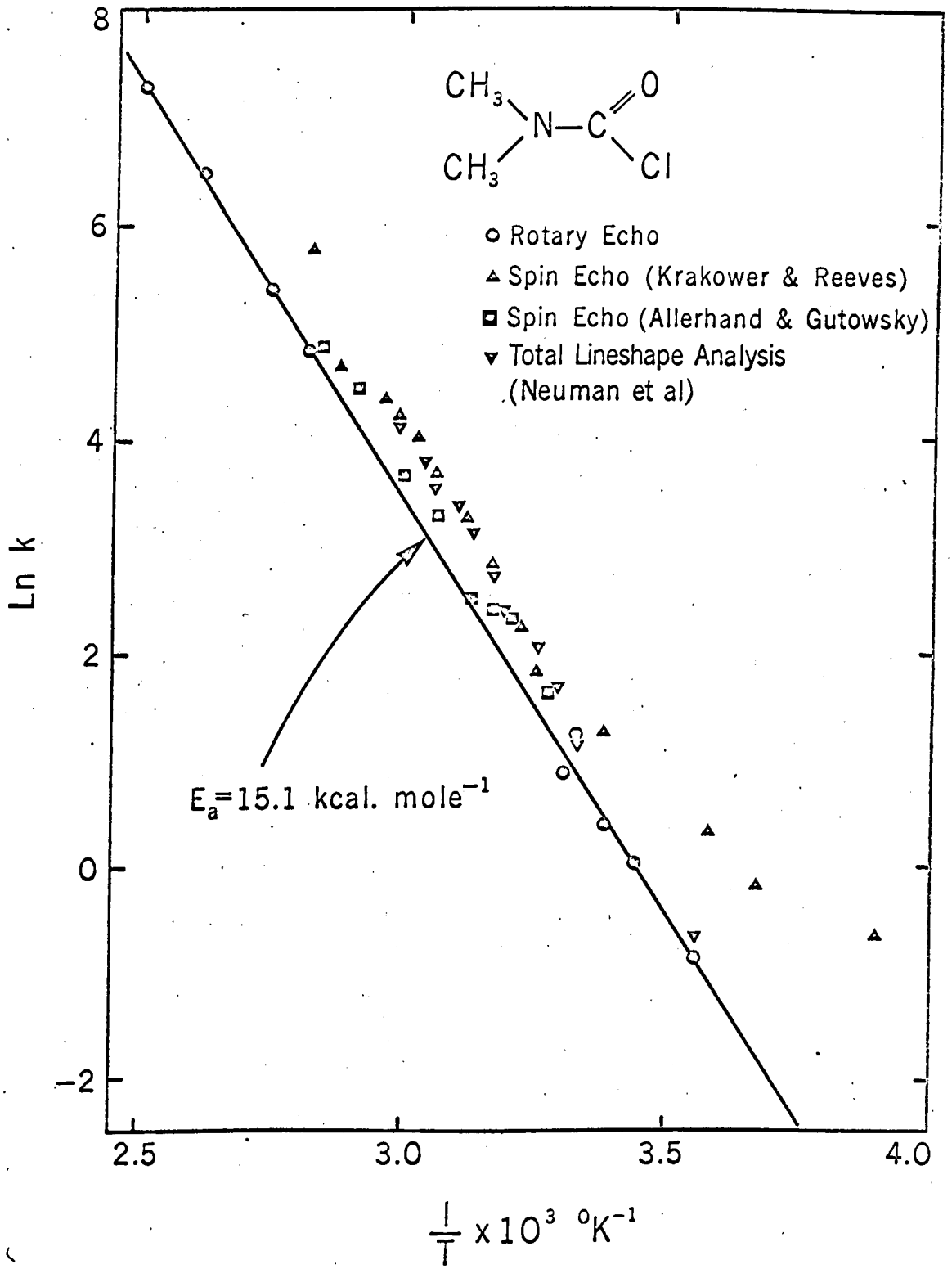

Fig. 3-3. Arrhenius plot for N,N-dimethylcarbamyl chloride.

temperatures were presented in Table II, the Arrhenius plot shown in Fig. 3-3 and the activation parameters listed in Table III.

(b) N,N-dimethylnitrosamine (DMNA)

T_1 was determined by the method of adiabatic passage with sampling (APS) fully described by Anderson (39) and was found to be quite temperature independent within experimental errors, over the temperature range from 54° to 134°C, T_1 = 10 ± 0.7 sec. The temperature independence can be attributed as the result of two effects counteracting each other, namely nuclear relaxation by magnetic dipole-dipole interactions in liquids demanding increase of relaxation times with increasing temperature while the production of small but increasing amounts of paramagnetic nitric oxide in the sample as the temperature is raised speeding up the relaxation (33).

Exchange rate calculated from the R_{2_r}'s assuming T_1 equal to T_2 gave a non-linear Arrhenius plot (Fig. 3-4). The discrepancies, particularly severe for k small were found to be due to differential contribution to the relaxation processes by scalar coupling to a quadrupolar nucleus (see Chapter IV). Correcting for J-coupling ($J_{\underline{H}CN\underline{N}}$ taken to be 1.24 hz and T_{1_N}, 5 msec.) the exchange rates were re-determined. The exchange rates at various temperatures in both cases were presented in Table IV, the Arrhenius plot shown in Fig. 3-4 and activation parameters listed in Table V.

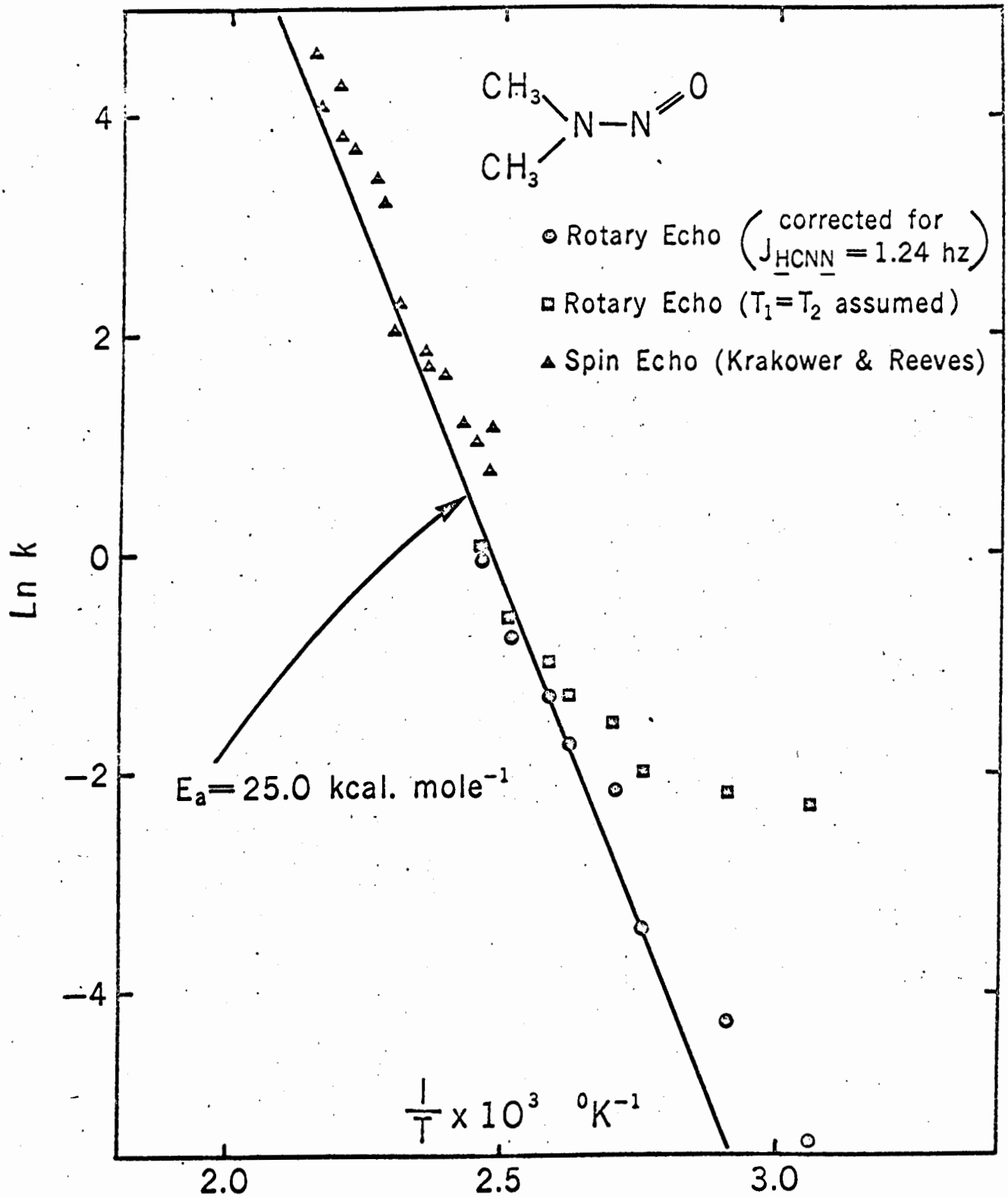

Fig. 3-4. Arrhenius plot for N,N-dimethylnitrosamine.

Table IV. Chemical exchange rates for N,N-dimethylnitrosamine.

Temp. (°C)	R_{2r}	k^*, $T_1=T_2$ assumed	k^*, corrected for J-coupling
54	.205	.105	.005
71	.214	.114	.014
90.5	.234	.134	.034
97.5	.315	.215	.115
108	.370	.270	.170
115	.461	.361	.261
126	.641	.541	.441
134	1.105	1.005	.905

*Obtained according to equation (3.4).

Table V. Comparison of activation parameters for N,N-dimethylnitrosamine

Method	E_a $(\frac{kcal}{mole})$	$\Delta H^{\ddagger}$ $(\frac{kcal}{mole})$ @ 463°K	ν_o	$\Delta S^{\ddagger}$ (eu) @ 463°K	Reference
Rotary-echo	25.0 ± 2.5	24.1	2.99×10^{13}	0.25	present
Spin-echo (off res.)	22.9 ± 1.7	22.0	6.04×10^{12}	- 3.92	33
Spin-echo (on res.)	21.9 ± 1.6	21.0	1.00×10^{12}	- 2.93	33
Spin-echo (off res)	19.7 ± 3.4	18.8	1.13×10^{11}	-10.9	29
Spin-echo (on res.)	25.5 ± 2.5	24.6	1.20×10^{14}	1.04	29
Steady-state (peak sep.)	23.0	22.1	0.70×10^{13}	- 2.85	31
Steady-state (int. ratio)	25.0 ± 5.0	24.1	1.60×10^{11}	-10.1	32

E. Discussion

It so happens that the two systems chosen in the present chemical exchange studies contain nuclei possessing quadrupole moments in the molecules apart from the protons of interest. Due to rapid relaxation of the chlorine and nitrogen nuclei in DMCC and of the nitrogen nuclei in DMNA by interaction of the quadrupolar moments with the electric field gradients in non-shperically symmetric environments, the indirect scalar coupling of the quadrupolar nuclei to the protons is not resolved. But under such conditions the quadrupolar nuclei usually provide a relaxation mechanism for the protons, known as scalar relaxation of the second type (40). It is observed that if the scalar relaxation contribution is sufficiently large it shows up in the rotary-echo decay rate R_{2r} (see Chapter IV).

In DMCC, such an effect is not detected in the rotary-echo measurements. This is not unexpected because the coupling constants between the protons and the quadrupolar nuclei are small and the relaxation times of the quadrupolar nuclei short. While the J_{HN}'s and T_{1N}'s for similar compounds are of magnitude about 0 to 0.5 hz (41) and 1 msec (42) respectively, the J_{HCl} between the protons and chlorine four bonds apart is practically zero and T_{1Cl}, for similar compounds are of magnitude about 10 to 100 μsec (43).

In DMNA the nitrogen nucleus α to the methyl groups has similar small J_{HN} and T_{1N} as in DMCC and gives negligible scalar relaxation as expected. However, the β-nitrogen is usually

comparatively more strongly coupled to the protons, $J_{\underline{HCC}\underline{N}}$ about 1.1 to 1.4 hz (41), and has relatively long T_{1N}, 4 to 6 msec (42). By a method of trial and error to obtain a best fit to theoretical results, values of 1.24 hz and 5 msec are obtained for the $J_{\underline{HCN}\underline{N}}$ and T_{1N} of the β-nitrogen. These correspond to an effect of 0.1 sec^{-1} in the rotary-echo decay rate. The temperature dependence of T_{1N} through an assumed activation process on the reorientational correlation time $\tau_2 = (\tau_2)_o e^{\epsilon/RT}$, $\epsilon \approx 2$ kcal $mole^{-1}$, is found to be of little significance here and is neglected in the calculation. On the same basis, the effect due to coupling to the α-nitrogen is more than an order of magnitude smaller and is not important in the experiment.

In the present study of hindered internal rotation the rotary-echo results are closely comparable to those of the spin-echo experiments (see Tables III and V). The smaller absolute values of $\Delta S^{\ddagger}$ obtained here for both the systems, DMCC and DMNA reflect that the activation parameters thus obtained are closer to their true values as the entropy of activation $\Delta S^{\ddagger}$ for the transition over the barrier hindering internal rotation should be around zero since there is little change in the degree of randomness in the activated complex.

The NMR methods which have thus far been applied to determine rate constants are i) the high-resolution steady-state methods (27), ii) the high-resolution multiple resonance methods (44, 45) and iii) the spin-echo methods (3, 19, 33, 38, 46-52).

A general limitation of the steady-state methods is that they are sensitive only for processes in which the exchange rate is comparable with the splitting, in radians/sec, being averaged out. Once the exchange narrowed limit of a single sharp line has been approached, further increases in rate do not affect the usual high-resolution steady-state spectrum appreciably. The method of total line shape fitting by high speed computers is not free from this limitation. Another drawback of the steady-state method is that the chemical shift has to be known in order to determine the exchange rate. The chemical shift is usually obtained by 'freezing out' the exchange either by making measurements on each species in the absence of the other, in dilute solution, or by going down to temperatures sufficiently low so that the effect of exchange on the chemical shift is negligible. But then it is still necessary to assume that the chemical shift is temperature-independent. If the opposite is the case, variations in the chemical shift with temperature may produce considerable errors in the calculated rates. The high-resolution multiple resonance methods also suffer from the limitation that the exchange rates must be below that corresponding to coalescence of signalsat different sites. So the applicable range is quite limited. The spin-echo methods employing a Carr-Purcell sequence cover not only the ranges accessible to the above methods but also extend to much faster rates. Some other desirable features of the method are i) that it is not necessary to make any assumptions about the values

of the chemical shift and the transverse relaxation time as in the steady-state method. These quantities are obtained as an extra bonus from the rate studies, and ii) that H_o inhomogeneity effects are eliminated in the spin-echo method and less expensive magnets can be used instead of the high-resolution magnets.

The main disadvantage of the spin-echo method is its lack of selectivity. The selective deuteration of sites unaffected by exchange is in general difficult enough to limit the scope of the spin-echo method when protons are observed. Also the effects of H_1 inhomogeneities in the spin-echo experiment will produce errors which are cumulative. These have not in general been considered in the rate studies to date and may probably be the most serious source of errors in the Carr-Purcell method for obtaining exchange rates. Such errors would cause experimental values of $\Delta H^{\ddagger}$ to be too low, as seems to be the case. With rotary echoes, the high-resolution of the method provides sufficient selectivity even among homonuclear systems and inhomogeneity effects of both H_1 and H_o are eliminated. Moreover, with the special capability of determining long relaxation times or low decay rates, the method extends its application at both ends to cover an overall range comparable to if not larger than that of the spin-echo method. The main drawback of the rotary-echo method to date is that it requires knowledge of the relaxation times and in some cases, the chemical shift to determine exchange rates.

To give some general ideas about the reliability of the

different NMR methods in chemical exchange studies, an approximate comparison of the ranges of applicability for the various methods is shown in Fig. 3-5. The ranges for the steady-state methods are generally quite limited mainly by the magnet inhomogeneity and by the sensitivity of the chosen parameters. Multiple resonance methods are of course only applicable below coalescence. The pulsed methods have much wider ranges. The dotted lines in the figure show possible extension of the ranges by either varying some experimental parameters or by taking greater pains in the experiments. The rotary-echo method, though not applicable for quite some range around the coalescence point, has quite a wide overall range from end to end. To a first approximation, the intrinsic reliability of the methods should be proportional to the range of experimental values covered by each. So it is obvious that the pulsed methods are more reliable on this basis. By and large, this newly-developed rotary-echo method, pulsing at sub-audio frequencies, possesses the resolution of the steady-state methods on one hand and has some of the merits of the pulsed methods on the other.

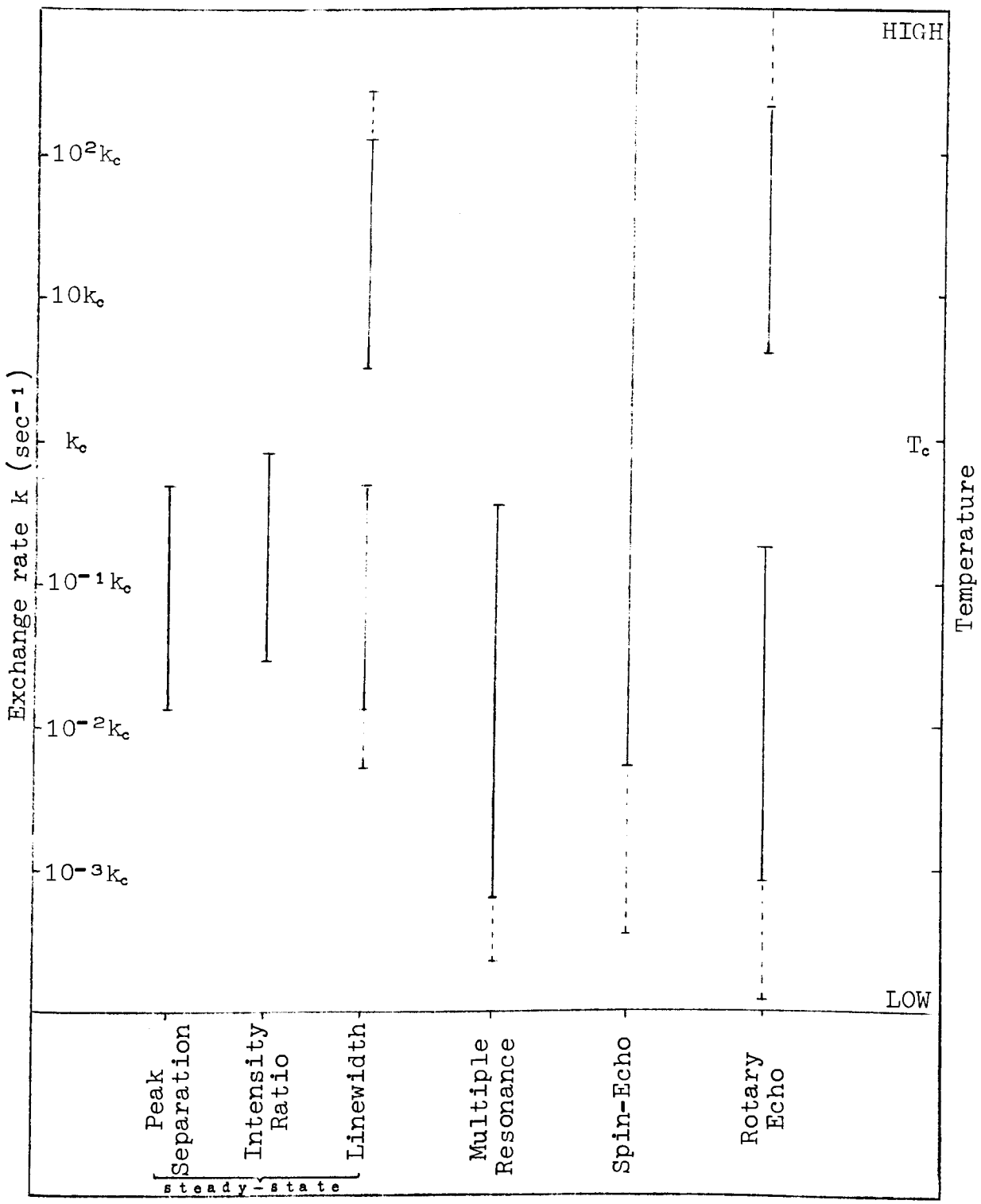

Fig. 3-5. Comparison of applicable ranges of exchange rates and temperature for various methods.

CHAPTER IV

SCALAR COUPLING WITH QUADRUPOLAR NUCLEI

In the chemical exchange studies by the rotary-echo method in the previous chapter, it was noted that differential contributions to T_1 and T_2 relaxation processes from scalar coupling of protons to a quadrupolar nucleus can show up in the proton rotary-echo decay rate R_{2r}. To substantiate that the rotary-echo decay, pulsing at sub-audio frequencies, is sensitive to unresolved scalar coupling to quadrupolar nuclei, the systems acetonitrile (CH_3CN) and chloroform ($CHCl_3$) were studied with the aim of obtaining $J_{\underline{H}C\underline{C}N}$ in CH_3CN and $J_{\underline{H}C\underline{C}l}$ in $CHCl_3$. The contributions of scalar relaxation to T_2 of the protons in these two systems were expected to be detectable.

A. Theory of Scalar Relaxation

In the systems CH_3CN and $CHCl_3$, reorientation of the molecules provides an effective relaxation mechanism for the nitrogen nucleus in the former and the chlorine nuclei in the latter through their quadrupole interaction (53) with the electric-field gradients fixed in the molecular frame. If τ_q is the appropriate correlation time for the reorientation of the field gradients, $\frac{e^2Qq}{\hbar}$ is the quadrupole coupling constant in radians per second and η is the asymmetry parameter, then the relaxation times (T_{1q} and T_{2q}) for the quadrupolar nucleus of spin

S in the extreme narrowing limit are given by (54)

$$\frac{1}{T_{1q}} = \frac{1}{T_{2q}} = \frac{3}{40}\frac{2S + 3}{S^2(2S - 1)}\left(1 + \frac{\eta^3}{3}\right)\left(\frac{e^2Qq}{\hbar}\right)^2\tau_q \quad . \qquad (4.1)$$

T_{1q} and T_{2q} are usually very short for quadrupolar nuclei in non-spherically symmetric environments. In these two systems, the fast relaxation of the quadrupolar nuclei induces rapidly fluctuating magnetic fields at the protons under observation through the indirect scalar coupling, $J_{\underline{HCCN}}$ in CH_3CN and $J_{\underline{HCCl}}$ in $CHCl_3$. This mechanism has been described as a type II scalar relaxation by Abragam (40). Specifically, the contributions to the relaxation processes for the spin I by the scalar interaction are

$$\left(\frac{1}{T_{1i}}\right)_{sc} = \frac{2(2\pi J)^2}{3}S(S + 1)\frac{T_{2q}}{1 + (\omega_i - \omega_s)^2T_{2q}^2} \qquad (4.2)$$

$$\left(\frac{1}{T_{2i}}\right)_{sc} = \frac{(2\pi J)^2}{3}S(S + 1)\left[T_{1q} + \frac{T_{2q}}{1 + (\omega_i - \omega_s)^2T_{2q}^2}\right] \qquad (4.3)$$

Generally, $$|(\omega_i - \omega_s)|T_{2q} >> 1 > T_{1q}, T_{2q}, \qquad (4.4)$$

so this mechanism does not usually contribute to T_{1i} but it does affect T_{2i} unless T_{2q} (along with T_{1q}) is so small that

$$(\omega_i - \omega_s)^2T_{2q}^2 << 1 \qquad (4.5)$$

when the contributions to both T_{1i} and T_{2i} are infinitesimally small. Combining the contribution (DD) due to dipole-dipole interaction and that due to scalar coupling, Solomon and Bloembergen (22) obtain the following for the relaxation times (T_1 and T_2) of a nuclear species coupled to a quadrupolar nucleus of spin S, itself relaxing with time constants T_{1q} and T_{2q}:

$$\frac{1}{T_1} = DD + \frac{2(2\pi J)^2}{3} S(S+1) \frac{T_{2q}}{1 + (\omega_i - \omega_s)^2 T_{2q}^2} \qquad (4.6)$$

$$\frac{1}{T_2} = DD + \frac{(2\pi J)^2}{3} S(S+1) \left[T_{1q} + \frac{T_{2q}}{1 + (\omega_i - \omega_s)^2 T_{2q}^2} \right] \qquad (4.7)$$

When the condition (4.4) is satisfied, the indirect scalar coupling, although only a weak interaction, can serve as an effective T_2 relaxation mechanism, and from (4.6) and (4.7). one obtains

$$\frac{1}{T_2} - \frac{1}{T_1} = \frac{(2\pi J)^2}{3} S(S+1) T_{1q} \ . \qquad (4.8)$$

To allow for the possibility that there are N equivalent quadrupolar nuclei in the molecule, more or less independently relaxed and coupled to spins under observation, the integral factor N has been introduced to equation (4.8) by Freeman, Ernst and Anderson (55) to give

$$\frac{1}{T_2} - \frac{1}{T_1} = \frac{N(2\pi J)^2}{3} S(S+1) T_{1q} \, . \qquad (4.9)$$

If the N quadrupolar nuclei do not relax independently, $NS(S+1)$ in equation (4.9) has to be replaced so that

$$\frac{1}{T_2} - \frac{1}{T_1} = \frac{(2\pi J)^2}{3} \overline{S(S+1)} T_{1q} \qquad (4.10)$$

where $\overline{S(S+1)}$ is the weighted contribution to $S(S+1)$ from the various resultant vector combinations of the N spins. Evaluation of $\overline{S(S+1)}$ for $N = 3$ is shown in Section C where the calculation is done.

B. Experimental

(a) Preparation of samples

Spectral grade acetonitrile and chloroform were further distilled once and then were degassed and sealed in cylindrical glass sample tubes of bore about 3 mm in diameter.

(b) Rotary-echo measurements

The rates of decay of the echo envelope in the rotating frame were obtained with the rotary-echo instruments described in Chapter I. The intensity of H_1 used was 2.5 milligauss and the frequencies of pulsing ranged from 1 to 5 sec^{-1}. The decay rates ($\frac{1}{T_{2r}}$) free from diffusion effects were obtained by extrapolation to infinite pulse rate.

(c) T_1 measurements

The longitudinal relaxation times T_1 were determined by the method of saturation-recovery with sampling with a Varian A56/60 high-resolution NMR spectrometer. This method employs a repetitive H_o field sweep and two levels of H_1, the saturating (~3 mG) and the sampling (~0.001 mG) levels. The Varian spectrometer was slightly modified so that i) it could be switched easily between two predetermined levels of H_1, and ii) connections to the dc sweep coils of the dc magnet were provided.

The repetitive H_o sweep was obtained by feeding recurrent waves from a Tektronix Type 162 waveform generater to the dc sweep coils. The recovery of the signal after the saturating H_1 was turned down was sampled with low H_1 and was recorded with a

Honeywell Electronik 19 recorder connected to the recorder output of the Varian spectrometer.

C. Calculation of Results

(a) Acetonitrile (CH_3CN)

The T_{1q} for N in CH_3CN was taken from the value 5.0 msec measured directly by an rf pulse method by Moniz and Gutowsky (42). $\frac{1}{T_1}$ and $\frac{1}{T_{2r}}$ measured in this experiment for the protons in CH_3CN were

$$\frac{1}{T_1} = 0.091 \text{ sec}^{-1}$$

$$\frac{1}{T_{2r}} = 0.19 \text{ sec}^{-1}.$$

But $$\frac{1}{T_{2r}} = \frac{1}{2}\left(\frac{1}{T_1} + \frac{1}{T_2}\right)$$

therefore $$\frac{1}{T_2} - \frac{1}{T_1} = 2\left(\frac{1}{T_{2r}} - \frac{1}{T_1}\right) = 0.198 \text{ sec}^{-1}.$$

Using equation (4.8)

$$J_{\underline{H}C\underline{C}\underline{N}} = 1.23 \text{ hz}.$$

(b) Chloroform ($CHCl_3$)

The T_{1q} for Cl in $CHCl_3$ was taken from the linewidth measurement for the chlorine nuclei in chloroform by Winter (56). Half width at half intensity of 22 gauss gave T_{1q} equal to 17.4 μsec. $\frac{1}{T_1}$ and $\frac{1}{T_{2r}}$ measured in this present experiment for the proton in $CHCl_3$ were

$$\frac{1}{T_1} = 0.0143 \text{ sec}^{-1}$$

$$\frac{1}{T_{2r}} = 0.0523 \text{ sec}^{-1}.$$

Therefore $\frac{1}{T_2} - \frac{1}{T_1} = 2(\frac{1}{T_{2r}} - \frac{1}{T_1}) = 0.076.$

Assuming the three chlorine nuclei are relaxing independently in the molecule and using equation (4.9)

$$J_{\underline{H}\underline{C}\underline{C}l} = 5.5 \text{ hz}$$

as was obtained by Winter (56).

It is very likely that the three chlorine nuclei do not relax independently, so we have to treat them as a whole. In this way, combining the three $\frac{3}{2}$ - spins vectorially there are

1 possible combination of total spin $\frac{9}{2}$
2 possible combinations of total spin $\frac{7}{2}$
3 possible combinations of total spin $\frac{5}{2}$
4 possible combinations of total spin $\frac{3}{2}$
2 possible combinations of total spin $\frac{1}{2}$.

The total number of possible combinations is 12, each of equal probability in the classical high temperature limit of molecular J states. Therefore the weighted mean

$$\overline{S(S+1)} = \frac{1}{12}\left[\frac{9}{2}\cdot\frac{11}{2} + 2\cdot\frac{7}{2}\cdot\frac{9}{2} + 3\cdot\frac{5}{2}\cdot\frac{7}{2} + 4\cdot\frac{3}{2}\cdot\frac{5}{2} + 2\cdot\frac{1}{2}\cdot\frac{3}{2}\right] \qquad (4.11)$$

$$= 8.25.$$

Using this value in (4.10), we get

$$J_{\underline{H}\underline{C}\underline{C}\underline{l}} = 6.3 \text{ hz}.$$

Actually there are two chlorine isotopes Cl^{35} and Cl^{37} both of spin $\frac{3}{2}$ and an isotopic ratio of 3 to 1. However, the ratio (57)

$$\frac{(J^2T_{1q})_{35}}{(J^2T_{1q})_{37}} = (\frac{\gamma_{35}}{\gamma_{37}})^2(\frac{Q_{37}}{Q_{35}})^2 \approx 0.9$$

and the contributions to $(\frac{1}{T_2} - \frac{1}{T_1})$ from either spin differ little so the complications due to the presence of two isotopes have been disregarded.

D. Discussion

(a) Acetonitrile (CH_3CN)

The experimentally determined T_1, 11.0 sec. is in agreement with the value obtained by Boden et al (58) for the methyl protons in the same compound. The calculated T_2, 3.46 sec. is much shorter than the $T_2°$, 11.2 sec. of Boden et al (58) obtained by the Carr-Purcell spin-echo method at high pulse rate. The difference is due to the fact that the contribution of scalar relaxation to the T_2 process is eliminated by the high frequency pulses (pulse separation smaller than the relaxation time for the quadrupolar nucleus). So T_2 of 3.46 sec. is the transverse relaxation time where both the dipole-dipole and the scalar contributions are effective as is given by (4.7), while $T_2°$ of 11.2 sec. results from only the dipole-dipole contribution and under the generally satisfied condition (4.4). $T_2°$ should be equal to T_1 according to equation (4.6). Thus Boden's $T_2°$

of 11.2 sec. is in agreement with our T_1 of 11.0 sec.

The calculated $J_{\underline{H}C\underline{C}N}$ of 1.23 hz is also in agreement with the value of 1.2 hz scaled down from the N^{15} coupling constant of Binsch et al (41) and with the value of 1.38 hz determined indirectly by Boden et al (58).

(b) Chloroform ($CHCl_3$)

Our experimentally determined T_1, 70 sec. is longer than that of Winter (56), 42 sec. for the proton in chloroform. The calculated T_2 from our T_{2r} is 11.1 sec., also slightly longer.

$J_{\underline{H}C\underline{C}l}$ of 5.5 hz is obtained as Winter on the same assumption that the three chlorine nuclei relax independently. Doing away with the assumption, fresh calculation gives $J_{\underline{H}C\underline{C}l}$ a value of 6.3 hz.

Coupling constants between proton and chlorine separated by two bonds are lacking for comparison. However, some values for the coupling between proton and fluorine two bonds apart have been reported: 60 hz for $J_{\underline{H}C\underline{F}}$ in monofluoroethane (59) and 81 hz for $J_{\underline{H}C\underline{F}}$ in 1-fluoro-2,2-dichloroethylene (60). Scaling by γ_{Cl}/γ_F according to the theory of nuclear spin-spin interaction (61), we get 6.26 hz and 8.45 hz for $J_{\underline{H}C\underline{C}l}$. The values of 6.3 hz for $J_{\underline{H}C\underline{C}l}$ calculated for chloroform appears to be better than the value of 5.5 hz obtained on assumption that the three nuclei relax independently.

From the above results in this present experiment, it is

obvious that the rotary-echo method with pulsing at sub-audio frequencies is sufficiently sensitive to detect the effects of unresolved scalar coupling to quadrupolar nuclei.

CHAPTER V

F^{19} SPIN-ROTATION RELAXATION IN THE LIQUID PHASE

The fluorine spin-rotation relaxation in liquid chlorodifluoromethane (CHF_2Cl) and difluoromethane (CH_2F_2) has been studied indirectly by selective rotary-echo experiments on the proton resonances, whose natural linewidths are dominated by the rapid relaxation by spin-rotation interaction of the fluorine nuclei coupled scalarly to the protons. A full report on the experiments is shown in the following sections.

A. Introduction

Spin-rotation interaction between the nuclear spin vector $\vec{I}$ and the overall molecular rotational angular momentum vector $\vec{J}$ is one of the hyperfine interactions important to microwave spectroscopy (62). This type of interaction, of form

$$\vec{I}.\underset{\approx}{C}.\vec{J},$$

where $\underset{\approx}{C}$ is the spin-rotation coupling tensor, was first found in the hydrogen molecule by Kellogg et al (63, 64) in 1939 using molecular-beam techniques. Since then there have been a number of measurements on this interaction in which a variety of techniques were used to suit the molecule and the particular measurement desired.

Because the spin-rotation interaction involves the nu-

clear spin and is magnetic in nature, its effects are also detectable in NMR measurements. In NMR, the interaction modulated by collisions which cause a time dependence in $\vec{J}$, can provide an effective relaxation mechanism (65) for the spins. It is found that the effect is particularly important with systems in the gaseous phase and with systems containing heavier magnetic nuclei. Generally, from experimental data obtained so far, the spin-rotation contribution to relaxation is at least two orders of magnitude bigger in the gaseous phase than in the liquid phase (66). The protons in gaseous methane and its deuterated modifications (67, 68) and the fluorines in the gaseous fluoromethanes (69, 70) have been found to be relaxed mainly by spin-rotation interaction. In liquids proton spin-rotation effects are negligible but those of fluorine and other heavier magnetic nuclei are still dominant (66, 71, 72) at temperatures around the ice point or above. That the spin-rotation interaction is small for the proton and much larger for fluorine is implicit in the proportionality which Ramsey (73) has pointed out between the spin-rotation interaction constant and the second-order paramagnetic term in the nuclear magnetic shielding, in as much as the latter is small for protons (73) and large for fluorines (72).

Theories of nuclear magnetic relaxation by spin-rotation interaction in gases (68, 74, 75) and in liquids (66, 76, 77) have been developed. Experimentally the problem has been tackled

by two approaches: direct and indirect. In the direct method, the relaxation times of the nuclei relaxed by spin-rotation interaction are measured directly and the spin-rotation contributions separated from the other contributions if necessary. This method has been applied quite extensively to both gases (67, 68, 74, 78, 79) and liquids (66, 80, 81, 82). In the second method one needs not look at the nuclei relaxed by spin-rotation interaction. Instead one observes the relaxation of the other nuclei, indirectly or scalarly coupled to the nuclei relaxed by spin-rotation interaction. For CH_2F_2 and CH_3CHF_2 in the gaseous phase where the fluorines relax predominantly by spin-rotation interaction, Flynn and Baldeschwieler (70) obtained the fluorine transition probabilities from the differential linewidths of the proton resonances without looking at the fluorines at all. In the liquid state, high-resolution spectral linewidths are determined mainly by magnet inhomogeneity. The differential relaxation observed in the gaseous phase is covered up by inhomogeneity effects. Using the nuclear Overhauser effect (20, 83), Kuhlmann and Baldeschwieler (84) and Kanazawa (85) were able to study the F^{19} spin-rotation interaction of the difluoroethylenes in solutions by working on the proton resonances only. In this chapter we wish to report a second indirect but straight-forward method in the studies of the F^{19} spin-rotation relaxation in liquid CHF_2Cl and CH_2F_2 using high-resolution rotary-echo techniques.

B. Proton Resonances in A_nX_2 Systems

In the systems we study A is H^1 and X, F^{19}. n takes on the values 1 for CHF_2Cl and 2 for CH_2F_2.

(a) An AX_2 system — CHF_2Cl

The Hamiltonian for the AX_2 system (CHF_2Cl) can be written as

$$\mathcal{H} = -\omega_H K_Z(H) - \omega_F K_Z(F) + \mathcal{R}_{HF} [\vec{I}(1)\cdot\vec{I}(2) + \vec{I}(1)\cdot\vec{I}(3)] \qquad (5.1)$$

where $\vec{K}(H) = \vec{I}(1)$

$\vec{K}(F) = \vec{I}(2) + \vec{I}(3)$

$\omega_H = \gamma_H H_o$

$\omega_F = \gamma_F H_o$

$\mathcal{R}_{HF}$ is the scalar coupling constant between the proton and the fluorine,

γ_H and γ_F are the magnetogyric ratios of proton and fluorine respectively,

and H_o is the applied dc magnetic field.

The spin-product basis functions for the system can be readily written and the appropriate linear combinations of these basis functions consistent with the C_s symmetry of CHF_2Cl are given in Table VI.

In this representation the Hamiltonian is diagonal and therefore the basis functions are the eigenfunctions. The allowed proton transitions with their relative widths due to rapid fluorine relaxation are shown in Table VII.

A schematic energy-level diagram for the system is shown

Table VI. Wave functions for an AX_2 system.

Basis functions	Spin-product functions	F_z	K_z (H)	K_z (F)	Symmetry	$\langle \varphi_i \mid \mathcal{H} \mid \varphi_i \rangle$
φ_1	$\alpha\alpha\alpha$	3/2	$\frac{1}{2}$	1	A'	$-\frac{1}{2}(\omega_H+2\omega_F-\mathcal{R}_{HF})$
φ_2	$\frac{1}{\sqrt{2}}\,\alpha(\alpha\beta+\beta\alpha)$	$\frac{1}{2}$	$\frac{1}{2}$	0	A'	$-\frac{1}{2}\omega_H$
φ_3	$\frac{1}{\sqrt{2}}\,\alpha(\alpha\beta-\beta\alpha)$	$\frac{1}{2}$	$\frac{1}{2}$	0	A''	$-\frac{1}{2}\omega_H$
φ_4	$\alpha\beta\beta$	$-\frac{1}{2}$	$\frac{1}{2}$	-1	A'	$-\frac{1}{2}(\omega_H-2\omega_F+\mathcal{R}_{HF})$
φ_5	$\beta\alpha\alpha$	$\frac{1}{2}$	$-\frac{1}{2}$	1	A'	$\frac{1}{2}(\omega_H-2\omega_F-\mathcal{R}_{HF})$
φ_6	$\frac{1}{\sqrt{2}}\,\beta(\alpha\beta+\beta\alpha)$	$-\frac{1}{2}$	$-\frac{1}{2}$	0	A'	$\frac{1}{2}\omega_H$
φ_7	$\frac{1}{\sqrt{2}}\,\beta(\alpha\beta-\beta\alpha)$	$-\frac{1}{2}$	$-\frac{1}{2}$	0	A''	$\frac{1}{2}\omega_H$
φ_8	$\beta\beta\beta$	-3/2	$-\frac{1}{2}$	-1	A'	$\frac{1}{2}(\omega_H+2\omega_F+\mathcal{R}_{HF})$

Table VII. Allowed transitions in the H^1 spectrum of CHF_2Cl.

Label	Transitions	Energy	K(F)	K_z (F)	Symmetry	Rel. width
S_1^-	$\varphi_1 \rightarrow \varphi_5$	$\omega_H-\mathcal{R}_{HF}$	1	1	A'	$k_s + k_a$
C_1	$\varphi_2 \rightarrow \varphi_6$	ω_H	1	0	A'	$2k_s + k_a$
S_1^+	$\varphi_4 \rightarrow \varphi_8$	$\omega_H+\mathcal{R}_{HF}$	1	-1	A'	$k_s + k_a$
C_0	$\varphi_3 \rightarrow \varphi_7$	ω_H	0	0	A''	$3k_a$

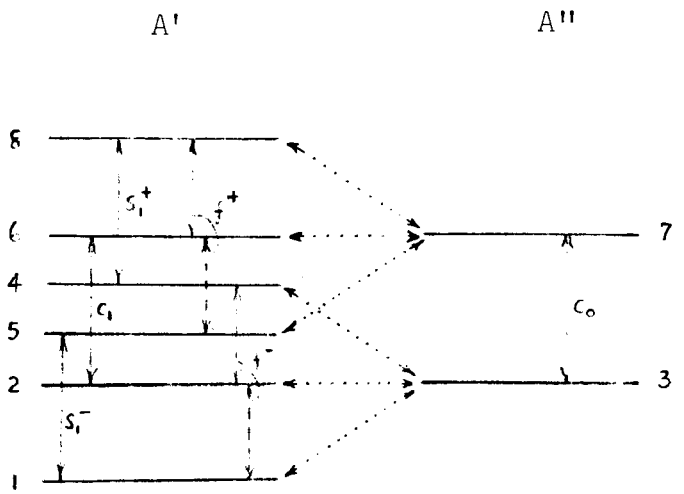

Fig. 5-1. Schematic energy-level diagram for an AX_2 system.

in Fig. 5-1. The levels belonging to the A' and A'' representations are shown separately. The allowed proton transitions are shown by full lines while the allowed fluorine transitions by dashed lines between the levels. Antisymmetric fluorine transitions are shown by dotted lines. High-resolution proton spectra of the system in the liquid and gaseous phase are similar to those for CH_2F_2 in Fig. 5-4. With reference to Fig. 5-1, it is clear that rapid fluorine relaxation will provide an effective transverse relaxation mechanism for the proton transitions between states with parallel fluorine spins, K(F) = 1. Proton transitions between states with antiparallel fluorine spins, K(F) = 0 are not affected by the symmetric fluorine relaxation but by the much less frequent antisymmetric transitions. Therefore the central component in the proton triplet is made up of one broad and one sharp line superimposed on each other as shown

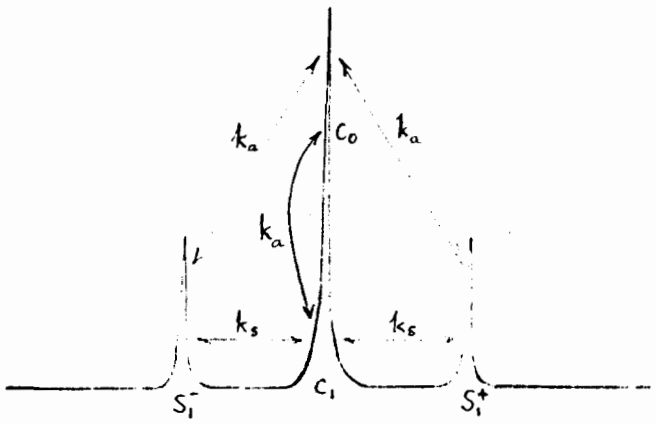

Fig. 5-2. Schematic PMR spectrum for $A_n X_2$ systems. ($A = H^1$, $X = F^{19}$)

schematically in Fig. 5-2. In rotary-echo experiments, if a proton transition, say the S_1^- is irradiated selectively, (see Fig. 5-1) the population of the levels 1 and 5 will be disturbed and transient effects will take place via the rapid fluorine transitions. These rapid fluorine transitions show up as proton relaxation in the rotary-echo measurements. Let us define

k_s as the symmetric fluorine transition probability,

$\Delta m_F = \pm 1$,

and k_a as the antisymmetric fluorine transition probability,

$\Delta m_F = \pm 1, 0$.

Then by considering the rapid fluorine transitions as a means of transferring magnetization among the proton resonance lines with rates k_s and k_a as shown in Fig. 5-2, or by considering the contribution of the rapid fluorine relaxation to the line widths of the proton transitions in a way similar to that used by Flynn

and Baldeschwieler (86), the proton decay rates in the rotating frame for the various components in the proton multiplet can be written in terms of R_{1H}, R_{2H} and the k's as shown below:

$$R_{2rH}(C_1) = \frac{1}{2}(R_{1H} + R_{2H}) + 2k_s + k_a \qquad (5.2)$$

$$R_{2rH}(C_0) = \frac{1}{2}(R_{1H} + R_{2H}) + 3k_a \qquad (5.3)$$

$$R_{2rH}(S_1) = \frac{1}{2}(R_{1H} + R_{2H}) + k_s + k_a \qquad (5.4)$$

(b) An A_2X_2 system — CH_2F_2

The Hamiltonian for the A_2X_2 system (CH_2F_2) can be written as

$$\mathcal{H} = -\omega_H K_Z(H) - \omega_F K_Z(F) + \mathcal{R}_{HF}[\vec{I}(1)\cdot\vec{I}(3) + \vec{I}(1)\cdot\vec{I}(4) + \vec{I}(2)\cdot\vec{I}(3) + \vec{I}(2)\cdot\vec{I}(4)] \qquad (5.5)$$

where $\vec{K}(H) = \vec{I}(1) + \vec{I}(2)$

$\vec{K}(F) = \vec{I}(3) + \vec{I}(4)$.

The basis functions consistent with the C_{2v} symmetry of CH_2F_2 are the eigenfunctions of the Hamiltonian and are shown in Table VIII. The allowed proton transitions with their relative widths due to rapid fluorine relaxation are shown in Table IX. A schematic energy-level diagram for the system is shown in Fig. 5-3. The levels belonging to the A_1 and B_1 representations are shown separately. Full lines between levels show the allowed proton transitions, dashed lines, allowed fluorine transitions and dotted lines, the antisymmetric fluorine transitions. High-resolution proton spectra of this system in the liquid and gaseous phase are shown in Fig. 5-4. The set of equations (5.2)-(5.4) also applies here. A high-resolution fluorine spectrum of CH_2F_2 in

Table VIII. Wave functions for an A_2X_2 system.

Basis functions	Spin-product functions	F_z	$K_z(H)$	$K_z(F)$	Symmetry	$\langle \varphi_i \mid \mathcal{H} \mid \varphi_i \rangle$
φ_1	$\alpha\alpha\alpha\alpha$	2	1	1	A_1	$-\omega_H-\omega_F+\mathcal{R}_{HF}$
φ_2	$\sqrt{\frac{1}{2}}\alpha\alpha(\alpha\beta+\beta\alpha)$	1	1	0	A_1	$-\omega_H$
φ_3	$\sqrt{\frac{1}{2}}\alpha\alpha(\alpha\beta-\beta\alpha)$	1	1	0	B_1	$-\omega_H$
φ_4	$\sqrt{\frac{1}{2}}(\alpha\beta+\beta\alpha)\alpha\alpha$	1	0	1	A_1	$-\omega_F$
φ_5	$\sqrt{\frac{1}{2}}(\alpha\beta-\beta\alpha)\alpha\alpha$	1	0	1	B_1	$-\omega_F$
φ_6	$\alpha\alpha\beta\beta$	0	1	-1	A_1	$-\omega_H+\omega_F-\mathcal{R}_{HF}$
φ_7	$\frac{1}{2}(\alpha\beta+\beta\alpha)(\alpha\beta+\beta\alpha)$	0	0	0	A_1	0
φ_8	$\frac{1}{2}(\alpha\beta-\beta\alpha)(\alpha\beta-\beta\alpha)$	0	0	0	A_1	0
φ_9	$\frac{1}{2}(\alpha\beta+\beta\alpha)(\alpha\beta-\beta\alpha)$	0	0	0	B_1	0
φ_{10}	$\frac{1}{2}(\alpha\beta-\beta\alpha)(\alpha\beta+\beta\alpha)$	0	0	0	B_1	0
φ_{11}	$\beta\beta\alpha\alpha$	0	-1	1	A_1	$\omega_H+\omega_F-\mathcal{R}_{HF}$
φ_{12}	$\sqrt{\frac{1}{2}}\beta\beta(\alpha\beta+\beta\alpha)$	-1	-1	0	A_1	ω_H
φ_{13}	$\sqrt{\frac{1}{2}}\beta\beta(\alpha\beta-\beta\alpha)$	-1	-1	0	B_1	ω_H
φ_{14}	$\sqrt{\frac{1}{2}}(\alpha\beta+\beta\alpha)\beta\beta$	-1	0	-1	A_1	ω_F
φ_{15}	$\sqrt{\frac{1}{2}}(\alpha\beta-\beta\alpha)\beta\beta$	-1	0	-1	B_1	ω_F
φ_{16}	$\beta\beta\beta\beta$	-2	-1	-1	A_1	$\omega_H+\omega_F+\mathcal{R}_{HF}$

Table IX. Allowed transitions in the H^1 spectrum of CH_2F_2.

Label	Transitions	Energy	K(F)	$K_z(F)$	Symmetry	Rel. width
S_1^-	$\varphi_1 \rightarrow \varphi_4$ $\varphi_4 \rightarrow \varphi_{11}$	$\omega_H-\mathcal{R}_{HF}$	1	1	A_1	$k_s + k_a$
C_1	$\varphi_2 \rightarrow \varphi_7$ $\varphi_7 \rightarrow \varphi_{12}$	ω_H	1	0	A_1	$2k_s + k_a$
S_1^+	$\varphi_6 \rightarrow \varphi_{14}$ $\varphi_{14} \rightarrow \varphi_{16}$	$\omega_H+\mathcal{R}_{HF}$	1	-1	A_1	$k_s + k_a$
C_0	$\varphi_3 \rightarrow \varphi_9$ $\varphi_9 \rightarrow \varphi_{13}$	ω_H	0	0	B_1	$3k_a$

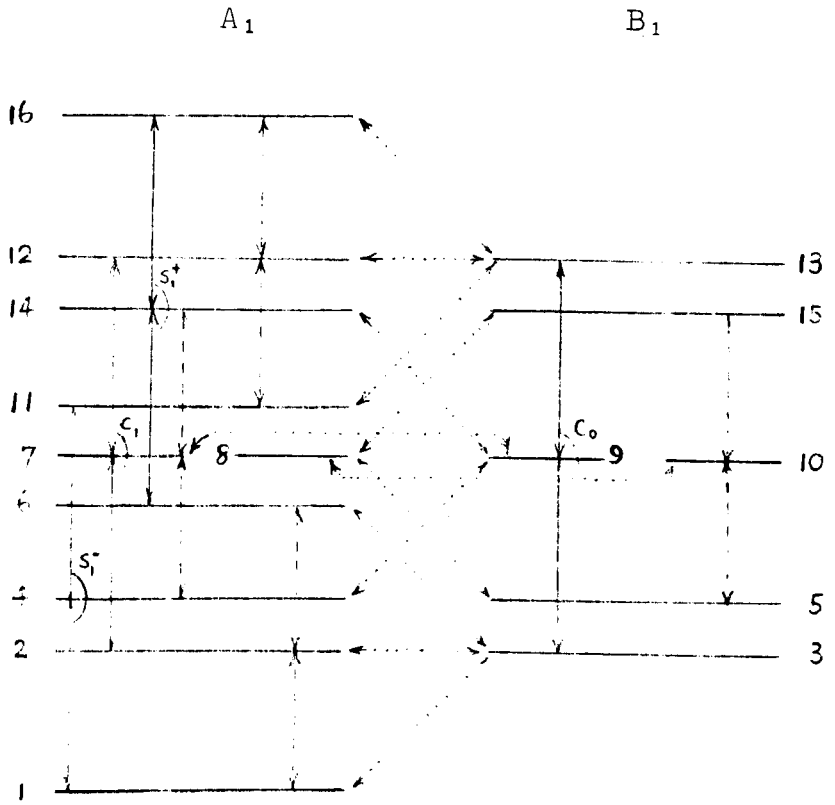

Fig. 5-3. Schematic energy-level diagram for an A_2X_2 system.

the gaseous phase is shown in Fig. 5-5. The line widths of the fluorine resonances are equal within experimental errors to those of the side transitions in the gas phase proton spectrum of the compound as expected.

C. Experimental

(a) Preparation of samples

The CHF_2Cl and CH_2F_2 were purchased from the Matheson Co. Inc. and the Pierce Chemical Co. respectively. No further purification was made except for a simple vacuum distillation prior

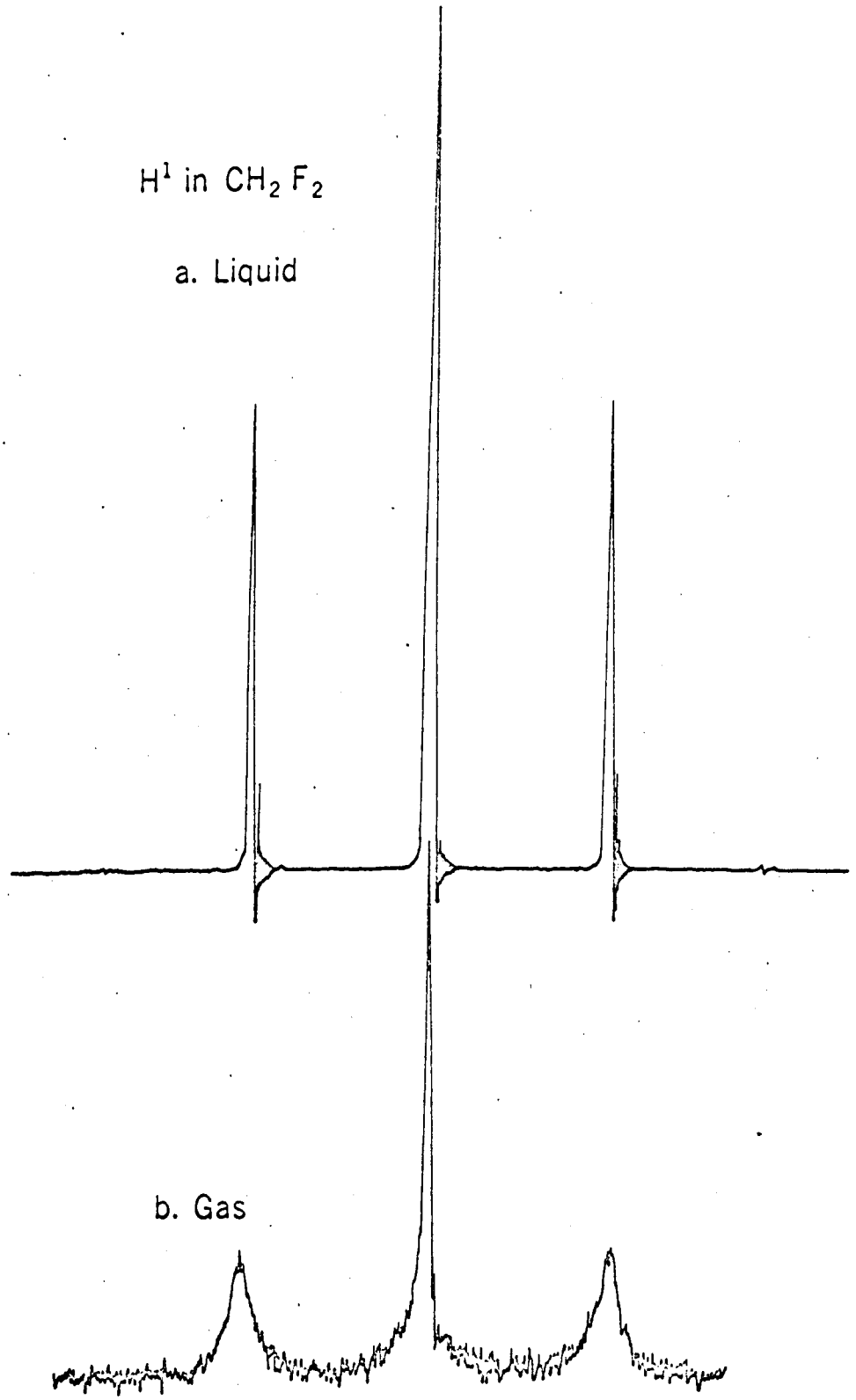

Fig. 5-4. High-resolution PMR spectra of CH_2F_2. (Pressure of gas ~10 atmospheres)

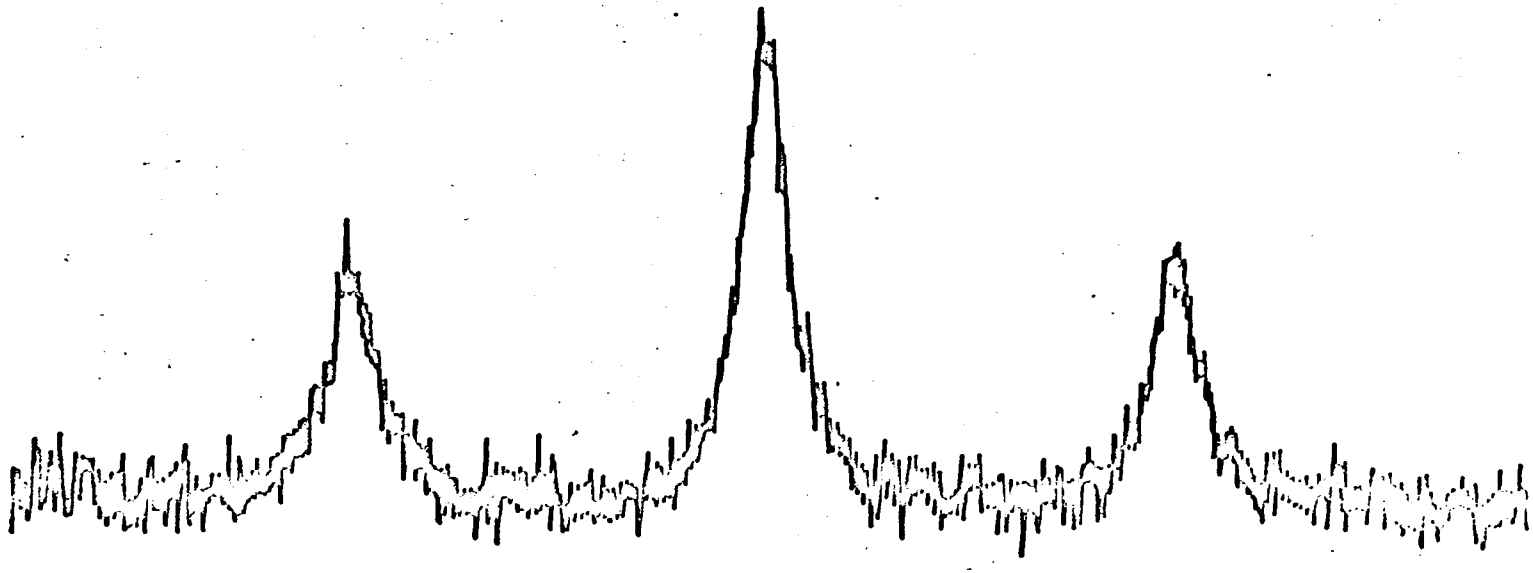

Fig. 5-5. Gas phase high-resolution F^{19} spectrum of CH_2F_2.

to the preparation of sample in tubes. For each compound the samples were prepared in pyrex glass tubes of two different sizes: 3 mm i.d. - 5 mm o.d. tubes for work with the Varian A56/60 spectrometer and 6 mm i.d. - 8 mm o.d. tubes with the NMR specialties pulse machine. Degassing was done by the usual freeze-pump-thaw method repeated four times. Several samples prepared this way gave consistent T_1 values for the protons, showing that negligible amount of paramagnetic impurities (e.g. oxygen) is present.

(b) Rotary-echo measurements

The decay of the rotary-echo train for the protons was measured selectively on each individual component of the proton multiplets using the Varian A56/60 high-resolution NMR spectrometer modified for the purpose. For the side peaks in the proton triplet, the decays are the same within experimental errors and are governed by a single exponential. For the central peak a double exponential decay is observed as expected, in that the central peak is a superposition of a broad and a sharp line of equal intensity. The decay rates in the rotating frame, $R_{2rH}(C_1)$, $R_{2rH}(C_0)$ and $R_{2rH}(S_1)$ were obtained from semi-log plots of the rotary-echo amplitudes against time.

(c) High-resolution steady-state measurements

Steady-state spectra were obtained on the Varian A56/60 high-resolution NMR spectrometer for both protons and fluorines.

The gas phase spectra were improved by signal-averaging using a Fabri-Tek 1064 instrument computer with a Model SD-2 digitizer and a Model SW-3 NMR field stabilizer and sweep control.

(d) T_1 and T_2 measurements

Proton T_1's were measured by two methods: i) saturation-recovery with sampling on the Varian A56/60 high-resoltuion NMR spectrometer, ii) π - $\pi/2$ pulse sequence on the NMR Specialties pulse machine. The T_1's are consistent from individually prepared samples. Fluorine T_1's were measured by only the second method but at two different frequencies, 15 and 56.4 Mhz. All T_2's were measured by the Carr-Purcell spin-echo method on the NMR Specialties pulse machine. The proton T_2's depend on pulse separation. For the shortest pulse separation (2τ = 0.5 msec.) available for the present work because of the large time base used, only the spin-rotation contribution was pulsed out ($2\tau << T_{1F}, 1/J_{HF}$) while the scalar relaxation due to coupling to the quadrupolar chlorine in CHF_2Cl was not ($2\tau >> T_{1Cl}$). With our shortest pulse separation the measured T_{2F} for CHF_2Cl was still not free from the scalar relaxation of the coupled quadrupolar chlorine.

(e) Sample temperature control

For work with the Varian A56/60 high-resolution NMR spectrometer the sample temperature was maintained in the built-in variable temperature probe by a gas-flow system and the tempera-

ture regulated by a Varian V-6040 temperature control. Temperatures were calibrated with the ethylene glycol and methanol samples provided. For work with the NMR Specialties pulse machine, the sample temperature was maintained by an Alnor temperature control system consisting of a DN-20 pyrotroller and a S5 percentage power control unit. The temperatures were calibrated by sticking in a thermometer taking the position of the sample in the probe. For both temperature controls the sample temperature attained was steady and accurate with ±0.5°K.

D. Results

The experimental relaxation rates are given in Table X. Using equations (5.2)-(5.4) the fluorine transition probabilities are calculated and shown in Table XI. The fluorine transition probabilities k's are assumed to be due to spin-rotation interaction predominantly, as the dipole-dipole contribution given essentially by the proton relaxation rates is found to be much smaller than that of the former mechanism over the temperature range in our experiment. The contribution from chemical shift anisotropy has been found to be negligible (66), $(\frac{1}{T_{1F}})_{CSA} < 10^{-2}$. In confirmation, we find the fluorine relaxation rates to be field-independent. Semi-log plots of the fluorine transition probabilities k's and the proton relaxation rates R's against the inverse of the absolute temperature are shown in Fig. 5-6 for both CHF_2Cl and CH_2F_2.

Some scalar coupling constants for the compounds are found

Table X. Experimental relaxation rates for CHF_2Cl and CH_2F_2.

Relaxation rates	CHF_2Cl (°C)						CH_2F_2 (°C)						Methods used
	42°	20°	0°	-25°	-40°	-56°	42°	20°	0°	-25°	-40°	-56°	
$R_{2r_H}(C_1)$ central	.950	.890	.825	.710	.675	.665	.785	.675	.660	.635	.595	.575	Rotary-echo
$R_{2r_H}(C_0)$ central	.210	.205	.195	.180	.165	.165	.140	.140	.145	.150	.160	.180	
$R_{2r_H}(S_1)$ side	.565	.520	.480	.420	.400	.395	.425	.370	.365	.360	.350	.355	
R_1H	.018	.024	.032	.046	.062	.081	.022	.029	.039	.055	.077	.110	SRS & $\pi-\frac{\pi}{2}$ sequence
R_2H (2τ = .5 ms)	.230	.220	.195	.165	.140	.135	.023	.030	.039	.057	.079	.112	Carr-Purcell
R_1F	.490	-	-	-	-	-	.415	-	-	-	-	-	$\pi-\frac{\pi}{2}$ sequence
R_2F (2τ = 16 ms)	1.325	-	-	-	-	-	.420	-	-	-	-	-	Carr-Purcell

Table XI. Fluorine transition probabilities for CHF_2Cl and CH_2F_2.

Systems	CHF_2Cl						CH_2F_2					
Temp.(°C) / Transition probabilities $\frac{1}{T} \times 10^3$	42°	20°	0°	-25°	-40°	-56°	42°	20°	0°	-25°	-40°	-56°
	3.18	3.42	3.66	4.03	4.29	4.61	3.18	3.42	3.66	4.03	4.29	4.61
k_s	.385	.370	.345	.290	.275	.270	.360	.305	.295	.275	.245	.220
k_a	.029	.028	.027	.025	.021	.019	.039	.037	.036	.031	.023	.023

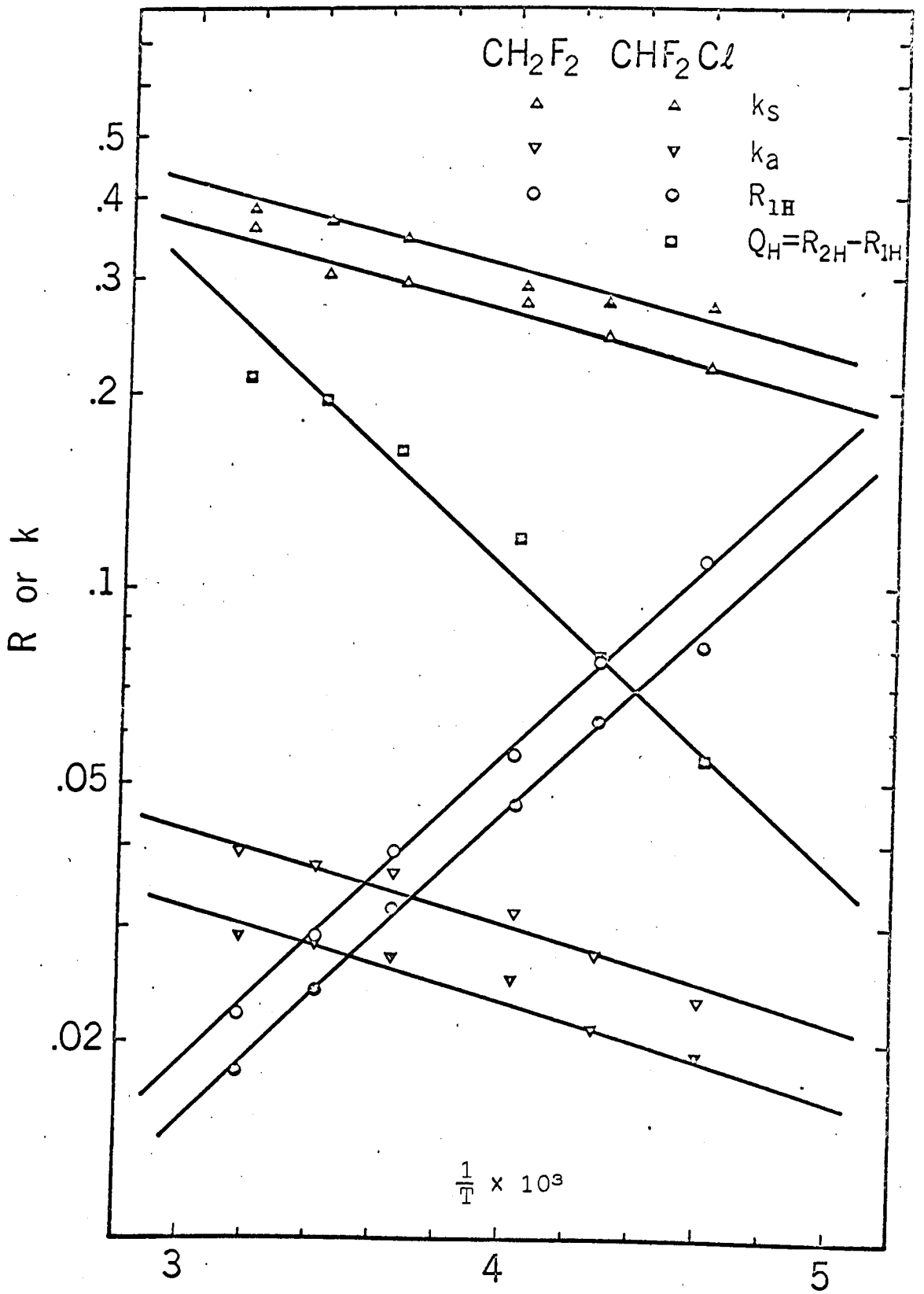

Fig. 5-6. Semi-log plot of relaxation rates and transition probabilities vs 1/T for CHF_2Cl and CH_2F_2.

Table XII. Scalar coupling constants for CHF_2Cl and CH_2F_2.

Compound	J_{HF} (hz)	$J_{C^{13}H}$ (hz)
CHF_2Cl	63.3±.2	228.4±.5
CH_2F_2	50.2±.2	183.4±.5

from the liquid phase high-resolution spectra and are listed in Table XII.

High-resolution steady-state fluorine NMR measurements at 315°K show that the fluorines absorb at 4187 hz in CHF_2Cl and 8313 hz in CH_2F_2 both towards high field with reference to CCl_3F. Using the fluorine nuclear shielding constant scale of Hindermann and Cornwell (87), the fluorine paramagnetic shielding σ_F^p for CHF_2Cl and CH_2F_2 are obtained. According to Ramsey (88) and Flygare (89) the second order paramagnetic term in the shielding is proportional jointly to the product of the spin-rotation interaction constant (C) and the moment of inertia (I) characteristic of each system. Using an approximate equation for an asymmetric-top molecule (89)

$$\sigma_F^p = \frac{MC}{4mg_FG} - \frac{e^2}{3mc^2}\sum_i Z_i r_i \qquad (5.6)$$

where M is the proton mass,

m is the electron mass,

g_F is the nuclear g factor for the nucleus F,

G is the average rotational constant

e is the electronic charge

c is the velocity of light,

Z_i is the atomic number of the ith atom in the molecule,

r_i is the distance between the nucleus F in question and the ith nucleus and

i numbers all the nuclei in the molecule except the nucleus F

and $I = \frac{1}{3}(I_{xx} + I_{yy} + I_{zz})$ of the inertia tensors calculated for the systems in Appendix B, the constant $C = \frac{1}{3}(C_{xx} + C_{yy} + C_{zz})$ of the spin-rotation interaction tensor (Appendix C) for each system is found and listed in Table XIII along with the moment of inertia (I). From Hubbard's theory of nuclear magnetic relaxation by spin-rotation interactions in liquids (76) assuming isotropic rotational diffusion we have

Table XIII. Some molecular parameters for CHF_2Cl and CH_2F_2.

Parameters	CHF_2Cl	CH_2F_2
C	-2.11×10^4 hz	-4.07×10^4 hz
I	1.67×10^{-38} gm. cm^2.	6.58×10^{-39} gm. cm^2.
τ_1^* at 315°K	2.10×10^{-14} sec.	1.21×10^{-14} sec.
τ_2^* at 315°K	7.04×10^{-13} sec.	4.48×10^{-13} sec.
ϵ_2	2.17 ± .1 kcal mole.	2.16 ± .1 kcal mole.

$$\left(\frac{1}{T_1}\right)_{SR} = \frac{2kTC^2I}{\hbar^2}\tau_1 \qquad (5.7)$$

in the extreme narrowing limit. Putting the experimental R_{1F}'s obtained for the systems at 315°K and the calculated values of C

*τ_1 and τ_2 are correlation times for the change in angular momentum and for molecualr reorientation respectively.

and I in equation (5.7), the τ_1 for each system is obtained and shown in Table XIII. The τ_2's at 315°K are also obtained (Table XIII) from the experimental R_{1H}'s for the systems at the same temperature assuming that the R_{1H}'s are predominantly due to intramolecular dipole-dipole interactions. The activation energies (ϵ_2) for molecular reorientation are obtained from the slopes of the R_{1H} vs $1/T$ plots (Fig. 5-6) and are listed in Table XIII.

E. Discussion

For the spin $\frac{1}{2}$ nuclei in the two systems studied, the probable relaxation mechanisms that may be effective in the liquids are the dipole-dipole interaction and chemical shift anisotropy modulated by molecular reorientation, spin-rotation interaction modulated by collisions and scalar relaxation due to coupling indirectly to a quadrupolar chlorine in one of the systems, CHF_2Cl. These are discussed in this section in the light of our experimental results.

For the protons, spin-rotation and anisotropic chemical shift contributions are negligible and only the dipole-dipole interaction contributes to the R_{1H}'s. From the general BPP theory (65) it can be shown that for this relaxation process,

$$R_{1H} = \frac{2}{3} \gamma_H^2 \langle H^2 \rangle_{AV} \tau_2 \qquad (5.8)$$

$$R_{1F} = \frac{2}{3} \gamma_F^2 \langle H^2 \rangle_{AV} \tau_2 \qquad (5.9)$$

where $\langle H^2 \rangle_{AV}$ is the mean square magnitude of the field fluctuation at each nucleus,

τ_2, the correlation time for molecular reorientation. Because $\gamma_H \approx \gamma_F$ and τ_2 is virtually the same for H and F as both nuclei are in the same essentially rigid and nearly spherical molecule

$$R_{1H} \approx R_{1F}.$$

The observed difference in R_{1H} and R_{1F} will be discussed later in this section.

Usually in the extreme narrowing limit $R_1 = R_2$. This is observed in the R_{1H} and R_{2H} for CH_2F_2. In CHF_2Cl the proton R_{2H} is quite different from R_{1H}. As described by Abragam (40), the rapid relaxation of the quadrupolar chlorine induces rapidly fluctuating magnetic fields at the proton through the scalar relaxation of the second type and contributes only to T_2 under the condition

$$(\omega_H - \omega_{Cl})^2 T_{1Cl}^2 >> 1$$

where ω_H and ω_{Cl} are the proton and chlorine resonant frequencies respectively and T_{1Cl}, the chlorine spin-lattice relaxation time. Accordingly (40)

$$Q_{H-Cl} = R_{2H} - R_{1H} = \frac{\hbar_{H-Cl}^2}{3} S(S + 1) T_{1Cl} = k_1 T_{1Cl} \qquad (5.10)$$

where S is the spin of the chlorine nucleus.

But T_{1Cl} is given by (54)

$$\frac{1}{T_{1Cl}} = \frac{1}{10}\left(1 + \frac{\eta^2}{3}\right)\left(\frac{e^2 Qq}{\hbar}\right)^2 \tau_2 = k_2 \tau_2, \qquad (5.11)$$

therefore

$$Q_{H-Cl} = \frac{k_1}{k_2 \tau_2}. \qquad (5.12)$$

τ_2 is the correlation time for molecular reorientation and should be the same as the τ_2 in the dipole-dipole contribution. Semi-log plot of Q_{H-Cl} for CHF_2Cl against the inverse temperature (Fig. 5-6) gives, within experimental errors, an inverse temperature dependence to that of the dipole-dipole contribution (the R_{1H}'s) as expected from theories.

For the fluorines scalar relaxation contributes only to the T_2 by the same token as above and does not affect the fluorine T_1. The fluorine transition probabilities are due overwhelmingly to the spin-rotation interaction modulated by collisions. Contribution from anisotropy of the fluorine chemical shift has been shown to be negligibly small (66), $(\frac{1}{T_{1F}})_{CSA} < 10^{-2}$. In addition the fluorine relaxation rates have been found to be field-independent, within experimantal errors. Over the temperature range covered in the experiment the dipole-dipole contribution can also be neglected in comparison to the spin-rotation contribution.

In considering the contribution to relaxation by the spin-rotation interaction it is found that this interaction contains two time-dependent parts——the molecular reorientation and the angular momentum modulated by collisions. Approximate expressions have been derived (76, 77, 84, 90) for the correlation functions by assuming that the angular momentum and the orientation of the molecule are independent.* This should be a good approximation if the correlation time for the change in angular moment-

*For an alternate treatment on a less restrictive assumption, see Ref. 67, Appendix B.

um, τ_1, is very different from that for molecular reorientation, τ_2.

When $\tau_1 \ll \tau_2$, according to Kuhlmann and Baldeschwieler (84) the fluorine transition probability (k_s) between states of the same symmetry is given by

$$k_s = W_{aa'} = \frac{2}{3}\gamma_F^2 \tau_1 \left[\sum_{i,j=x,y,z} (C_{ij}^A)^2\right] \langle J_o^2 \rangle_{AV} \left| \langle a | I_{A\pm1}(F) | a' \rangle \right|^2 \qquad (5.13)$$

where $\Delta m_F = \pm 1$

$$I_{A\pm1} = \mp\frac{1}{\sqrt{2}} \left[\{I_x(1) + I_x(2)\} \pm i\{I_y(1) + I_y(2)\}\right]$$

$\langle J_o^2 \rangle_{AV}$ = the mean square angular momentum

and $\underset{\approx}{C}^A$ is the totally symmetric part of the spin-rotation interaction tensor in the molecule-fixed co-ordinate system.

For transitions between states of different symmetry, and $\tau_1 \ll \tau_2$, the antisymmetric fluorine transition probability (k_a) is given by

$$k_a = W_{ab} = \frac{2}{3}\gamma_F^2 \tau_1 \left[\sum_{i,j,=x,y,z} (C_{ij}^B)^2\right] \langle J_o^2 \rangle_{AV} \left| \langle a | I_{BM}(F) | b \rangle \right|^2 \qquad (5.14)$$

where $M = \Delta m_F = \pm 1$ or 0

$$I_{BM} = I_M(1) - I_M(2)$$

and $\underset{\approx}{C}^B$ is the antisymmetric spin-rotation interaction tensor in the molecule-fixed co-ordinate system.

Thus when $\tau_1 \ll \tau_2$ the symmetric and antisymmetric transition probabilities are all governed by the same correlation time τ_1. They then have the same temperature dependence and their ratio is

independent of temperature but depends on the magnitudes of the symmetric and antisymmetric spin-rotation interaction tensors.

When $\tau_1 >> \tau_2$, Kuhlmann and Baldeschwieler (84) showed that the symmetric transition probability depends on both τ_1 and τ_2, (τ_1 will dominate due to the condition $\tau_1 >> \tau_2$ unless the spin-rotation interaction tensor is very anisotropic) and the anitsymmetric transition probability is dominated by τ_2. Thus k_s and k_a will show different temperature dependence.

From our plot (Fig. 5-6) the fluorine transition probabilities, due predominantly to spin-rotation interaction, show marked differences in the temperature dependence from that of the dipole-dipole interaction as expected from theories. For both of the systems the k_s and k_a lines are parallel showing the same temperature dependence. It is thus apparent that within the framework of the theory the condition $\tau_1 << \tau_2$ holds for both CH_2F_2 and CHF_2Cl between 217° and 315°K. At 315°K values of τ_1 and τ_2 calculated from experimental relaxation rates show confirmatively that $\tau_1 << \tau_2$ (see Table XIII). For lower temperatures the condition must be true as τ_1 decreases while τ_2 increases as the temperature drops. The ratios between the symmetric and antisymmetric transition probabilities are independent of temperature and for CHF_2Cl

$$\frac{k_a}{k_s} = \frac{C_{xx}^2 + C_{yy}^2 + C_{zz}^2 + C_{yz}^2 + C_{zy}^2}{C_{xy}^2 + C_{xz}^2 + C_{yx}^2 + C_{zx}^2} \approx 13$$

and for CH_2F_2

$$\frac{k_s}{k_a} = \frac{C_{xx}^2 + C_{yy}^2 + C_{zz}^2}{C_{xz}^2 + C_{zx}^2} \approx 9.$$

The symmetric and antisymmetric spin-rotation interaction tensors for the systems are shown in Appendix C.

In ordinary longitudinal relaxation processes the relaxation rate R_1 is made up of both the symmetric and antisymmetric transition probabilities. For both CHF_2Cl and CH_2F_2 the indirectly found fluorine transition probabilities k_s and k_a at 315°K add up to be equal, within experimental errors, to the directly measured R_{1F} at the same temperature (see Tables X and XI).

In our experiment the fluorine longitudinal relaxation rate R_{1F} in CHF_2Cl is found to be greater than that for CH_2F_2.

$$\frac{R_{1F}(CHF_2Cl)}{R_{1F}(CH_2F_2)} = \frac{.490}{.415} = 1.18.$$

Hubbard's isotropic rotation theory (76) of spin-rotation relaxation in liquids shows that for a particular temperature the spin relaxation rates are proportional to $C^2I\tau_1$ in the extreme narrowing limit. Since τ_1 is proportional to I/τ_2 for a particular temperature (76)

$$(R_{1F})_{SR} \alpha \frac{C^2I^2}{\tau_2}$$

using the values of C, I and τ_2 obtained separately from other sources

$$\frac{(\frac{C^2I^2}{\tau_2})CHF_2Cl}{(\frac{C^2I^2}{\tau_2})CH_2F_2} = 1.10,$$

in reasonably good agreement to the experimental ratio of 1.18.

Transient homonuclear Overhauser experiments* done on the protons of the systems show that the rate for a transition to attain a new steady state when another transition is irradiated by a strong H_2 is much faster than the rate of return of the transition to thermal equilibrium when H_2 is removed. The time required for 'heating' up is found to be comparable to the T_{1F}'s, while that for 'cooling' down comparable to the T_{1H}'s. This is because that the rate-controlling steps are different for the two transient processes. The rate of attaining a new steady state in the presence of H_2 is determined primarily by the fluorine relaxation probability, while the rate of return to thermal equilibrium is determined by the proton relaxation probabiltiy.

The rotary-echo method used in the present study gives quite similar results as the other indirect method using one observing and one irradiating fields of different intensity. Essentially the method reported here employs the same rf field both for irradiating and for observing. Thus this method provides a straightforward though indirect means of studying spin-rotation relaxation in liquids.

---

*Double resonance experiments performed on a Varian HA100 high-resolution NMR spectrometer.

CHAPTER VI

A CHALLENGING SYSTEM

N,N-DIMETHYL-2,3-DIHYDROXY-3-PHENYLPROPIONAMIDE

$\Phi CH(OH)CH(OH)CON(CH_3)_2$

This compound is a very interesting system. It has two dissimilar asymmetric carbon atoms and therefore exhibits optical isomerism and at the same time diastereoisomerism. There are altogether four isomers, the d-erythro, the l-erythro, the d-threo and the l-threo forms. Not considering the isomeric modifications, each isomer in itself presents a sufficiently challenging system. It has lone pairs of electrons on the oxygen and nitrogen atoms in the amido group and can act as a ligand. Being an amide, the C-N bond has a partial double bond character hindering internal rotation about that bond. The two vicinal hydroxyl groups give an interesting research idea about proton exchange in the glycol. In the following sections, we venture to take a further look into the above mentioned properties.

A. Preparation of the Compound

Attempts to prepare dl-erythro-N,N-dimethyl-2,3-dihydroxy-3-phenylpropionamide by the usual organic peracid hydroxylation of dl-trans-N,N-dimethylcinnamamide gave unexpectedly a 40:60 mixture of both diastereomers, the threo form being predominant. The anomaly prompted a closer investigation of each of the inter-

A non-stereospecific alkene hydroxylation. Stereochemistry of the ring opening of *dl-cis-* and *dl-trans-N,N*-dimethyl-3-phenylglycidamide by acids

S. O. CHAN AND E. J. WELLS
Chemistry Department, Simon Fraser University, Burnaby, British Columbia
Received December 28, 1966

Attempts to prepare *dl-erythro-N,N*-dimethyl-2,3-dihydroxy-3-phenylpropionamide by the usual organic peracid hydroxylation of *dl-trans-N,N*-dimethylcinnamamide gave unexpectedly a 40:60 mixture of both diastereomers, the *threo* form being predominant. The anomaly prompted a closer investigation of each of the intermediate stages in the overall hydroxylation process. Epoxidation of *dl-trans-N,N*-dimethylcinnamamide by monoperphthalic acid gave only *dl-trans-N,N*-dimethyl-3-phenylglycidamide. Opening of the epoxide ring by acids gave a mixture of *dl-erythro* and *dl-threo* diols in a ratio of 40:60. *cis-N,N*-Dimethyl-3-phenylglycidamide, when subjected to the same ring-opening processes, also gave a mixture, but in a ratio of 75:25.

Canadian Journal of Chemistry. Volume **45**, 2123 (1967)

The hydroxylation of an alkene by acid-catalyzed hydrolytic cleavage of the epoxide ring initially given by the reaction with organic peracids is commonly regarded (1–3) as leading stereospecifically to *trans* addition. In this paper we draw attention to an olefinic system which yields predominantly the *cis* addition product when subjected to this treatment.

Hydroxylation

dl-trans-N,N-Dimethylcinnamamide (*trans* I), m.p. 94–95 °C, was hydroxylated by the standard method with hydrogen peroxide and formic acid (**4**). The epoxide II that was first formed was rapidly opened in the formic acid solvent to give the hydroxy formyloxy compound III. Hydrolysis of the monoformate III with base gave *N,N*-dimethyl-2,3-dihydroxy-3-phenylpropionamide (IV). IV, after recrystallization from benzene, melted sharply at 92–93 °C; the product could not be separated by thin-layer or column chromatography on alumina.

The 60 MHz proton magnetic resonance spectrum of IV in $CDCl_3$ or D_2O at 42 °C displays not one but two *N*-methylamide doublets around τ 7.2 of different intensity, the intensity ratio being independent of temperature over the range −50 (in $CDCl_3$) to +200 °C (in molten neat product). The splitting within each pair is the normal amide chemical shift caused by the magnetic anisotropy of the carbonyl bond, and by hindered rotation about the carbon–nitrogen bond (5–7). The coalescence temperature for both pairs was 60–65 °C in $CDCl_3$, and 75–80 °C in D_2O. The two lines remaining above 75 °C did not coalesce even up to 200 °C in the molten product. In addition, the proton magnetic resonance spectrum shows two AB quartets around τ 5.2 arising from the vicinal methine protons, the less intense quartet having J about 5 Hz, and the more intense having J about 6 Hz. The intensity ratio of these quartets is identical (within experimental error) with that of the *N*-methyl group. The doubling of both the *N*-methyl

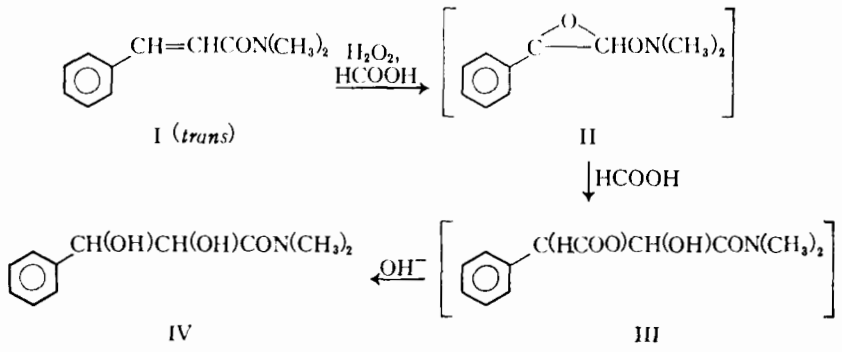

I (*trans*) II

IV III

and the vicinal methine proton spectrum cannot be ascribed to rotameric isomerization in IV caused by hindered rotation about the CH—CH bond as a result of intramolecular hydrogen bonding or by steric factors, etc., because (*i*) the intensity ratio is temperature independent (8), (*ii*) the observed value for $J_{H_\alpha H_\beta}$ (5–6 Hz) is indicative of an averaged vicinal coupling over the three rotamers (9, 10), and (*iii*) the hydroxyl proton resonance in $CDCl_3$ at $\tau \approx 6.2$ shows no evidence of a strong intramolecular hydrogen bond (11).

We therefore ascribe the doubling observed in the spectrum of IV to a mixture of diastereomers. Specific *trans* hydroxylation of *trans* I would yield *erythro* IV, whereas non-stereospecific hydroxylation gives both the *erythro* and *threo* isomers. Integration of the peak heights in the nuclear magnetic resonance spectra of three independently prepared samples yielded a relative intensity ratio of $1:(1.5 \pm 0.2)$ for the two isomer concentrations.

The above interpretation was confirmed by comparison of the spectrum of IV with that of the *threo* IV (m.p. 117–118 °C) obtained by hydroxylation of *trans* I with $KMnO_4$ (12), and by mixed spectra of the two products. The proton spectrum of the *threo* isomer is identical with that of the major component of the organic peracid hydroxylation product. As a further check, the synthesis of pure *erythro* diol amide (*erythro* IV) by $KMnO_4$ hydroxylation of *cis*-*N*,*N*-dimethylcinnamamide (*cis* I) was desirable, but attempts to prepare *cis* I were unsuccessful. However, we conclude that the performic acid hydroxylation of *dl*-*trans*-*N*,*N*-dimethylcinnamamide (*trans* I) gives predominantly *cis* hydroxylation in a 60:40 ratio.

Epoxidation

To discover where the non-stereospecificity occurs, each of the individual stages involved in the overall hydroxylation process was investigated. Oxidation of *dl*-*trans*-*N*,*N*-dimethylcinnamamide (*trans* I) by monoperphthalic acid gave only *trans* epoxide (*trans* II), as expected for specific *cis* addition to the double bond (2, 3, 13–16). The *trans* epoxide was identified by comparison of its nuclear magnetic resonance spectral parameters (Table I) with those obtained by Tung *et al.* (17) for *trans*-*N*,*N*-diethyl-3-phenylglycidamide. A mixture of *cis*- and *trans*-*N*,*N*-dimethyl-3-phenylglycidamide was also prepared from benzaldehyde and *N*,*N*-dimethyl-α-chloroacetamide by Darzens condensation (17, 18); the isomers were separated by chromatography on alumina to give a light-yellow liquid (b.p. 176 °C under 3 mm pressure) and a colorless solid (m.p. 96–97 °C). The nuclear magnetic resonance spectrum of the liquid was identical with that of *trans* II prepared by epoxidation of *trans* I with monoperphthalic acid; the spectral parameters of the solid in $CDCl_3$ agreed with those for *cis*-*N*,*N*-diethyl-3-phenylglycidamide (17), and confirmed the assignment of the *cis* form to this isomer.

Epoxide Ring Opening

Treatment of *dl*-*trans*-*N*,*N*-dimethyl-3-phenylglycidamide (*trans* II) with 80% aqueous formic acid, followed by base hydrolysis, and treatment with 25% sul-

TABLE I

Nuclear magnetic resonance data at 60 MHz and 42 °C

Compound	Solvent	Chemical shifts						
		CH_3 (τ)		$\delta_{CH_3-CH_3}$ (Hz)	H_α (τ)	H_β (τ)	$\delta_{\alpha\beta}$ (Hz)	$J_{H_\alpha H_\beta}$ (Hz)
trans I	$CDCl_3$	7.01		—	3.18	2.42	45.5	15.5
trans II	$CDCl_3$	7.03	6.92	6.5	6.38	5.96	25.0	2.0
cis II	$CDCl_3$	7.29	7.12	10.0	6.13	5.79	20.5	4.5
threo IV	$CDCl_3$	7.61	7.17	26.5	5.63	5.33	18.0	6.5
	D_2O	7.41	7.27	8.5	5.32	5.21	6.5	7.0
erythro IV	$CDCl_3$	7.26	7.11	9.0	5.37	5.09	17.0	5.5
	D_2O	7.09	6.98	6.5	5.19	5.13	3.5	6.0

furic acid in aqueous acetone both gave a mixture of diastereomeric glycols (approximately 40% *erythro* (inversion) and 60% *threo* (retention), as in the performic acid hydroxylation product). Formic acid was deliberately used in the opening of the epoxide to make the reaction conditions in this isolated step as similar as possible to those involved in the hydrogen peroxide – formic acid hydroxylation process. The ring opening was repeated with dilute sulfuric acid to avoid using a base in the process. The possibility of isomerization in the alkaline hydrolysis of the glycol monoester was excluded by the observations of Curtin *et al.* (19) and by the fact that the same mixture was obtained from ring openings with and without alkaline hydrolysis. Opening of the ring in *dl-cis-N,N*-dimethyl-3-phenylglycidamide (*cis* II) with the same two processes gave approximately 75% of *erythro* IV (retention) and 25% of *threo* IV (inversion).

We point out that, in the present case, *trans* epoxide gave a mixture of diastereomeric diols when the ring was cleaved with dilute sulfuric acid, in agreement with the results of Curtin *et al.* (19) but in contrast to the results of Tung *et al.* (17), who obtained only *erythro* diol from *trans-N,N*-diethyl-3-phenylglycidamide. Our *cis* epoxide opened with more or less the same ease as the *trans*, giving also a mixture of diastereomers, again in contrast to the observation of Tung *et al.* (17), whose *cis* epoxyamide resisted ring opening under more or less the same conditions.

DISCUSSION

Epoxide ring opening has been the subject of several recent reviews (13–15). Normally the ring opening is accompanied by Walden inversion at the reaction site independently of whether the reaction is conducted in acid, neutral, or basic media. This has led Parker and Issacs (14) to formulate the mechanism in terms of either a true S_N2 process or what they call a "borderline S_N2" process, a subtle distinction being drawn between the relative proportions of bond forming and bond breaking in the transition states. However, both descriptions imply configuration inversion. Acid-catalyzed cleavage proceeds by initial protonation of the epoxide oxygen (13), but the subsequent steps in the mechanism are apparently the same as those in neutral or alkaline ring opening. In acid media the possibility of an S_N1 mechanism through a stable carbonium ion yielding mixed stereochemical products seems to be ruled out by the great stereospecificity of the process in most cases.

On the other hand, there are a number of examples of ring openings which give complete retention of configuration (19–23). These cases are characterized by having an aryl and (or) a carbonyl group directly bonded to one or both of the epoxide ring carbon atoms. For complete retention of configuration, neither the S_N2 nor the S_N1 mechanism can be the general explanation. A retention scheme resulting from two inversions at the reaction site has been proposed by Wasserman and Aubrey (22)

by invoking neighboring-group participation (24, 25).

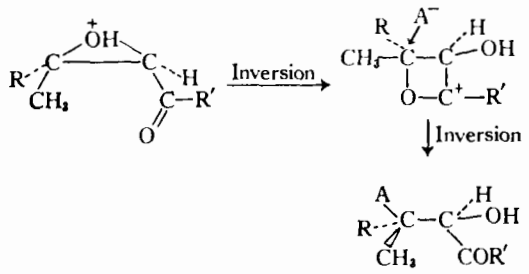

An alternative mechanism (proposed by Brewster (20)) that accounts for retention is ion-pair formation between the charged nucleophilic reagent and the charge center of the protonated oxygen and developing carbonium ion pair.

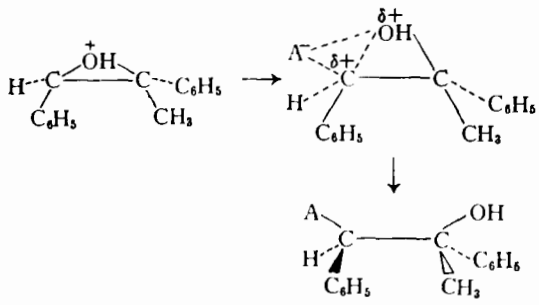

This ion-pair mechanism changes into the internal displacement mechanism (S_Ni) of Ingold (26) when the attacking ion is attached exclusively to the epoxide oxygen, and into the modified S_N2 mechanism of Parker and Isaacs (14) when the attacking ion is attached to the incipient carbonium center.

Moreover, there are several cases, in addition to the one reported here, of epoxide ring openings yielding both stereoisomeric products (19, 27–29). Again, the parent epoxides contain an aryl or carbonyl function attached to the epoxide carbon atom, and the double-inversion mechanism may be operative. Our results can be explained by the Wasserman–Aubrey sequence if the intramolecular complex at the transition state is weak, so that a balance is struck between the normal S_N2 inverting path and the path through the weak complex yielding retention. The higher specificity of the reaction from the *cis* isomer compared with that from the *trans* isomer is understandable in terms of a stabilization of the four membered ring transition complex relative to the *cis* reactant as a result of the aryl–carbonyl repulsion present in the *cis* reactant. In the case discussed here, the neighboring-group effect could operate alternatively through the lone pair on the nitrogen atom. We have no evidence to choose between the two, apart from analogy with the other carbonyl systems which give retention.

It is conceivable that the few non-stereospecific ring openings occur by an S_N1 mechanism through a stable carbonium ion. However, it is difficult to see why a carbonium ion should then not occur in those similar cases which lead specifically to retention of configuration. A related criticism may be levelled at the double-inversion process. Specific retention in the neighboring group participation scheme implies a specific stable intramolecular interaction; again, it is difficult to understand how such an interaction can compete with 100% effectiveness against the normal S_N2 process in most of the cases in which it is detectable.

Until answers to problems such as these are given, we agree with Curtin *et al.* (19) that epoxide ring openings, at present, are of dubious reliability for demonstrating configurational relationships.

EXPERIMENTAL

dl-trans-N,N-Dimethylcinnamamide (trans I)

The procedure was similar to that of Cromwell and Coughlan (30). A solution of dimethylamine (9.5 g, 0.21 mole) in 50 ml of benzene was added slowly, with constant stirring, to a solution of *trans*-cinnamoyl chloride (16.7 g, 0.1 mole) in 100 ml of benzene cooled in a water bath. After all of the amine solution had been added, the reaction mixture was stirred at room temperature for 4 h. The hydrochloride that precipitated was removed by filtration at the pump, and the filtrate was washed with two 100 ml portions of 3 *N* HCl–NaCl solution and then twice with 3 *N* NaCl solution. The benzene solution was dried over anhydrous sodium sulfate and the solvent removed under reduced pressure. The solid was recrystallized from a 50:50 mixture of benzene and petroleum ether (b.p. 65–110 °C), yield 90%, m.p. 94–95 °C.

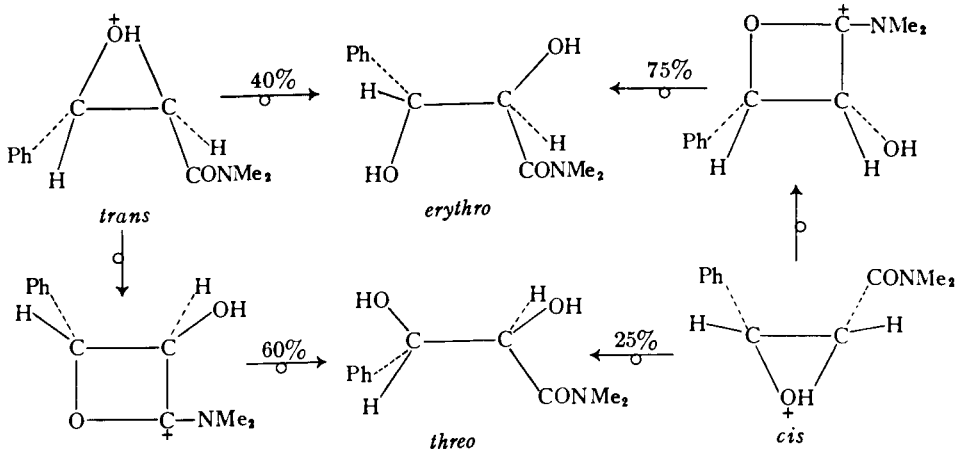

Hydroxylation of dl-trans-N,N-Dimethylcinnamamide (trans I) with Hydrogen Peroxide – Formic Acid

A solution of 17.5 g (0.1 mole) of *trans* I in 100 ml of 98–100% formic acid was cooled in a cold water bath; 25 g (~0.2 mole) of 30% hydrogen peroxide was added, with constant stirring, during about 10 min. Then the reaction mixture was kept at 40–45 °C, with constant stirring, for 24 h. The solvent was removed under reduced pressure and the residue heated under reflux with sufficient 3 *N* aqueous NaOH at 100 °C for 1 h. The product was extracted with chloroform, the extract dried, the solvent removed under reduced pressure, and the residue recrystallized from benzene, yield 40%, m.p. 92–93 °C.

dl-threo-N,N-Dimethyl-2,3-dihydroxy-3-phenylpropionamide (threo IV)

The procedure was similar to that of Boeseken (12). A solution of 17.5 g (0.1 mole) of *trans* I in 500 ml of 95% ethanol was cooled in an ice–salt bath. A solution of 18 g (0.12 mole) of $KMnO_4$ and 12 g (0.1 mole) of anhydrous $MgSO_4$ in 300 ml of water was then added during 2½ h, the temperature being kept at about −10 °C. The ice bath was removed and the reaction mixture stirred at room temperature for another 2½ h. The mixture was then filtered and the filtrate evaporated nearly to dryness under reduced pressure. The residue was treated with 250 ml of warm water and the solution filtered. The water was then removed under reduced pressure, the residue dried, and the solid recrystallized from benzene, yield 25%, m.p. 117–118 °C.

dl-trans-N,N-Dimethyl-3-phenylglycidamide (trans II)

A solution of 17.5 g (0.1 mole) of *trans* I in 100 ml of benzene was mixed with 36.5 g (0.2 mole) of monoperphthalic acid in 600 ml of ether, and refluxed for 6 h. The solvent was then removed under reduced pressure and the residue dried under vacuum. The solid was digested with 500 ml of chloroform that had been dried over anhydrous potassium carbonate, the mixture was filtered, and the solvent was removed from the filtrate, leaving a viscous oil. The oil was chromatographed on alumina, with benzene as eluent. Some unreacted *trans* I was washed down in the first portion, and the required epoxide in the following four. The epoxide was a light-yellow liquid boiling at 180 °C under 3.5 mm pressure, yield 30%.

cis- and trans-N,N-Dimethyl-3-phenylglycidamide by Darzens Condensation (17)

A solution of potassium *t*-butoxide (11.5 g, 0.103 mole) in 100 ml of dried *t*-butanol was added to a mixture of 10.6 g (0.1 mole) of benzaldehyde and 12.2 g (0.1 mole) of *N,N*-dimethyl-α-chloroacetamide under an atmosphere of nitrogen at about 10 °C during 1½ h. The reaction was allowed to proceed for another hour, and the alcohol was removed under reduced pressure. The residue was treated with 100 ml of ether and sufficient water to dissolve the potassium chloride. The ether solution was washed with saturated sodium chloride solution, dried with anhydrous sodium sulfate, and evaporated to dryness. The viscous oil was distilled under vacuum, and the fraction distilling at 170–175 °C under 3 mm pressure was collected, yield 65%.

Separation of cis and trans-N,N-Dimethyl-3-phenylglycidamide by Chromatography on Alumina

Five grams of the distilled epoxyamide was chromatographed on alumina. The series of eluents used was 50:50 hexane–benzene, benzene, 50:50 benzene–chloroform, and chloroform; 2.2 g of a light-yellow liquid was obtained from the first few portions of eluate, followed by about 0.8 g of mixed compounds and finally 1.5 g of a white solid. The yellow oil distilled at 176 °C under 3 mm pressure, and the solid, after being recrystallized from benzene, melted at 96–97 °C.

Treatment of trans-N,N-Dimethyl-3-phenylglycidamide (trans II) with Formic Acid and Sodium Hydroxide

To a mixture of 5 ml of 98–100% formic acid and 2 ml of water was added 1 g of *trans* II. The reaction mixture was kept at 40–45 °C in a water bath for

3 h and the solvent removed under reduced pressure. The residue was heated under reflux with sufficient dilute aqueous NaOH at 100 °C for 1 h. The product was extracted with chloroform, dried, and evaporated to dryness under reduced pressure. The residue was then used directly for nuclear magnetic resonance measurements without further recrystallization. The spectra showed that the sample was pure.

Treatment of trans-N,N-Dimethyl-3-phenylglycidamide (trans II) with Dilute Aqueous Sulfuric Acid

To a mixture of 10 ml of 30% sulfuric acid and 5 ml of acetone was added 1 g of *trans* II. The reaction mixture was kept at 40–45 °C in a water bath for 3 h, the solvent removed under reduced pressure, 10 ml of fresh water added, and the mixture extracted with chloroform. The chloroform extract was dried and evaporated to dryness under reduced pressure. The residue was then used for nuclear magnetic resonance measurements without further recrystallization.

Treatment of cis-N,N-Dimethyl-3-phenylglycidamide (cis II) with Formic Acid and Sodium Hydroxide

The procedure was the same as for *trans* II.

Treatment of cis-N,N-Dimethyl-3-phenylglycidamide (cis II) with Dilute Aqueous Sulfuric Acid

The procedure was the same as for *trans* II.

Nuclear Magnetic Resonance Spectra

The spectra were run on a Varian A56/60 instrument, with tetramethylsilane as an internal standard in those samples run in $CDCl_3$ at room temperature and below, and as an external standard in those samples run in D_2O.

ACKNOWLEDGMENTS

We thank Dr. Y. L. Chow for valuable discussion, and the referees for several penetrating comments that led to further work which improved our initial communication. We gratefully acknowledge a grant to E. J. W. from the National Research Council of Canada.

REFERENCES

1. D. SWERN. J. Am. Chem. Soc. **70**, 1235 (1948).
2. D. SWERN. Chem. Rev. **45**, 1 (1949).
3. D. SWERN. Org. Reactions, **7**, 378 (1953).
4. F. D. GUNSTONE. *In* Advances in organic chemistry. Vol. 1. Interscience Publishers, Inc., New York. 1960. p. 103.
5. W. D. PHILLIPS. J. Chem. Phys. **23**, 1363 (1955).
6. H. S. GUTOWSKY. Discussions Faraday Soc. **19**, 247 (1955).
7. H. S. GUTOWSKY and C. H. HOLM. J. Chem. Phys. **25**, 1228 (1956).
8. J. A. POPLE, W. G. SCHNEIDER, and H. J. BERNSTEIN. High-resolution nuclear magnetic resonance. McGraw-Hill Book Co., Inc., New York. 1959.
9. J. T. ARNOLD. Phys. Rev. **102**, 136 (1956).
10. A. A. BOTHNER-BY and R. E. GLICK. J. Chem. Phys. **25**, 362 (1956).
11. W. G. SCHNEIDER, H. J. BERNSTEIN, and J. A. POPLE. J. Chem. Phys. **28**, 601 (1958).
12. J. BOESEKEN. Rec. Trav. Chim. **47**, 683 (1928).
13. A. ROSOWSKY. *In* Heterocyclic compounds. A. Weissberger (*Editor*). Interscience Publishers, Inc., New York. 1964. Pt. 1. p. 1.
14. R. E. PARKER and N. S. ISSACS. Chem. Rev. **59**, 737 (1959).
15. S. WINSTEIN and R. B. HENDERSON. *In* Heterocyclic compounds. Vol. 1. R. C. Elderfield (*Editor*). John Wiley & Sons, Inc., New York. 1950. p. 1.
16. E. L. ELIEL. Steric effects in organic chemistry. M. S. Newman (*Editor*). John Wiley & Sons, Inc., New York. 1956. p. 106.
17. C. C. TUNG, A. J. SPEZIALE, and H. W. FRAZIER. J. Org. Chem. **28**, 1514 (1963).
18. M. S. NEWMAN and B. J. BAGERLEIN. Org. Reactions, **5**, 438 (1949).
19. D. Y. CURTIN, A. BRADLEY, and Y. G. HENDRICKSON. J. Am. Chem. Soc. **78**, 4064 (1956).
20. J. H. BREWSTER. J. Am. Chem. Soc. **78**, 4061 (1956).
21. C. C. TUNG and A. S. SPEZIALE. J. Org. Chem. **28**, 2009 (1963).
22. H. H. WASSERMAN and N. AUBREY. J. Am. Chem. Soc. **78**, 1726 (1956).
23. H. O. HOUSE. J. Org. Chem. **21**, 1306 (1956).
24. S. WINSTEIN and R. E. BUCKLES. J. Am. Chem. Soc. **64**, 2780 (1942).
25. S. WINSTEIN and R. B. HENDERSON. J. Am. Chem. Soc. **65**, 2196 (1943).
26. C. K. INGOLD. Structure and mechanism in organic chemistry. Cornell University Press, Ithaca, New York. 1953. p. 394.
27. B. WITKOP and C. M. FOLTZ. J. Am. Chem. Soc. **79**, 197 (1957).
28. C. M. FOLTZ and B. WITKOP. J. Am. Chem. Soc. **79**, 201 (1957).
29. M. SVOBODA and J. SICHER. Collection Czech. Chem. Commun. **20**, 1452 (1955).
30. N. H. CROMWELL and J. A. COUGHLAN. J. Am. Chem. Soc. **67**, 903 (1945).

mediate stages in the overall hydroxylation process. Epoxidation of dl-trans-N,N-dimethylcinnamamide by monoperphthalic acid gave only dl-trans-N,N-dimethyl-3-phenylglycidamide. Opening of the epoxide ring by acids gave a mixture of dl-erythro and dl-threo diols in a ratio of 40:60. Cis-N,N-dimethyl-3-phenylglycidamide, when subjected to the same ring-opening processes, also gave a mixture, but in ratio of 75:25. The usual trans-hydroxylation method being non-stereospecific here, the compound was finally prepared in its diastereoisomeric form viz. dl-threo-N,N-dimethyl-2,3-dihydroxy-3-phenylpropionamide by cis-hydroxylation with potassium permanganate. The details of the whole investigation have been reported in Canadian Journal of Chemistry, Volume 45, 2123-2128 (1967), a copy of the reprint being enclosed.

B. Effects of Metal Ions on the PMR of the Compound

It has been postulated that an amide is coordinated to metals via the carbonyl oxygen (91). Some researchers, however, believe in complexation via the amino nitrogen (92, 93). There have also been suggestions for an amide to be bridging or bidentate in complex formation (94, 95). Being an amide, the compound $\Phi CH(OH)CH(OH)CON(CH_3)_2$ is a potential ligand.

NMR methods have been applied to observe complex formation between metal ions and diamagnetic ligand molecules. If the metal ions are also diamagnetic, complex formation usually results

in small low field shifts of the NMR signals for the ligands. While free or unbonded diamagnetic metal ions produce negligible change in magnetic shielding they may lower the spin-lattice relaxation time of the magnetic nuclei slightly (96). If the metal ions in solution of the ligands are paramagnetic, fluctuation in the local field produced by the paramagnetic ions are great enough to broaden the absorption lines sufficiently to prevent detection unless the ions are only weakly paramagnetic or in very low concentration. This is because the electronic magnetic moments are very large (compared with those of the nuclei) and provide an efficient relaxation mechanism to shorten T_1 considerably (97). Bloembergen, Purcell and Pound (65) have derived an expression for T_1 in terms of the number N of paramagnetic ions of effective magnetic moment μ_{eff} in 1 c.c. in a solution of viscosity η as shown below.

$$\frac{1}{T_1} = 12\pi^2\gamma^2\eta N\mu_{eff}^2/5kT \qquad (6.1)$$

If the paramagnetic metal ions form complexes in solution the NMR spectrum of the nuclei in the ligand sometimes shows unusually large chemical shifts (98 - 101). These large shifts are thought to be due to a slight transfer of unpaired electron spin from the paramagnetic ion to the ligand molecule and the unpaired spin is then transmitted to the other nuclei in the ligand molecule by the contact mechanism. Also if complexation occurs in solution the apparent value of μ_{eff} will be concentration-dependent and can be used as a means of studying such equilibria. Another eff-

ect which may be used for the same purpose is the concentration-dependent shift of the NMR signals caused by the presence of paramagnetic ions (102, 103).

Some preliminary observations of the effects of the Zn^{++}, Cd^{++}, Fe^{++}, Ni^{++}, Cu^{++}, Cr^{+++}, Fe^{+++} and Mn^{++} ions on the PMR spectrum of the system $\Phi CH(OH)CH(OH)CON(CH_3)_2$ in deuterium oxide solution were done. With the diamagnetic Zn^{++} or Cd^{++} ions, solutions of the amide and metal ions in molar ratios of 1:1 and 2:1 respectively, gave no detectable shift nor broadening of the NMR signals of the ligand in deuterium oxide. The strongly paramagnetic ions, Cr^{+++}, Fe^{+++} or Mn^{++} even in quite low concentration (less than 0.05M) broaden the resonance lines to a nearly undetectable level. With Fe^{++}, Ni^{++}, or Cu^{++} ions, the resonance signals of the ligand are shifted up-field and at the same time broadened as the ion concentration increases. Variations of the chemical shift (δ) and half width at half height ($\Delta\omega_{\frac{1}{2}}$) of the signals with concentration of Fe^{++} ions in deuterium oxide solution were obtained as shown in Table XIV. For comparison, the variations of δ and $\Delta\omega_{\frac{1}{2}}$ for the absorption signal of pure water were obtained and shown in Table XV.

From these preliminary observations it is not possible to tell whether metal-amide complexes are formed in solution or not; neither can it be certain that the observed up-field shift of greater than half of a kilohertz is due to isotropic contact interactions or to the usual effects of paramagnetic ions or to an

Table XIV. Variation of Chemical shifts and half widths of proton resonances with concentration of Fe^{++} ions in D_2O solution of dl-threo-$\Phi CH(OH)CH(OH)CON(CH_3)_2$.

Fe^{++} ion concentration in mole/litre	H_2O - OH peak		Phenyl peak		N,N-dimethyl peak	
	δ hz	$\Delta\omega_{\frac{1}{2}}$ hz	δ hz	$\Delta\omega_{\frac{1}{2}}$ hz	δ hz	$\Delta\omega_{\frac{1}{2}}$ hz
0	258	1	412	1	159	1
.12	237	4.5	353	1.5	91	2
.17	193	13	221	1.5	-38	3
.25	150	18	112	2	-141	3.5
.5	38	35	-168	3	-410	4

Table XV. Variation of chemical shift and half width of the proton resonance in pure water with concentration of Fe^{++} ions.

Fe^{++} ion concentration in mole/litre	δ hz	$\Delta\omega_{\frac{1}{2}}$ hz
0	262	1.5
.12	234	4
.17	186	12
.25	145	20
.5	44	30

average effect of the two. The clarification of these points would be an interesting research problem but the techniques required for investigation are out of the scope of this work.

C. Hindered Internal Rotation

Due to magnetic anisotropy of the carbonyl bond and hindered internal rotation (see Chapter III, section A) about the carbon-nitrogen bond, the two N-methyl groups of dl-threo-$\Phi CH(OH)CH(OH)CON(CH_3)_2$ absorb at different frequencies, 155.5 hz and 164.0 hz from TMS in D_2O solution and 145 hz and 171.5 hz from TMS in $CDCl_3$ solution. On raising the temperature, the two methyl peaks collapse into one around 60-65°C in $CDCl_3$ and 75-80°C in D_2O. The coalesced line sharpens on further heating. NMR methods can be applied to study the hindered internal rotation here. Any one of the high-resolution steady-state methods can be used but with some limitations. For the case where the two peaks are wider apart the double resonance method (44, 45) is also applicable. Spin-echo methods employing high power rf pulses are not suitable as there are other protons not taking part in rotational exchange but they will be affected and sampled together with the methyl signals. On the other hand, the high-resolution rotary-echo method would be useful here as its frequency resolution makes it possible to study the methyl signals. A detailed study on this system has not yet been made. This point is raised here only to include all chemical or chemico-physical problems of interest that arise from the system $\Phi CH(OH)$-$CH(OH)CON(CH_3)_2$.

D. Proton Exchange

Another problem of interest presented by our compound is

proton exchange. The compound is a dissymmetric glycol. Apart from intramolecular exchange between the protons of the vicinal hydroxyl groups, intermolecularly there can also be direct and cross exchange between similar and dissimilar sites respectively in different molecules as shown in the following scheme:

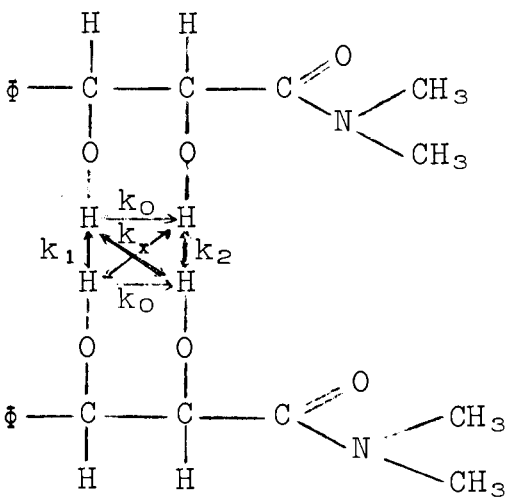

There are altogether four different exchange rates. They can be sorted out presumably by studying the differential collapse of the $J_{\underline{H}C\underline{O}\underline{H}}$ couplings in the basic AB pattern of the methine protons, or in the resonances of the hydroxyl protons or both.

Detailed studies along these lines have not been made but some interesting effects of differential proton exchange in the AB spectrum of the methine protons have been observed. Fig. 6-1 shows a sequence of temperature runs from 40° to 120°C of the AB methine proton and the hydroxyl proton resonances of the glycol in acetonitrile solution. At 40°C the exchange among the hydroxyl protons is moderately slow. The spectrum of the AB methine protons, each coupled to a hydroxyl proton, is not resolved and

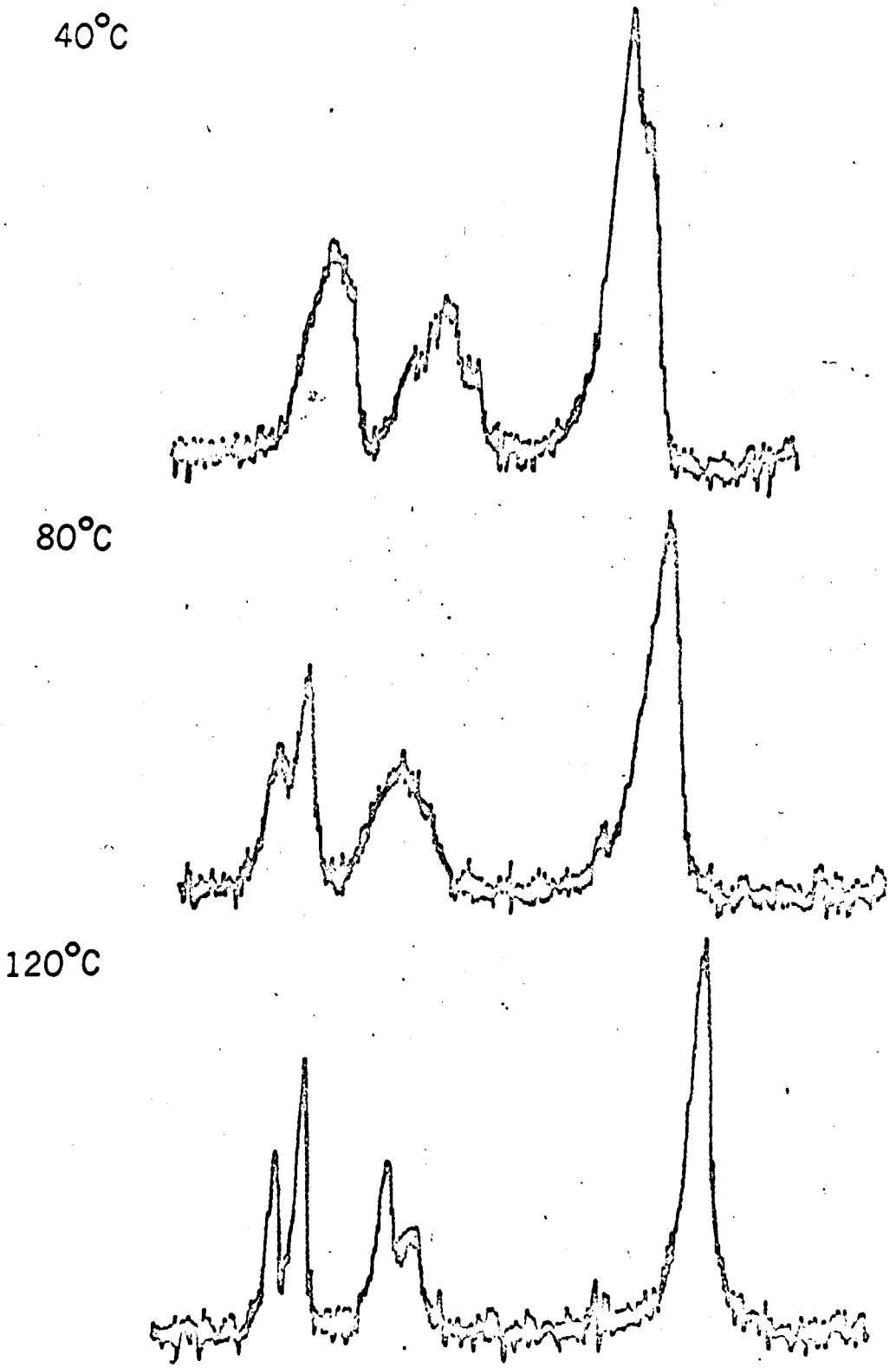

Fig. 6-1. The methine and hydroxyl proton resonances of dl-threo-ΦCH(OH)CH(OH)CON$(CH_3)_2$ in CH_3CN solution.

consists of two broad peaks corresponding to the A and B proton transitions respectively ($\delta\nu_0/J_{H_AH_B} \approx 3$). The hydroxyl proton resonances are also broad and nearly degenerate and appear as an overlapping of two unresolved doublets. As the exchange rates increase when the temperature is raised, the hydroxyl proton resonance sharpens up and the AB quartet begins to emerge but the A part and B part sharpen up at different rates reflecting the difference in the exchange rates k_1 and k_2.

In N,N-dimethylformamide solution, the methine protons and the hydroxyl protons of the glycol have more or less the same chemical shifts at 40°C. The spectrum consists of only non-resolvable broad features overlapping each other. Addition of traces of pyridine to the solution speeds up the exchange considerably and the AB quartet comes out distinctly on top of the hydroxyl proton resonances (Fig. 6-2). Lowering the temperature slows down the exchange and the coupling of a hydroxyl proton to each of the AB methine protons complicates the AB quartet which finally becomes broad and unresolved again. The differential exchange effect is not as distinct in this N,N-dimethylformamide solution as in the acetonitrile solution. A choice of the right solvent will therefore facilitate the study considerably.

In general, the difficulties in the present case are the temperature dependence of the hydroxyl proton resonances and the shift degeneracies among the methine and hydroxyl protons or between the hydroxyl protons alone. The shifting of the hydroxyl

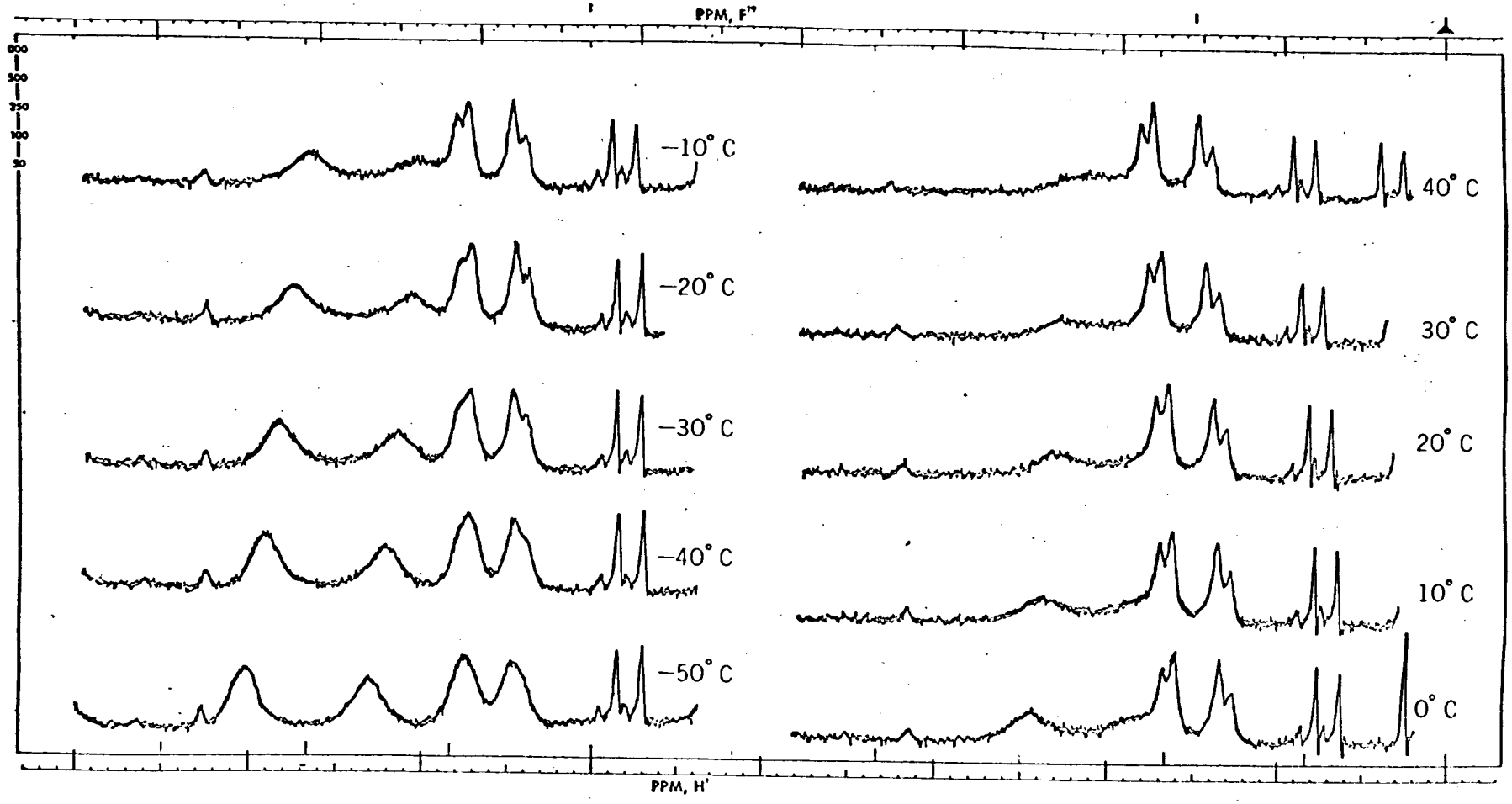

Fig. 6-2. The methine and hydroxyl proton resonances of dl-threo-$\Phi CH(OH)CH(OH)CON(CH_3)_2$ in $HCON(CH_3)_2$ solution.

proton resonances up-field as the temperature is increased is due to a varying extent of hydrogen bonding among the hydroxyl protons (104, 105). This effect, together with the shift degeneracies, makes the extraction of exchange data from NMR measurements harder. In conclusion, the present problem is complicated but interesting. Solution of such a problem requires high resolution and precision. The method of total line shape analysis of a high-resolution spectrum by computer is preferable but the selective rotary-echo method may provide an alternate way.

CHAPTER VII

SUMMARY AND CONCLUSION

The high-resolution NMR rotary-echo technique is a modification of Solomon's rotary-echo experiment. The difference is essentially in the means of obtaining a relative 180° phase change between the field H_1 and the y-component of the magnetization vector in the frame rotating at the Larmor frequency. The modified method proves to be particularly simple to apply with commercially available high-resolution NMR spectrometer and offers some advantages in echo amplitude stability. The effects of radiation damping are refocussed to first order and that the effects of molecular self-diffusion through the H_1 field gradients can be removed as in the Carr-Purcell spin-echo method.

A general theoretical treatment for the decay of the rotary-echo train is made. It is obtained that for γH_1 much larger than the natural relaxation rates involved, the rotary echoes decay exponentially to good approximation. The solution for the on-resonance rotary-echo decay can be obtained exactly but the off-resonance case is still unsolved. The effects of the inhomogeneities ΔH_0 in the static field H_0 can be made negligible as long as H_1 is larger than ΔH_0. Nuclear Overhauser effects arising from cross relaxation among the z-components of two or more spectral magnetization vectors does not affect the rotary-echo decay if none of the other magnetization vectors is much larger

than the one under observation and if γH_1 is much larger than the cross relaxation rate involved.

Exchange effects in high-resolution rotary echoes are considered. Due to the complexity of the problem closed formulae to include chemical exchange are still to be found but approximate equations for special limiting cases have been derived. Hindered internal rotation about the carbon-nitrogen bond in N,N-dimethylcarbamyl chloride (DMCC) and N,N-dimethylnitrosamine (DMNA) is studied. Activation energies and frequency factors of 15.1 and 25.0 kcal/mole and 2.70×10^{11} and 2.99×10^{13} sec^{-1} respectively are obtained for DMCC and DMNA respectively. These results are comparable to the spin-echo results and to some recent results of the high-resolution steady-state methods. The rotary-echo method, in chemical exchange studies, can cover quite a large overall range of exchange rates but it suffers from the drawback of requiring the knowledge of the relaxation times and in some cases, the chemical shift to determine exchange rates. Sometimes errors in the determination of the intermediate parameters may affect considerably the accuracy of the exchange rates obtained.

In rotary-echo experiments pulsing at sub-audio frequencies, it is found that the rotary-echo decay is sensitive to unresolved scalar coupling to quadrupolar nuclei. The method has been applied to determine the coupling constants $J_{\underline{H}C\underline{C}N}$ in acetonitrile (CH_3CN) and $J_{\underline{H}C\underline{C}l}$ in chloroform ($CHCl_3$). The results

obtained are in good agreement to those obtained by other researchers with other means.

The fluorine spin-rotation relaxation in liquid chlorodifluoromethane (CHF_2Cl) and difluro m ethane (CH_2F_2) has also been studied. An indirect method is used in which the fluorine transition probabilities are determined by observing only the resonances of the protons to which the fluorines are scalarly coupled. The method is based on the idea that the natural linewidths of the proton resonances are dominated by the rapid relaxation by spin-rotation interaction of the fluorine nuclei. With the elimination of magnetic inhomogeneity effects by the high-resolution rotary-echo method differential linewidths are observed among the proton triplet. Analytical equations are derived which lead to the determination of the fluorine transition probabilities from the rotary-echo decay rates R_{2rH} for the proton resonances. The symmetric and antisymmetric fluorine transition probabilities k_s and k_a respectively for the two systems are found at various temperatures ranging from 217° to 315°K. The same temperature dependences of k_s and k_a show that the correlation time τ_1 for the change in angular momentum is much shorter than the correlation time τ_2 for molecular reorientation. The ratios k_s/k_a are found to be about 13 for CHF_2Cl and about 9 for CH_2F_2 independent of temperature. Essentially this present method gives quite similar information as the double resonance method of Kuhlmann and Baldeschwieler.

In conclusion, the high-resolution NMR rotary-echo technique affords a frequency selective method for the study of slow relaxation properties of individual transitions in a high-resolution NMR spectrum. It has, in general, wide applications to problems of chemical exchange, heteronuclear relaxation, etc. To date the method is still in its first stage of developement. Regarding the instrumentation, the switching transients have to be further suppressed to give a better echo sequence. So far, only sufficiently concentrated solutions or neat liquids which give moderately strong signals can be used to give reasonably good echo sequences. To study weaker signals, the signal to noise ratio has yet to be improved. On the theoretical side, mathematical presentations of the rotary-echo decay with or without exchange for signals on or off resonance have to be refined. We believe that this method will acquire an important position in the NMR field as improvements along the above mentioned lines are made.

BIBLIOGRAPHY

BIBLIOGRAPHY

(1) E. M. Purcell, H. C. Torrey and R. V. Pound, Phys. Rev., 69, 37 (1946).

(2) F. Bloch, W. W. Hansen and M. E. Packard, Phys. Rev., 69, 127 (1946).

(3) A. Allerhand and H. S. Gutowsky, J. Chem. Phys., 41, 2115 (1964)..

(4) E. L. Hahn, Phys. Rev., 77, 297 (1950).

(5) E. L. Hahn, Phys. Rev., 80, 580 (1950).

(6) H. Y. Carr and E. M. Purcell, Phys. Rev., 94, 630 (1954).

(7) I. Solomon, Phys. Rev Letters, 2, 301 (1959).

(8) E. J. Wells and K. H. Abramson, Journal of Magnetic Resonance (to be published).

(9) S. Meiboom and D. Gill, Rev. Sci. Instr., 29, 688 (1958).

(10) H. C. Torrey, Phys. Rev., 76, 1059 (1949).

(11) N. Bloembergen and R. V. Pound, Phys. Rev., 95, 8 (1954).

(12) C. R. Bruce, R. E. Norberg and G. E. Pake, Phys. Rev., 104, 419 (1956).

(13) S. Bloom, J. Applied Phys., 28, 800 (1957).

(14) A. Szoke and S. Meiboom, Phys. Rev., 113, 585 (1959).

(15) A. Abragam, "Principles of Nuclear Magnetism", Oxford University Press, London, 1961, p. 73.

(16) W. R. Smythe, "Static and Dynamic Electricity", McGraw-Hill Inc., New York, 1950, p. 271.

(17) "Handbook of Chemistry and Physics", 49th Ed., Chemical Rubber Publishing Co., Cleveland, 1968, p. A-167.

(18) F. Bloch, Phys. Rev., 70, 460 (1946).

(19) H. S. Gutowsky, R. L. Vold and E. J. Wells, J. Chem. Phys., 43, 4107 (1965).

(20) A. W. Overhauser, Phys. Rev., 92, 411 (1953).

(21) I. Solomon, Phys. Rev., 99, 559 (1955).

(22) I. Solomon and N. Bloembergen, J. Chem. Phys., 25, 261 (1956)..

(23) R. Kaiser, J. Chem. Phys., 42, 1838 (1965).

(24) M. Cocivera, J. Chem. Phys., 47, 1112 (1967).

(25) A. A. Brooks, J. D. Cutnell, E. O. Stejskal and V. W. Weiss, J. Chem. Phys., 49, 1571 (1968).

(26) L. Pauling, "The Nature of the Chemical Bond", 3rd. Ed., Cornell University Press, Ithaca, New York, 1960, p. 207.

(27) A. Lowenstein and T. Connor, Ber. Bunsenges Physik Chem., 67, 280 (1963).

(28) M. T. Rogers and J. C. Woodbrey, J. Phys. Chem., 66, 540 (1962)..

(29) E. Krakower, Ph. D. Thesis, University of British Columbia (1966)..

(30) R. C. Neuman, Jr., D. N. Roark and V. Jonas, J. Am. Chem. Soc., 89, 3412 (1967)..

(31) W. D. Phillips, Ann. N. Y. Acad. Sci., 70, 817 (1958).

(32) D. J. Blears, J. Am. Chem. Soc., Supp. 2, 6256 (1964).

(33) K. H. Abramson, P. T. Inglefield, E. Krakower and L. W. Reeves, Can J. Chem., 44, 1685 (1966).

(34) A. Allerhand, H. S. Gutowsky, J. Jonas and R. Meinzer, J. Am. Chem. Soc., 88, 3185 (1966).

(35) E. L. Hahn and D. E. Maxwell, Phys. Rev., 88 1070 (1952)..

(36) H. M. McConnell, J. Chem. Phys., 28, 430 (1958).

(37) L. Piette and W. A. Anderson, J. Chem. Phys., 30, 899 (1959)..

(38) M. Bloom, L. W. Reeves and E. J. Wells, J. Chem. Phys., 42, 1615 (1965).

(39) W. A. Anderson, "NMR and EPR Spectroscopy", Pergamon Press, New York, 1960, Chap. 12.

(40) Ref. 15, p. 309.

(41) G. Binsch, J. B. Lambert, B. W. Roberts and J. D. Roberts, J. Am. Chem. Soc., 86, 5564 (1964).

(42) W. B. Moniz and H. S. Gutowsky, J. Chem. Phys., 38, 1155 (1963).

(43) Y. Saito, Can. J. Chem., 43, 2530 (1965).

(44) S. Forsén and R. A. Hoffman, J. Chem. Phys., 39, 2892 (1963).

(45) S. Forsén and R. A. Hoffman, J. Chem. Phys., 40, 1189 (1964).

(46) D. E. Woessner, J. Chem. Phys., 35, 41 (1961).

(47) L. W. Reeves and E. J. Wells, Disc. Far. Soc., 34, 177 (1962).

(48) Z. Luz and S. Meiboom, J. Chem. Phys., 39, 366(1963).

(49) J. G. Powles and J. H. Strange, Mol. Phys., 8, 169 (1964).

(50) A. Allerhand and H. S. Gutowsky, J. Chem. Phys., 42, 1587 (1965).

(51) A. Allerhand and H. S. Gutowsky, J. Chem. Phys., 42, 4203 (1965).

(52) A. Allerhand and E. Thiele, J. Chem. Phys., 45, 902 (1966).

(53) T. P. Das and E. L. Hahn, in "Nuclear Quadrupole Resonance Spectroscopy in Solid-State Physics", edited by F. Seitz and D. Turnbull, Academic Press Inc., New York, 1958, Suppl. 1.

(54) Ref. 15, p. 313.

(55) R. Freeman, R. R. Ernst and W. A. Anderson, J. Chem. Phys., 46, 1125 (1967).

(56) J. Winter, Compt. Rend., 249, 1346 (1959).

(57) Ref. 15, p. 332.

(58) N. Boden, J. Deck, E. Gore and H. S. Gutowsky, J. Chem. Phys., 45, 3875 (1966).

(59) H. S. Gutowsky, L. H. Meyer and D. W. McCall, J. Chem. Phys., 23, 982 (1955).

(60) H. M. McConnell, C. A. Reilly and A. D. McLean, J. Chem. Phys., 24, 479 (1956).

(61) N. F. Ramsey and E. M. Purcell, Phys. Rev., 85, 143 (1952).

(62) C. H. Townes and A. L. Schawlow, "Microwave Spectroscopy", McGraw-Hill, Inc., New York, 1955, p. 217.

(63) J. M. B. Kellogg, I. I. Rabi, N. F. Ramsey and J. R. Zacharias, Phys. Rev., 56, 728 (1939).

(64) J. M. B. Kellogg, I. I. Rabi, N. F. Ramsey and J. R. Zacharias, Phys. Rev., 57, 677 (1940)..

(65) N. Bloembergen, E. M. Purcell and R. V. Pound, Phys. Rev., 73, 679 (1948)..

(66) R. J. C. Brown, H. S. Gutowsky and K. Shimomura, J. Chem. Phys., 38, 76 (1963).

(67) M. Bloom, F. Bridges and N. N. Hardy, Can. J. Phys., 45, 3533 (1967)..

(68) C. S. Johnson and J. S. Waugh, J. Chem. Phys., 35, 2020 (1961)..

(69) C. S. Johnson, J. S. Waugh and J. N. Pinkerton, J. Chem. Phys., 35, 1128 (1961)..

(70) G. W. Flynn and J. D. Baldeschwieler, J. Chem. Phys., 37, 2907 (1962).

(71) H. S. Gutowsky, I. J. Lawrenson and K. Shimomura, Phys. Rev. Letters, 6, 349 (1961)..

(72) H. S. Gutowsky and D. E. Woessner, Phys. Rev., 104, 843 (1956)..

(73) N. F. Ramsey, "Nuclear Moments", John Wiley & Sons, Inc., New York, 1953, p. 73.

(74) C. S. Johnson and J. S. Waugh, J. Chem. Phys., 36, 2266 (1962)..

(75) G. T. Needler and W. Opechowski, Can. J. Phys., 39, 870 (1961).

(76) P. S. Hubbard, Phys. Rev., 131, 1155 (1963).

(77) W. T. Huntress, Jr., J. Chem. Phys., 48, 3524 (1968).

(78) M. Lipsicas and M. Bloom, Can. J. Phys., 39, 881 (1961).

(79) M. Bloom and R. Dorothy, Can J. Phys., 45, 3411 (1967).

(80) J. H. Chaffin III and P. S. Hubbard, J. Chem. Phys., 46, 1511 (1967).

(81) C. MacLean, E. L. Mackor and C. W. Hilbers, J. Chem. Phys., 46, 3393 (1967).

(82) M. Bloom and H. S. Sandhu, Can J. Phys., 40, 289 (1962).

(83) F. Bloch, Phys. Rev., 102, 104 (1956).

(84) K. F. Kuhlmann and J. D. Baldeschwieler, J. Chem. Phys., 43, 572 (1965).

(85) Y. Kanazawa, J. Chem. Phys., 47, 5357 (1967).

(86) G. W. Flynn and J. D. Baldeschwieler, J. Chem. Phys., 38 226 (1963).

(87) D. K. Hindermann and C. D. Cornwell, J. Chem. Phys., 48, 4148 (1968).

(88) N. F. Ramsey, Phys. Rev., 78, 699 (1950).

(89) W. H. Flygare, J. Chem. Phys., 41, 793 (1964).

(90) P. W. Atkins, Mol. Phys., 12, 133 (1967).

(91) W. E. Bull, S. K. Madan and J. E. Willis, Inorg. Chem., 2, 303 (1963).

(92) M. Martinette, S. Mizushima and J. V. Quagliano, Spectrochim. Acta, 15, 77 (1959).

(93) M. M. Fein, J. Green, J. Robinski and M. S. Cohen, Inorg. Chem., 4, 583 (1965).

(94) K. W. Bagnall, D. Brown and A. M. Deane, J. Chem. Soc., 1611 (1961).

(95) A. J. Carty and D. G. Tuck, J. Chem. Soc., Suppl. 2, 6012 (1964).

(96) S. Brcersma, Bull. Amer. Phys. Soc., 30, 43 (1955).

(97) L. O. Morgan, J. Murphy and P. E. Cox, J. Am. Chem. Soc., 81, 5043 (1959).

(98) H. M. McConnell and D. B. Chesnut, J. Chem. Phys., 28, 107 (1958).

(99) H. M. McConnell and C. H. Holm, J. Chem. Phys., 27, 314 (1957).

(100) D. R. Eaton, A. D. Josey, W. D. Phillips and R. E. Benson, Mol. Phys., 5, 407 (1962).

(101) R. S. Milner and L. Pratt, Disc. Far. Soc., 34, 88 (1962).

(102) P. Grivet and Y. Ayant, Compt. Rend., 232, 1094 (1951).

(103) D. F. Evans, J. Chem. Soc., 2003 (1959).

(104) J. T. Arnold and M. E. Packard, J. Chem. Phys., 19, 1608 (1951).

(105) U. Liddel and N. F. Ramsey, J. Chem. Phys., 19, 1608 (1951).

APPENDICES

APPENDIX A

PHENOMENOLOGICAL TREATMENT OF EXCHANGE BETWEEN TWO SITES

The average fractional loss of magnetization for every transfer of spins from one site to another can be obtained by taking the mean over a cycle of the fractional loss of magnetization $F(\theta)$ when a transfer occurs with an original phase angle θ of the magnetization vector, provided the following conditions hold:

$$k \ll \omega_1 \qquad (A.1)$$

$$k \ll \frac{1}{2\tau} \quad . \qquad (A.2)$$

Condition (A.1) assures that there is a chance for a transfer at any value of θ between $0°$ and $360°$, while condition (A.2) assures that the chance for one particular spin to undergo more than one transfer between two pulses is negligible.

(a) For transfers from the on-resonance site to the off-resonance site

Fig. A-1 shows the projection of the precession paths of the on- and off-resonance magnetization vectors on the xz-plane, the y-axis being perpendicular to the xz-plane and pointing outwards. Starting from OA at $t = 0$, the on-resonance vector precesses in a circle about H_1 and is represented by AOK while the off-resonance vector precesses in a cone about H_{eff} represented by OAL. Consider a transfer from on-resonance to off-resonance at an angle θ where θ is the phase angle attained when the vec-

tor precesses about H_1 from OA to OB. After the transfer the vector will precess about H_{eff} in a cone represented by OFG. The phase angle φ of OB with respect to the new cone of precess-

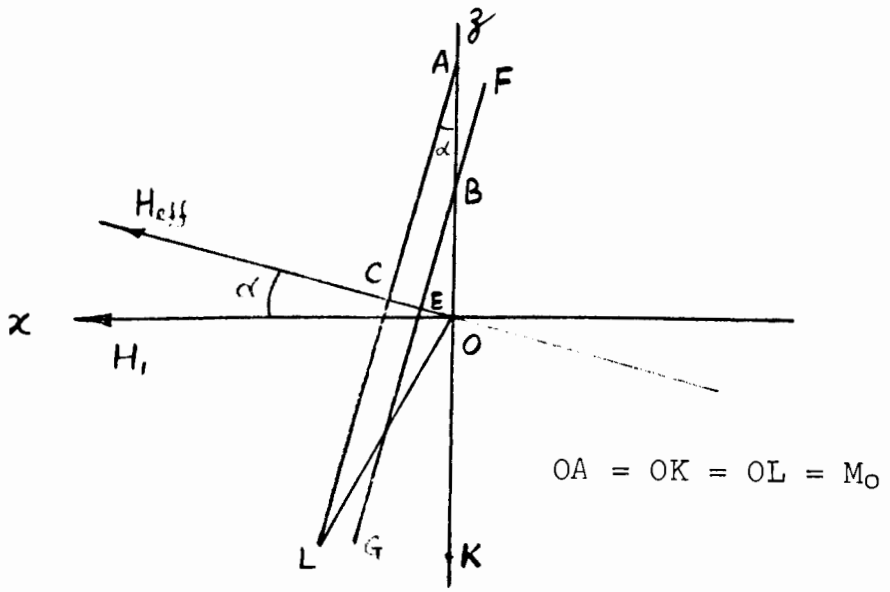

Fig. A-1. Projection of the precession paths of the magnetization vectors on the xz-plane.

ion is given by

$$\tan \varphi = \frac{M_o \sin\theta}{M_o \cos\theta \cos\alpha} = \frac{\sin\theta}{\cos\theta\cos\alpha} \qquad (A.3)$$

and

$$FE = M_o \sqrt{\sin^2\theta + \cos^2\theta\cos^2\alpha}\ . \qquad (A.4)$$

There is also a phase change $(\varphi - \theta)$ in the transfer. If

$$\frac{\omega_1}{(\omega_1^2 + \delta^2)^{\frac{1}{2}}} \approx 1,$$

the loss of magnetization is mainly due to the phase difference resulting from the transfer and the effective new amplitude after the transfer for the vector of original amplitude M_o is $FE\cos(\varphi - \theta)$. Simplifying, we get

$$\text{new effective amplitude} = M_o(\cos^2\theta\cos\alpha + \sin^2\theta).$$

Therefore, the decrease of magnetization due to one transfer

$$= M_o(1 - \cos^2\theta\cos\alpha - \sin^2\theta)$$

$$= 2M_o\sin^2\frac{\alpha}{2}\cos^2\theta$$

and the fractional loss $F(\theta)$ is given by

$$F(\theta) = 2\sin^2\frac{\alpha}{2}\cos^2\theta \qquad (A.5)$$

for a transfer occurring at an original phase angle θ.

(b) For transfers from the off-resonance site to the on-resonance site

Similar treatment as the above leads to fractional loss

$$F(\theta) = 2\sin^2\frac{\alpha}{2}\cos^2\theta - \sin\alpha\tan\alpha\cos\theta. \qquad (A.6)$$

Taking the mean over a complete cycle and since

$$\frac{1}{2\pi}\int_o^{2\pi}\cos\theta d\theta = 0 \quad \text{and}$$

$$\frac{1}{2\pi}\int_o^{2\pi}\cos^2\theta d\theta = \frac{1}{2},$$

the mean fractional loss for a correlated transfer (A→B and B→A simultaneously) between two sites is equal to $\sin^2\frac{\alpha}{2}$

where $\alpha = \tan^{-1}(\frac{\delta}{\omega_1})$.

APPENDIX B

INERTIA TENSORS FOR CHF_2Cl AND CH_2F_2

(a) Chlorodifluoromethane (CHF_2Cl)

With reference to Fig. B-1 and using the known atomic and molecular parameters shown therein, the elements of the inertia tensor for chlorodifluoromethane (CHF_2Cl) are obtained.

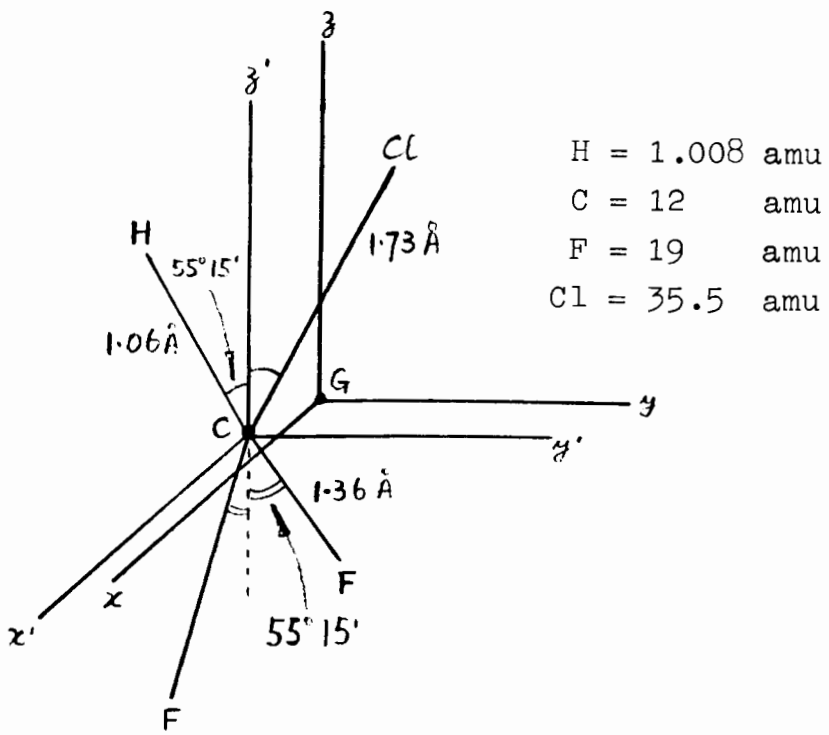

Fig. B-1. The CHF_2Cl molecule.

The primed frame has its origin at the central carbon atom and the y'z'-plane is a plane of symmetry of the molecule. The two fluorine atoms fall in the x'z'-plane. By the principle of moments and by symmetry, the centre of gravity G of the system is found at (0, 0.573, 0.071 in Å). The frame having its

origin at G is unprimed and has all its axes parallel to those of the primed frame. With reference to the frame at G, the inertia tensor $\underset{\approx}{I}(G)$ for the molecule is found to be

$$\underset{\approx}{I}(G) \approx \begin{bmatrix} 101 & 0 & 0 \\ 0 & 105 & -46 \\ 0 & -46 & 95 \end{bmatrix} \text{ amuÅ}^2. \qquad \text{(B.1)}$$

Diagonalization of (B.1) results in the inertia tensor $\underset{\approx}{I}(P)$ with respect to the principal axes of reference for the molecule as given by

$$\underset{\approx}{I}(P) \approx \begin{bmatrix} 101 & 0 & 0 \\ 0 & 146 & 0 \\ 0 & 0 & 53 \end{bmatrix} \text{ amuÅ}^2. \qquad \text{(B.2)}$$

The principal axes are obtained by a rotation about the x-axis in the counterclockwise direction through an angle of about 42°.

(b) Difluoromethane (CH_2F_2)

With reference to Fig. B-2 and using the known atomic and molecular parameters shown therein, the elements of the inertia tensor for the system are calculated.

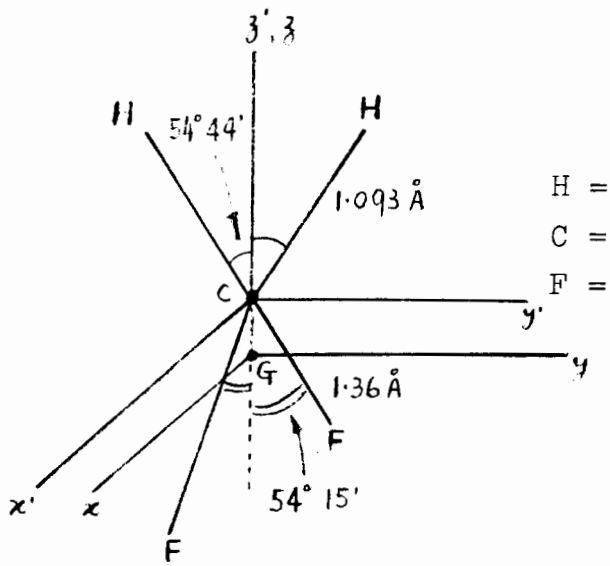

Fig. B-2. The CH_2F_2 molecule.

The primed frame has its origin at the central carbon atom and the y'z'-plane is a plane of symmetry of the molecule. The two fluorine atoms fall in the x'z'-plane. By the principle of moments and by symmetry, the centre of gravity G of the system is found at (0, 0, -0.566 in Å). The frame having its origin at G is unprimed and has all its axes parallel to those of the primed frame. The inertia tensor $\underset{\approx}{I}(G)$ with respect to this frame is found to be

$$\underset{\approx}{I}(G) \approx \begin{bmatrix} 16 & 0 & 0 \\ 0 & 55 & 0 \\ 0 & 0 & 48 \end{bmatrix} \text{ amuÅ}^2 \qquad \text{(B.3)}$$

which is diagonal. The x-, y- and z-axes are, therefore, the principal axes for the molecule.

APPENDIX C

SPIN-ROTATION INTERACTION TENSORS FOR CHF_2Cl AND CH_2F_2

The symmetric and antisymmetric spin-rotation interaction tensors $\underset{\approx}{C}^A$ and $\underset{\approx}{C}^B$ respectively in a molecule-fixed co-ordinate system are given by

$$\underset{\approx}{C}^A = \tfrac{1}{2} \left(\underset{\approx}{C}_1 + \underset{\approx}{C}_2 \right) \qquad (C.1)$$

$$\underset{\approx}{C}^B = \tfrac{1}{2} \left(\underset{\approx}{C}_1 - \underset{\approx}{C}_2 \right) \qquad (C.2)$$

where $\underset{\approx}{C}_1$ and $\underset{\approx}{C}_2$ are the tensors for the first and second fluorine nuclei with reference to the same molecule-fixed co-ordinate system.

(a) Chlorodifluoromethane (CHF_2Cl)

With reference to Fig. B-1, in the unprimed frame, the tensor $\underset{\approx}{C}_1$ for a fluorine nucleus can be written as

$$\underset{\approx}{C}_1 = \begin{bmatrix} C_{xx} & C_{xy} & C_{xz} \\ C_{yx} & C_{yy} & C_{yz} \\ C_{zx} & C_{zy} & C_{zz} \end{bmatrix} . \qquad (C.3)$$

The tensor $\underset{\approx}{C}_2$ for the other fluorine nucleus can be obtained by a symmetry operation which interchanges the two fluorine nuclei. Here a reflection with respect to the yz-plane interchanges the fluorine nuclei and the application of the transformation to $\underset{\approx}{C}_1$ gives

$$\underset{\approx}{C}_2 = \begin{bmatrix} C_{xx} & -C_{xy} & -C_{xz} \\ -C_{yx} & C_{yy} & C_{yz} \\ -C_{zx} & C_{zy} & C_{zz} \end{bmatrix} . \qquad (C.4)$$

From equations (C.1)-(C.4)

$$\underset{\approx}{C}^{A} = \begin{bmatrix} C_{xx} & 0 & 0 \\ 0 & C_{yy} & C_{yz} \\ 0 & C_{zy} & C_{zz} \end{bmatrix} \tag{C.5}$$

and

$$\underset{\approx}{C}^{B} = \begin{bmatrix} 0 & C_{xy} & C_{xz} \\ C_{yx} & 0 & 0 \\ C_{zx} & 0 & 0 \end{bmatrix} . \tag{C.6}$$

(b) Difluoromethane (CH_2F_2)

With reference to Fig. B-2, in the unprimed frame, the tensor $\underset{\approx}{C}_1$ for a fluorine nucleus can be written as

$$\underset{\approx}{C}_1 = \begin{bmatrix} C_{xx} & 0 & C_{xz} \\ 0 & C_{yy} & 0 \\ C_{zx} & 0 & C_{zz} \end{bmatrix} \tag{C.7}$$

since $\underset{\approx}{C}_1$ must be invariant under reflection with respect to the xz-plane. The tensor $\underset{\approx}{C}_2$ for the other fluorine nucleus can be obtained by a symmetry operation which interchanges the two fluorine nuclei. For example, 180° rotation about the z-axis interchanges the fluorine nuclei and the application of the transformation to $\underset{\approx}{C}_1$ gives

$$\underset{\approx}{C}_2 = \begin{bmatrix} C_{xx} & 0 & -C_{xz} \\ 0 & C_{yy} & 0 \\ -C_{zx} & 0 & C_{zz} \end{bmatrix} . \tag{C.8}$$

From equations (C.1), (C.2), (C.7) and (C.8)

$$\underset{\approx}{C}^{A} = \begin{bmatrix} C_{xx} & 0 & 0 \\ 0 & C_{yy} & 0 \\ 0 & 0 & C_{zz} \end{bmatrix} \tag{C.9}$$

and

$$\underset{\approx}{C}^{B} = \begin{bmatrix} 0 & 0 & C_{xz} \\ 0 & 0 & 0 \\ C_{zx} & 0 & 0 \end{bmatrix}. \qquad (C.10)$$